AD_____

Award Number: W81XWH-04-1-0213

TITLE: Structure-Based Design, Synthesis and Testing of Non-Peptide, Cell-Permeable, Potent Small Molecule Smac Mimetics as a New Therapy for Prostate Cancer"

PRINCIPAL INVESTIGATOR: Shanomeng Wang Ph. D.

CONTRACTING ORGANIZATION: University of Michigan
Ann Arbor, Michigan 48109-0934

REPORT DATE: February 2007

TYPE OF REPORT: Revised Final Report

PREPARED FOR: U.S. Army Medical Research and Materiel Command
Fort Detrick, Maryland 21702-5012

REPORT DOCUMENTATION PAGE

Form Approved
OMB No. 0704-0188

1. REPORT DATE *(DD-MM-YYYY)*	**2. REPORT TYPE**	**3. DATES COVERED** *(From - To)*
1-FEB-2007	REV Final	15 JAN 2004 - 14 JAN 2007

4. TITLE AND SUBTITLE
Structure-Based Design, Synthesis and Testing of Non-Peptide, Cell-Permeable, Potent Small Molecule Smac Mimetics as a New Therapy for Prostate Cancer"

5a. CONTRACT NUMBER

5b. GRANT NUMBER
W81XWH-04-1-0213

5c. PROGRAM ELEMENT NUMBER

6. AUTHOR(S)
Shanomeng Wang Ph. D.

E-Mail: Shaomeng@umich.edu

5d. PROJECT NUMBER

5e. TASK NUMBER

5f. WORK UNIT NUMBER

7. PERFORMING ORGANIZATION NAME(S) AND ADDRESS(ES)
University of Michigan
Ann Arbor, Michigan 48109-0934

8. PERFORMING ORGANIZATION REPORT NUMBER

9. SPONSORING / MONITORING AGENCY NAME(S) AND ADDRESS(ES)
U.S. Army Medical Research and Materiel Command
Fort Detrick, Maryland 21702-5012

10. SPONSOR/MONITOR'S ACRONYM(S)

11. SPONSOR/MONITOR'S REPORT NUMBER(S)

12. DISTRIBUTION / AVAILABILITY STATEMENT
Approved for Public Release; Distribution Unlimited

13. SUPPLEMENTARY NOTES

14. ABSTRACT
XIAP (X-linked inhibitor of apoptosis protein) is a promising new therapeutic target for the design of an entirely new class of effective and non-toxic cancer therapy to improve survival and quality of life of prostate cancer patients. New therapies targeting XIAP may prove to be especially effective to overcome apoptosis-resistance of prostate cancer cells. Using a powerful computational structure-based design strategy, we have designed and synthesized new, non-peptide, cell-permeable small-molecule inhibitors of XIAP. The most potent inhibitors bind to XIAP with nanomolar affinities and are highly potent in inhibition of cell growth in androgen-independent human prostate cancer cell lines. Furthermore, such inhibitors are highly effective in enhancing the activity of other anticancer drugs in human prostate cancer cells. Importantly, these inhibitors have a low toxicity to normal cells. Taken together, our studies have led to the discovery of highly promising small-molecule inhibitors of XIAP. Further optimization of these promising lead compounds may ultimately lead to the development of a new class of anticancer drugs for the treatment of advanced human prostate cancer.

15. SUBJECT TERMS

16. SECURITY CLASSIFICATION OF:			**17. LIMITATION OF ABSTRACT**	**18. NUMBER OF PAGES**	**19a. NAME OF RESPONSIBLE PERSON**
					USAMRMC
a. REPORT	**b. ABSTRACT**	**c. THIS PAGE**		88	**19b. TELEPHONE NUMBER** *(include area code)*

Table of Contents

Introduction

Androgen withdraw remains the only effective form of systematic therapy for men with advanced prostate cancer, with objective response in 80% of patients. Unfortunately, progression to androgen independence occurs within a few years in the majority of these cases. Despite extensive clinical trials, chemotherapy has limited antitumor activity, with an objective response rate of less than 50% and no demonstrated survival benefit. Thus, androgen-independent (hormone-refractory) disease is the main obstacle to improving the survival and quality of life in patients with advanced prostate cancer. There is an urgent need for novel therapeutic strategies for advanced prostate cancer by targeting the fundamental molecular basis of resistance of androgen-independent disease to chemotherapy.

Most of the current chemotherapeutic agents for advanced prostate cancer work by indirectly inducing programmed cell death or apoptosis in cancer cells. The aggressive cancer-cell phenotype is the result of a variety of genetic and epigenetic alterations leading to deregulation of intracellular signaling pathways. Such alterations include an impaired ability of the cancer cell to undergo apoptosis. Indeed, hormone-refractory prostate cancer is very resistant to apoptosis induced by chemotherapeutic agents and radiation. Thus, current and future efforts toward designing and developing new therapies to improve survival and quality of life of prostate cancer patients must include strategies that specifically target prostate cancer-cell resistance to apoptosis. Therefore, developing new and specific anticancer drugs that target critical apoptosis regulators by overcoming apoptosis of prostate cancer cells is a very exciting and fruitful area of research to improve the outcome of current anticancer therapies.

Inhibitor of apoptosis proteins (IAPs) have been identified as a class of central negative apoptosis regulators. XIAP is the most potent anti-apoptotic member among all the IAPs and has a key function in the negative regulation of apoptosis in both the cell surface death receptor- and the mitochondria-mediated pathways. Prostate cancer PC-3, DU-145 and LnCap cell lines have much higher levels of XIAP protein than normal prostate epithelial cells. XIAP has been implicated to play a key role in apoptosis-resistance of prostate cancer cells to chemotherapies. Because XIAP blocks apoptosis

at the effector phase, a point where multiple signaling pathways converge, new therapies targeting XIAP may prove to be especially effective to overcome apoptosis-resistance of prostate cancer cells and to develop an entirely new class of cancer therapy to improve survival and quality of life of prostate cancer patients.

Smac/DIABLO is a potent pro-apoptotic protein, which directly interacts with XIAP and other IAPs and promotes apoptosis by antagonizing the anti-apoptotic function of IAP proteins. Micro-injection of Smac protein was shown to promote apoptosis in prostate cancer cells. Three recent studies showed that short Smac-based peptides, consisting of the first 4 to 8 residues of the N-terminus of Smac tethered to a carrier peptide for intracellular delivery, sensitize various tumor cells *in vitro* for apoptosis induced by TRAIL or chemotherapeutic drugs and greatly enhance the anti-tumor activity of therapeutic agents *in vivo*. Importantly, Smac-based peptides show little or no toxicity to animals. These studies thus provide the important proof-of-concept that Smac-based small molecule inhibitors may have a great therapeutic potential for treating prostate cancer with XIAP overexpression.

Peptide-based inhibitors have several intrinsic limitations to be developed as potential drugs, including poor cell-permeability and poor *in vivo* stability. For this reason, in this IDEA Development Grant, we propose to design and synthesize potent, non-peptide**,** cell-permeable, small molecule inhibitors of XIAP (Smac mimetics) and to test their therapeutic potential for the treatment of prostate cancer using a powerful structure-based design strategy based upon a class of most promising non-peptide small molecule inhibitors we have already discovered in our laboratory. Successful carried out, our studies will represent an exciting step and lay the foundation for developing an entirely new class of anticancer drugs by targeting a central apoptosis regulator protein. It is predicted that such a drug will have very few side effects and will be able to significantly improve the outcome of current clinical treatment protocols by specifically overcoming apoptosis-resistance of prostate cancer cells to chemotherapeutic agents through targeting the fundamental molecular basis of apoptosis-resistance in prostate caner cells.

Body of the report:

In this project, we have pursued the design, synthesis and evaluation of two different classes of small-molecule inhibitors of XIAP. The first class of small-molecule inhibitors of XIAP is based upon the core structure of Embelin. Embelin is a natural product and was discovered as a fairly potent small-molecule inhibitor of XIAP through computational structure-based database searching in our laboratory. The second class of small-molecule inhibitors of XIAP was designed starting from the Smac AVPI sequence. In both cases, potent, cell-permeable small-molecule inhibitors of XIAP were identified. Below we divide the report into two sections, each of which focuses on one class of compounds.

A. Design, synthesis and evaluation of novel small-molecule inhibitors of XIAP based upon Embelin as the initial lead compound

Through structure-based database searching, we have previously discovered embelin as a non-peptide, small-molecule inhibitor of XIAP. Embelin was determined to bind to the XIAP BIR3 domain with an IC_{50} value of 4.7 μM (K_i = 400 nM, Table 1) in our optimized, competitive fluorescence-polarization (FP)-based assay. To the best of our knowledge, embelin is the only known class of non-peptide inhibitor that binds to the XIAP BIR3 domain, whose chemical structure is not related to the AVPI peptide in Smac. Hence, embelin represents a promising initial lead for optimization toward our ultimate goal of developing a new class of anticancer drugs to target XIAP. We have therefore pursued design, synthesis and evaluation of new embelin analogues to improve their binding affinities to XIAP and other activity in inhibition of cell growth and induction of cell death in human prostate cancer cells with high levels of XIAP.

Embelin consists of the dihydroxyquinone core and a long hydrophobic tail. Our modeling suggested that the hydrophilic dihydroxyquinone core forms a number of hydrogen bonds with XIAP and the hydrophobic tail interacts with hydrophobic pocket where the isoleucine residue in the AVPI Smac peptide binds. Our initial modifications focused on the hydrophobic tail portion of the molecule.

A series of embelin analogues **4a**-**4h** with different hydrophobic tails were designed and synthesized. The synthesis of compounds **4a-4h** is shown in **Scheme 1**. Briefly, commercially available, different phosphonium salts **1a-1h** were treated with 1:1 equivalent of *n*-butyllithium, followed by reaction with aldehyde **2,** which was prepared according to a published method. Hydrogenation afforded the key intermediates **3a-3h**. The final target compounds **4a-4h** were obtained by the oxidation of **3a-3h** with ceric ammonium nitrate, followed by hydrolysis with 70% perchloric acid and concentrated hydrochloric acid.

Scheme 1. Synthesis of designed new embelin analogues.

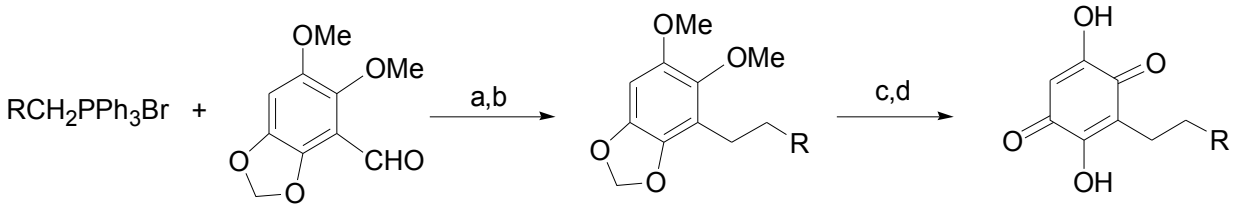

1a-1h **2** **3a-3h** **4a-4h**

Reagents and conditions: (a) n-BuLi, THF, 0 °C, 10 min; (b) H2, 10 % Pd-C, EtOAc, room temperature; (c) CAN, CH3CN-H2O, 0 °C, 1 h; (d) HClO4, HCl, dioxane, room temperature, 48 h.

Compounds **4a-4h** were tested for their binding affinities to recombinant XIAP BIR3 protein using our established quantitative fluorescence-polarization(FP)-based

competitive binding assay and compared directly to embelin (**1**) and the Smac AVPI peptide. The results are summarized in Table 1.

Compound **4a** was designed to test the importance of the $C_{11}H_{23}$ long hydrophobic tail, in which the $C_{11}H_{23}$ tail was replaced by an ethyl group. Our FP-based binding assay showed that compound **4a** has a K_i value of 10.4 μM to XIAP BIR3, thus 25-times less potent than embelin. This suggests that the $C_{11}H_{23}$ long hydrophobic tail is critical for the binding of embelin to XIAP BIR3. Based upon this result, we have designed and synthesized compound **4b** with a *n*-octyl side chain. Compound **4b** has a K_i value of 1.25 μM. Thus, although compound **4b** is 3-times less potent than embelin, it is 8-times more potent than compound **4a,** further confirming the importance of the long hydrophobic tail in the binding of embelin to XIAP BIR3.

The crystal structure of XIAP BIR3 in complex with Smac showed that the binding of Smac to XIAP BIR3 is mediated by AVPI four amino acid residues in Smac and a well-defined surface binding groove in XIAP BIR3. While the alanine residue in the Smac AVPI binding motif forms an extensive hydrogen bonding network with XIAP BIR3, the proline residue has hydrophobic contacts with Trp323 in XIAP. Our modeling suggested that the hydrophilic dihydroxyquinone core in embelin mimics the alanine residue in the Smac AVPI peptide to form a network of hydrogen bonding network. We have designed two new analogues, **4c** and **4d**, to explore whether a phenyl ring would be able to mimic the interaction between the proline ring in the Smac AVPI peptide and Trp323 in XIAP. As can be seen, while compound **4c** with a $(CH_2)_4$ linker between the dihydroxyquinone group and the phenyl ring has a K_i value of 1.3 μM, compound **4d**

with a $(CH_2)_2$ linker has a K_i value of 0.71 μM. We have therefore made additional modifications based upon compound **4d**.

In the Smac AVPI peptide, the isoleucine residue binds to a hydrophobic pocket and plays an important role for the binding of the AVPI peptide to XIAP BIR3. Our modeling suggested that the long hydrophobic tail in embelin interacts with this hydrophobic pocket in XIAP. This is further supported by the binding data of embelin and compound **4b**. We have thus designed and synthesized a series of new analogues based upon compound **4d** in an attempt to capture the hydrophobic interaction between the isoleucine residue in the Smac AVPI peptide and the hydrophobic pocket in XIAP BIR3.

Figure 1. Model between XIAP-BIR3 and **4h**

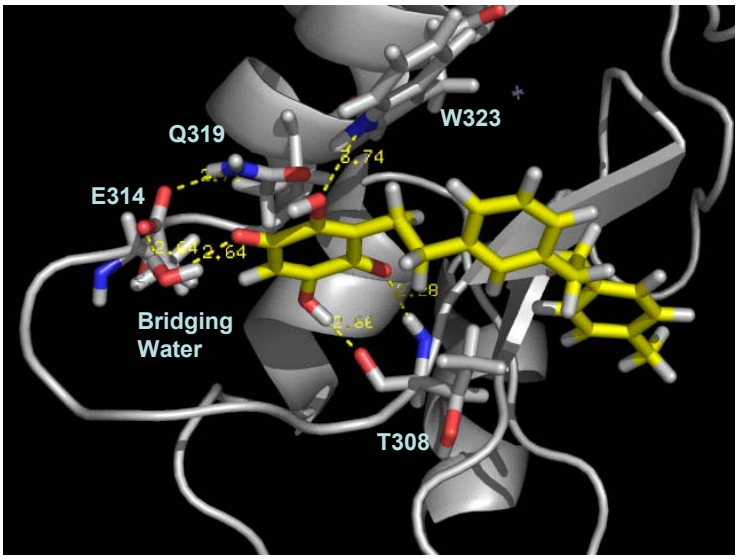

Compound **4e** with a n-butyl group attached to the *meta*-position on the phenyl ring in compound **4d** has a Ki value of 0.48 μM, which is more potent than **4d**. Encouraged by this result, we replaced the butyl group with an ethylphenyl group since it was previously shown that replacement of the isoleucine in the Smac AVPI peptide by

a phenylalanine residue increased the binding affinity of the resulting peptide. This resulted in compound **4f**, which has a K_i value of 0.38 μM binding to XIAP. Thus, compound **4f** is as potent as embelin.

Two additional compounds were designed and synthesized to further explore the interaction between the terminal phenyl ring and XIAP by installation a methyl group either on the *meta*- or *para*-position. The resulting compounds **4g** and **4h** have Ki values of 180 nM and 140 nM, respectively. Hence, compound **4g** and **4h** are more potent inhibitors of XIAP than embelin. The binding model predicted for compound **4h** in complex with XIAP BIR3 domain is shown in Figure 1.

We have tested these compounds for their activity to inhibit cancer cell growth in human PC-3 human prostate cancers using 4-day standard WST-based assay. The results are summarized in Table 1. As can be seen, consistent with its high binding affinity, compound **4g** potently inhibits cell growth in PC-3 cancer cells with an IC50 value of 9.1 μM.

In summary, embelin represents a novel class of non-peptide small-molecule inhibitors of XIAP. Through computational design and chemical modifications, we have now obtained very potent small-molecule inhibitors of XIAP. For example, compounds **4g** and **4h** have K_i values of 180 nM and 140 nM, respectively for binding to XIAP. In addition, compound **4g** is effective in inhibition of cancer cell growth in PC-3 human prostate cancer cell line with an IC_{50} value of 9.1 μM. Hence, compound **4g** represents a promising lead compound for further optimization toward our ultimate goal of developing a new class of anticancer drugs by targeting XIAP and promoting apoptosis in cancer cells.

Table 1. Binding affinities to the XIAP BIR3 in an FP-based binding assay for **4a-h**

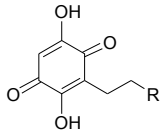

Compounds	R	$K_i \pm SD$ (μM) FP-Based Binding Assay	IC_{50} (Inhibition of cell growth in PC-3 cells)
1	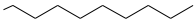	0.40 ± 0.13	8. 0
4a	H	10.4 ± 1.3	128
4b	$-CH_2CH_2CH_2CH_2CH_2Me$	1.25 ± 0.9	52. 0
4c	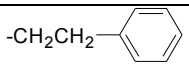	1.3 ± 0.3	16. 4
4d		0.71 ± 0.17	21. 8
4e	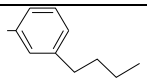	0.48 ± 0.3	15. 8
4f	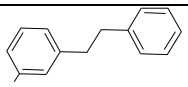	0.38 ± 0.09	14. 3
4g	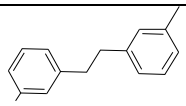	0.18 ± 0.09	9. 1
4h	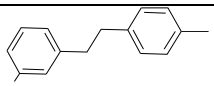	0.14 ± 0.05	16. 3

B. Design, synthesis and evaluation of novel, conformationally constrained Smac mimetics as inhibitors of XIAP

B1. Design of non-peptide, monovalent and bivalent Smac mimetics

High-resolution, experimental three-dimensional (3D) structures of the BIR3 domain of XIAP in complex with Smac protein and peptide have been determined (**Figure 1**).The N-terminal tetrapeptide of Smac (Ala-Val-Pro-Ile) recognizes a surface groove on the BIR3 domain of XIAP through several hydrogen-bonding interactions and van der Waals contacts. The interaction between BIR3 and caspase-9 has also been shown to involve four residues (Ala-Thr-Pro-Phe, or AVPI) on the amino terminus of the small subunit of caspase-9 to the same surface groove on the BIR3 domain. Several recent studies have convincingly demonstrated that Smac promotes the catalytic activity of caspase-9 by competing with caspase-9 for the same binding groove on the surface of the BIR3 domain.

Unlike most protein-protein interactions, the Smac-XIAP interaction is mediated by only four amino acid residues (AVPI) on the Smac protein and a well-defined surface groove on the BIR3 domain of XIAP. The K_d value of Smac peptide AVPI to XIAP (K_d =400 nM) is essentially the same as the mature Smac protein (K_d = 420 nM). This well-defined interaction site is ideal for the design of non-peptide, drug-like small molecules that mimic the binding of Smac to XIAP. Indeed, our NMR and computational modeling studies have shown that Embelin binds to this site.

Figure 1. X-ray structure of Smac in complex with XIAP BIR3. Carbon atoms are shown in green for Smac AVPI peptide. Hydrophobic carbon atoms on the side chain of Alanine, Proline ring and Isoleucine in Smac peptide are shown in yellow. Hydrogen bonds are depicted in light-blue dashed lines. Oxygen and nitrogen atoms are shown in red and blue, respectively. Carbon atoms in XIAP BIR3 protein are shown in black.

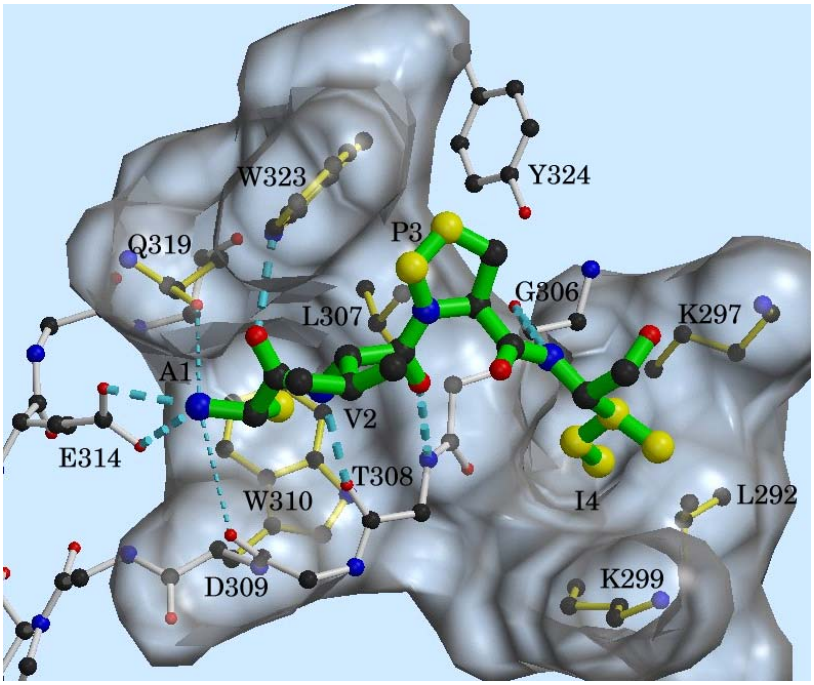

Based upon the X-ray structure of XIAP BIR3 in complex with Smac, we have designed **SM-122** as a conformationally constrained Smac mimetic to closely mimic the binding of Smac to XIAP BIR3 domain (**Figure 2**). Our cyclization strategy converts the two natural amino acids (valine and proline) into a non-amino-acid, bicyclic, lactam ring system, and the resulting Smac mimetics become non-peptide, i.e. there is no amino-acid bond in these Smac mimetics (**Figure 2**). Using our established fluorescence-polarization-based (FP-based) competitive binding assays, we have determined that **SM-122** binds to recombinant XIAP BIR3 protein with a K_i value of 27 nM, and to recombinant XIAP BIR2 protein with a K_i value of 2 μM. These data suggest that **SM-**

122 binds to XIAP BIR3 preferably but also has a significant binding to BIR2 domain of XIAP.

Figure 2. Designing conformationally constrained, non-peptide, bivalent Smac mimetics.

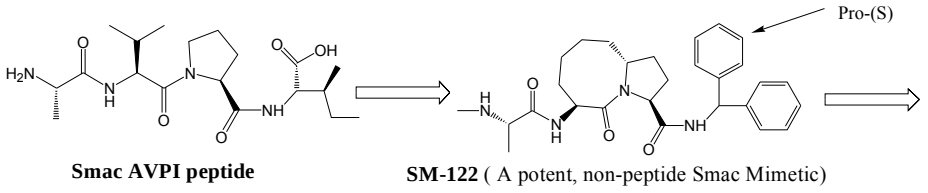

Smac AVPI peptide **SM-122** (A potent, non-peptide Smac Mimetic)

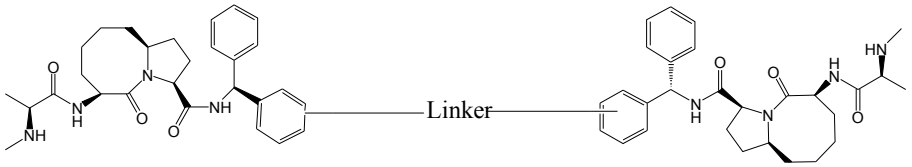

Basic template for bivalent Smac mimetics

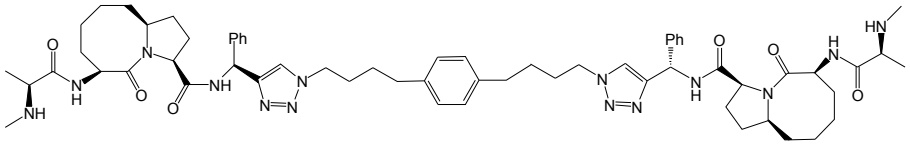

SM-164 (A Conformationally constrained non-peptide bivalent Smac Mimetic)

XIAP contains three baculoviral IAP repeat (BIR) domains (**Figure 3**). Its BIR2 domain, together with the linker before the BIR2 domain, binds to effector caspases-3 and -7 and inhibits their activity and its BIR3 domain binds to and inhibits an initiator caspase-9. In this manner, XIAP efficiently inhibits apoptosis by binding to and inhibiting the activity of not only caspase-9 but also caspase-3 and -7, whose activity is crucial for execution of apoptosis. We hypothesize that small-molecule inhibitors designed to concurrently target both the BIR2 and BIR3 domains of XIAP will be much more efficient in antagonizing XIAP in cells. We predict that such compounds, which are called "**bivalent Smac mimetics**" will achieve a higher binding affinity to XIAP and will be far

more effective than agents that target only the BIR2 or the BIR3 domain in promoting apoptosis in cancer cells.

Figure 3. XIAP inhibits caspase-9 through its BIR3 domain and caspase-3/-7 through its BIR2 domain together with the linker before BIR2. Smac protein forms a dimer and binds to both BIR2 and BIR3 domains in XIAP and effectively antagonizes the function of XIAP.

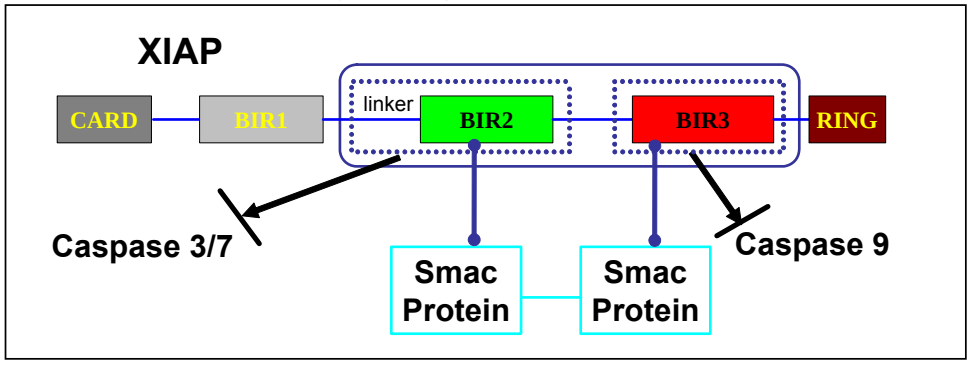

Using **SM-122** as the monovalent Smac mimetic, we have designed bivalent Smac mimetics to target both the BIR2 and BIR3 domains of XIAP. Analysis of our predicted binding models of **SM-122** to XIAP BIR3 showed that the phenyl ring at the pro-(*S*) position in **SM-122** can be used for chemical tethering (**Figure 2**), since this phenyl ring is exposed to solvent and is not in contact with any protein atoms. A series of bivalent Smac mimetics were designed with the basic template structure shown in **Figure 2**. To date, we have synthesized more than 10 such bivalent Smac mimetics with different types of chemical linkers. **SM-164** is one of the most potent and promising inhibitors (**Figure 2**).

SM-164 was determined to bind to XIAP protein containing both the BIR2 and BIR3 domains (residues 120-356) with an IC_{50} value of 1.9 nM (estimated Ki value

equal to 200 pM) in our competitive FP-based assay (**Figure 4**). Of note, the hill-slope of the binding curve is 1, suggesting the formation of 1:1 complex between **SM-164** and XIAP. In addition, gel-filtration experiments showed that our designed bivalent Smac mimetics form 1:1 complex with the XIAP protein containing BIR2 and BIR3 domain (data not shown), consistent with our FP-based binding results.

Figure 4. Competitive binding of designed monovalent and bivalent Smac mimetics to recombinant XIAP L-BIR2-BIR3 protein as determined using our FP-based binding assay.

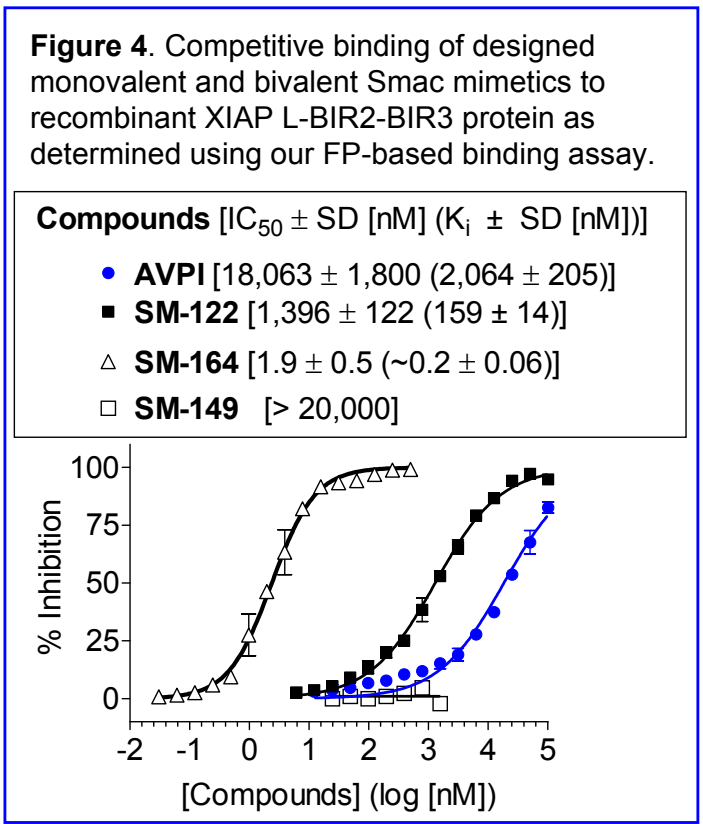

In comparison, **SM-122** has an IC_{50} value of 1.4 μM (Ki = 159 nM) to XIAP protein containing BIR2 and BIR3 domains and the AVPI Smac peptide has an IC50 value of 18 μM (K_i value of 2.1 μM). Hence, **SM-164** is 800-times more potent than the Smac AVPI peptide and 28-times more potent than the monovalent **SM-122**. **SM-164** represents the most potent Smac mimetic discovered to date. Since **SM-164** is non-

peptide, it is predicted that it will have major advantages over peptide-based Smac mimetics for its cell-permeability, *in vivo* stability and bioavailability.

Bivalent Smac mimetics potently inhibit cell growth in PC-3 and DU-145 cells

Figure 5. Inhibition of cell growth by **SM-164** in PC-3 and DU-145 cell lines, as determined using WST-based assays when cells were treated for 4 days.

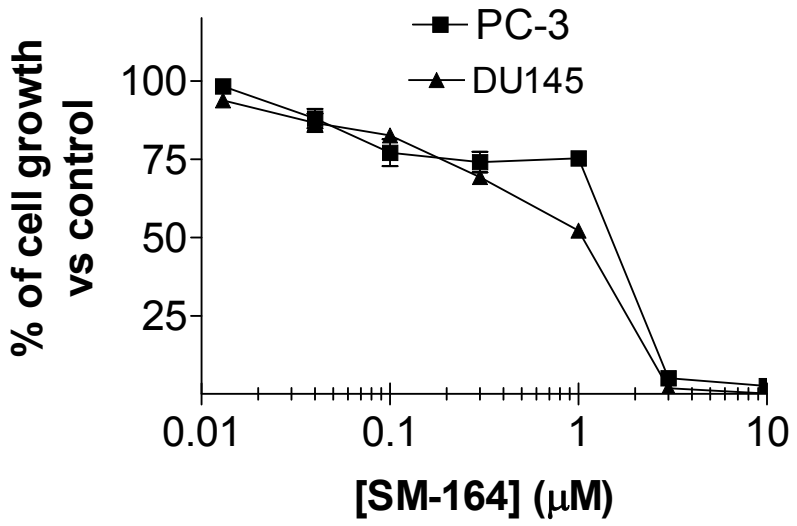

SM-164 was evaluated for its ability to inhibit cell growth in PC-3 and DU-145 cells. **SM-164** quite potently inhibited cell growth in both PC-3 and DU-145 cells with IC_{50} values of 1.5 and 1 μM, respectively (**Figure 5**). In direct comparison, **SM-164** is at least 50-times more potent than the monomeric **SM-122** (data not shown). This is consistent with its higher binding affinity to XIAP for **SM-164** than for **SM-122**.

SM-164 *is highly effective in enhancing the activity of taxotere in human prostate cancer PC-3 cells*

Since bivalent Smac mimetics such as **SH-164** are expected to effectively antagonize the inhibition of XIAP to not only caspase-9 but also caspase-3/-7, we

predict that they may be able to greatly enhance the activity of other chemotherapeutic agents. To this end, we have evaluated **SM-164** for its ability to enhance the activity of taxotere, which is an agent approved by the FDA as a treatment in combination with prednisonefor patients with androgen independent (hormone refractory) metastatic prostate cancer.

Figure 6. **SM-164** strongly synergizes with taxotere in the PC-3 human prostate cancer cell line. Cells were treated for 4 days and cell growth was determined using the WST-based assays when

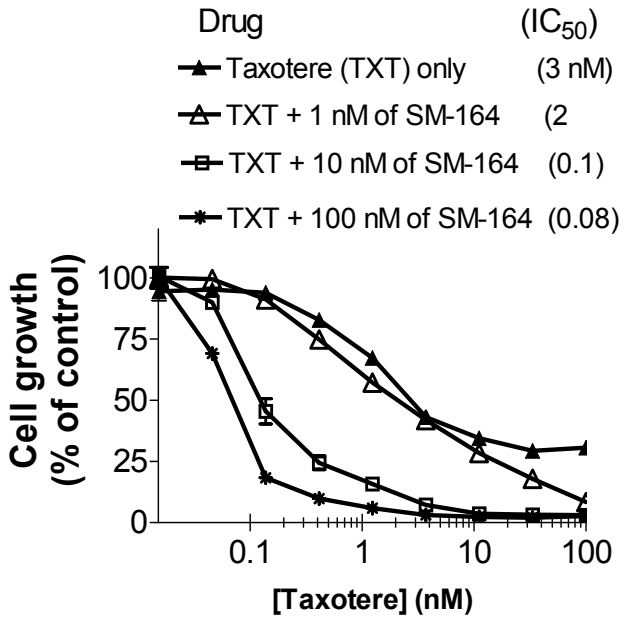

Our results show that **SM-164** is highly effective in enhancing the activity of taxotere in androgen-independent, PC-3 prostate cancer cells (**Figure 6**). Taxotere alone has an IC_{50} value of 3 nM in inhibition of cell growth. Combination with as low as 10 nM of SM-164 enhance the activity of taxotere by 30-times. Of note, since 10 nM of **SM-164** has no effect on its own, **SM-164** in combination with taxotere achieves a truly synergistic effect. Based upon the exciting in vitro results, we plan to carry extensive in

vivo studies to further evaluate the therapeutic potential of **SM-164** in combination with taxotere as a potentially new therapeutic strategy for the treatment of androgen, independent human prostate cancer.

SM-164 *is highly effective in enhancing the activity of TRAIL in human prostate cancer PC-3 cells*

Another agent we have evaluated in combination with **SM-164** is TRAIL (TNF-related apoptosis-inducing ligand). TRAIL was shown to be effective in inducing apoptosis in some cancer cells and importantly has a low toxicity to normal cells and tissues. TRAIL has been considered as a promising new anticancer therapy for the treatment of human cancer and is currently in clinical development. Unfortunately, TRAIL resistance is common in both preclinical and clinical studies.

PC-3 prostate cancer cells are insensitive to TRAIL, having IC_{50} values >300 ng/ml in the cell growth inhibition assay (**Figure 7A**). **SM-164** greatly enhances the activity of TRAIL in the PC-3 prostate cancer cell line. Combination of 10 nM and 100 nM of **SM-164** with TRAIL decreases the IC_{50} value of TRAIL from >300 ng/ml to 16 and 1 ng/ml, respectively. Importantly, since **SM-164** alone has minimal activity at as high as 500 nM, the dramatic enhancement in the activity of TRAIL by **SM-164** in the PC-3 cell line is also a true synergistic effect. **SM-149**, the inactive control, has no enhancement on the activity of TRAIL, indicating that the effects by **SM-164** are specific and correlate with its potent binding to XIAP protein.

Figure 7. Bivalent Smac mimetic **SH-164** dramatically synergizes the activity of TRAIL in human prostate cancer PC-3 cell line. (**A**). PC-3 cells were treated for 4 days and cell growth inhibition was determined by the WST-based assay; (**B**). PC-3 cells were treated for 12 hours and apoptosis was determined by flow cytometric analysis by Propidium iodide (P.I.) and ANNEXIN-V double staining.

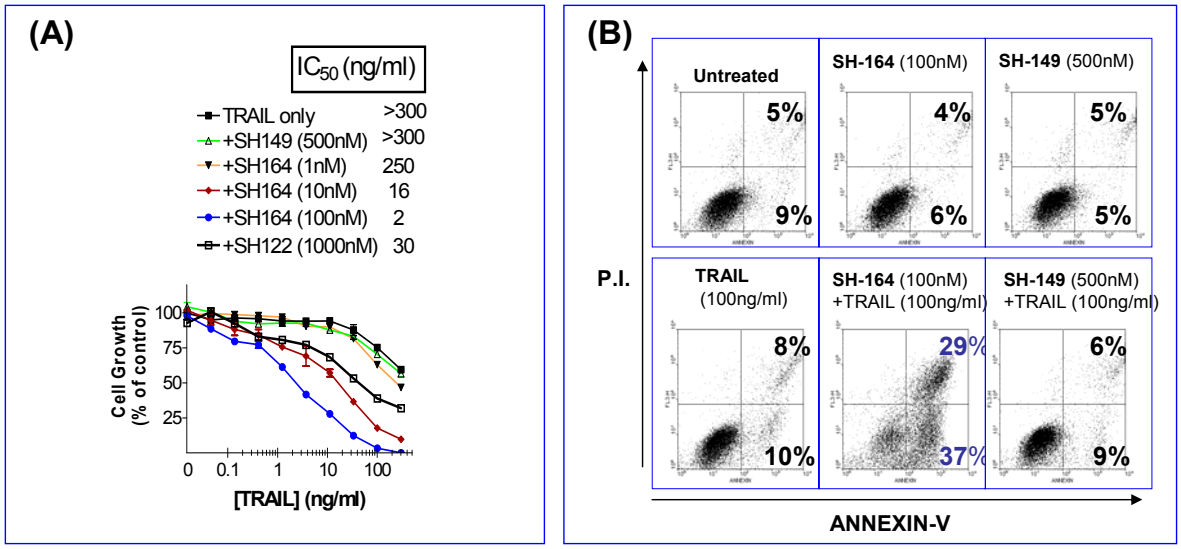

SM-164 *enhances the apoptosis induced by TRAIL in the PC-3 cells*

We have further evaluated **SM-164** for its ability to enhance apoptosis induction by TRAIL in PC-3 cells using Annexin-V/PI double staining. It was found that while treatment of PC-3 cells by TRAIL alone at 100 ng/ml for 24 hours resulted in 18% apoptotic cells, the combination of 100 nM of **SM-164** with 100 ng/ml TRAIL increased the apoptotic cells to 65% (**Figure 7B**). There was no increase in apoptotic cells when TRAIL was combined with 100 nM of the inactive control **SM-149** as compared to TRAIL alone.

Western blotting analysis showed that there is a marked increase in the processing of caspase-8, caspase-9 and caspase-3, and cleavage of PARP (**Figure 8**). Our Western analysis provided strong evidence that SM-164 greatly enhances the activity of TRAIL at the molecular level.

Figure 8. Western blot analysis of caspases, cleaved PARP, Cyto-C release and Bid cleavage in PC-3 cells treated by TRAIL, or **SM-164**, inactive control SM-149, or combination for 10 hours.

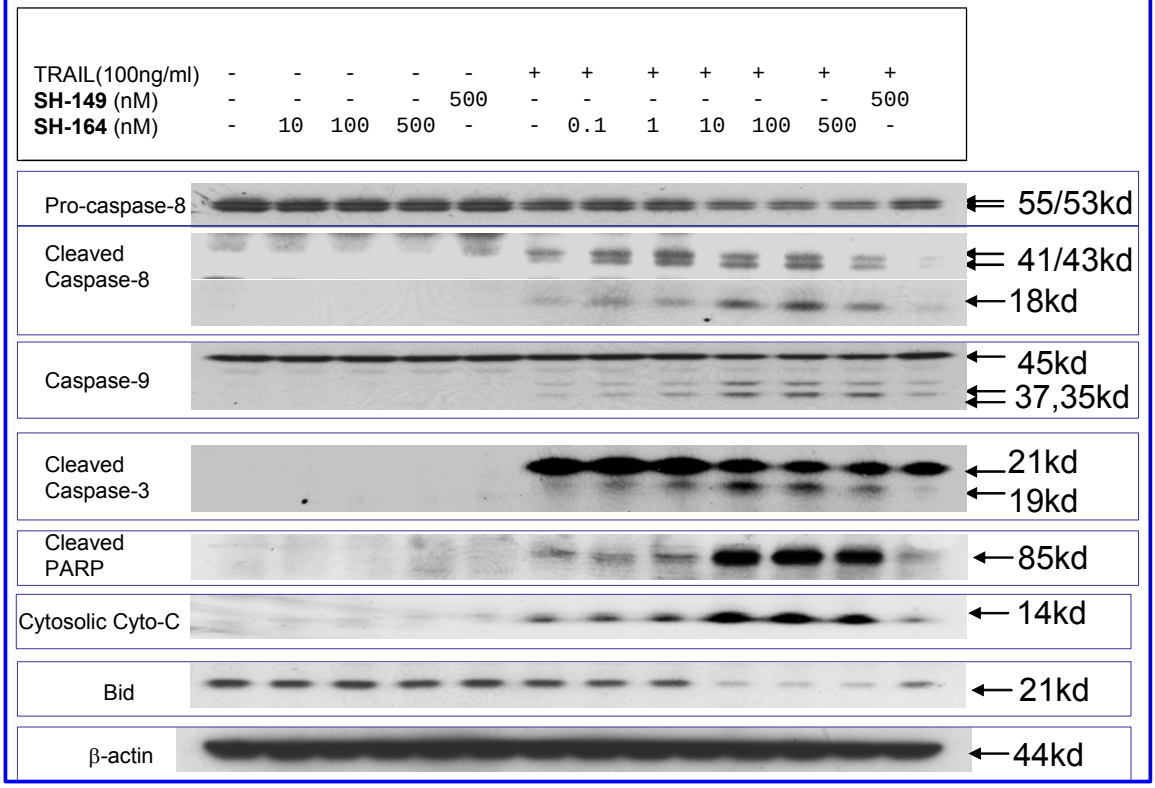

SM-164 *is not toxic to normal prostate epithelial cells*

SM-164 was tested for its toxicity to normal prostate epithelial cells (PrEC). As shown in Figure 9, **SM-164** is much less toxic to normal prostate epithelial cells and fibroblasts than to human prostate cancer cells. While SM-164 at 3 μM completely inhibited cell growth in PC-3 and DU-145 androgen-independent human prostate cancer cell lines, it has not or minimal effect in human prostate epithelial cells and WI-38 fibroblasts.

Figure 9. Inhibition of cell growth by **SM-164** in normal prostate epithelial cells (PrEC) and WI-38 fibroblasts. Cells were treated for 5 days and cell growth was determined using the standard WST-based assay.

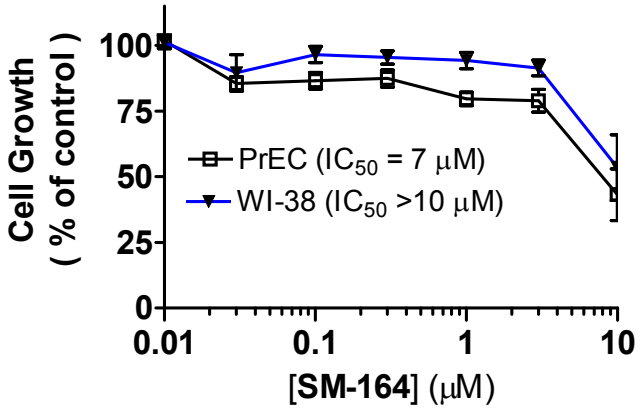

Preliminary toxicity evaluation of SM-164 in mice

In the last several months, we have synthesized sufficient amount of SM-164 for our proposed *in vivo* studies of SM-164 as a potential new therapeutic agent for the treatment of androgen-independent prostate cancer. As the first step, we have evaluated SM-164 for its toxicity in both nude and SCID mice. SM-164 is found to be well tolerated in mice with intravenous (i.v.) administration. **SM-164** at 5 mg/kg (i.v.) once a day (5 days a week) for 2 weeks did not cause any animal weight loss, or other sign of toxicity. In addition, combination of SM-164 (5 mg/kg, i.v. once a day, 5 times a week for 2 weeks) with taxotere (7.5 mg/kg, i.v., once a week for 2 weeks) is also well tolerated. These dose-schedules will be used for our proposed *in vivo* efficacy experiment using the PC-3 xenograft model of human prostate cancer to test the antitumor activity of SM-164 alone and in combination with taxotere. Taxotere is a clinically approved anticancer drug for the treatment of advanced prostate cancer. A success of our in vivo efficacy study will thus provide the rationale and impetus for future clinical evaluations of our Smac mimetics as a new therapy for the treatment of human prostate cancer, in combination with taxotere. We expect that our *vivo* efficacy study will be finished within the next 12 weeks.

Key Research Accomplishments:

(A). Starting from Embelin as the initial lead compound, our optimization has yielded new compounds with higher affinities to XIAP. The two most potent lead compounds, **4g** and **4h,** bind to XIAP BIR3 with K_i values of 180 and 140 nM, respectively. Compound **4g** potently inhibits cell growth in PC-3 androgen-independent human prostate cancer cell line and represents a promising new lead compound for further optimization. We have now synthesized a large quantity of this compound for extensive *in vitro* and *in vivo* studies to further determine its therapeutic potential for the treatment of androgen-independent human prostate cancer.

(B). Starting from the Smac AVPI peptide, we have designed conformationally constrained, non-peptide Smac mimetics with extremely high binding affinities. For example, SM-164 binds to XIAP with an IC_{50} value of 1.9 nM (Ki value = 200 pM), representing the most potent small-molecule inhibitor of XIAP discovered to date. **SM-164** potently inhibits cell growth in PC-3 and DU-145 androgen-independent human prostate cancer cell lines. In addition, **SM-164** is highly potent and effective to sensitize PC-3 prostate cancer cells to taxotere and TRAIL at low nanaomolar concentrations and achieves a true synergistic effect. Importantly, **SM-164** displays a minimal toxicity to normal prostate epithelial cells. Our studies showed that SM-164 represents a highly promising lead compound for extensive *in vitro* and *in vivo* evaluation to further evaluate its therapeutic potential for the treatment of advanced human prostate cancer.

(c). To date, one manuscript has been published on the design, synthesis and evaluation of Embelin analogues. A PDF file is included for this report. Another manuscript has been accepted for publication by the *Journal of the American Chemical Society* on the design, synthesis and initial characterization of SM-164 as a potent antagonist of XIAP. A PDF file of this manuscript is attached. A third manuscript specifically on the evaluation of SM-164 in human prostate cancer models *in vitro* and *in vivo* is being written. We are in the

process of completing the planned in vivo experiment using the PC-3 xenograft model.

In summary, our studies provide the initial but important proof-of-the-concept that small-molecule inhibitors of XIAP may have a great therapeutic potential for the treatment of advanced, androgen-independent prostate cancer. We are at the present time performing extensive *in vivo* studies of compound 4g and SM-164 in animal models of human prostate cancer.

Reportable Outcomes:

(1). A manuscript described the design, synthesis and biochemical and biological characterization of Embelin-based compounds has been published.

Jianyong Chen, Zaneta Nikolovska-Coleska, Guoping Wang, Su Qiu and Shaomeng Wang, Design, synthesis, and characterization of new embelin derivatives as potent inhibitors of X-linked inhibitor of apoptosis protein, *Bioorganic & Medicinal Chemistry Letters*, *Volume 16, Issue 22*, *15 November 2006*, *Pages 5805-5808.* A PDF file is included. This DOD grant was acknowledged in the paper.

(2). Another manuscript has been accepted for publication by the *Journal of the American Chemical Society* on the design, synthesis and initial characterization of SM-164 as a potent antagonist of XIAP. A PDF file of this manuscript is attached. This DOD grant was acknowledged in the paper.

(3). A third manuscript specifically on the evaluation of SM-164 in human prostate cancer models *in vitro* and *in vivo* is being written. We are in the process of completing the planned in vivo experiment using the PC-3 xenograft model.

(4). A patent application was filed on SM-164 and its analogues as antagonists of XIAP and potential novel anticancer agents for the treatment of human prostate cancer and other types of human cancer.

Conclusions: XIAP represents a promising molecular target for the design and development of an entirely new class of anticancer drugs for the treatment of human prostate cancer by overcoming apoptosis resistance of prostate cancer cells. Our studies, supported by the DOD prostate cancer IDEA grant, have yielded two different classes of potent, cell-permeable and non-peptide small-molecule inhibitors of XIAP. Our data suggest that these potent small-molecule inhibitors of XIAP may have a great therapeutic potential for the treatment of human prostate cancer. Further optimization for these promising lead compounds and extensive testing may ultimately lead to an entirely new class of anticancer therapy for the treatment of androgen-independent human prostate cancer by targeting XIAP.

Available online at www.sciencedirect.com
ScienceDirect
Bioorganic & Medicinal Chemistry Letters 16 (2006) 5805–5808
Bioorganic & Medicinal Chemistry Letters

Design, synthesis, and characterization of new embelin derivatives as potent inhibitors of X-linked inhibitor of apoptosis protein

Jianyong Chen, Zaneta Nikolovska-Coleska, Guoping Wang, Su Qiu and Shaomeng Wang*

Comprehensive Cancer Center and Departments of Internal Medicine, Pharmacology and Medicinal Chemistry, University of Michigan, 1500 E. Medical Center Drive, Ann Arbor, MI 48109, USA

Received 24 July 2006; revised 15 August 2006; accepted 15 August 2006
Available online 8 September 2006

Abstract—X-Linked inhibitor of apoptosis protein (XIAP) is a promising molecular target for the design of new anticancer drugs aiming at promoting apoptosis in cancer cells. We have previously identified embelin as an inhibitor of XIAP through computational structure-based database screening. Herein, we report the design, synthesis, and evaluation of new embelin analogues as inhibitors of XIAP. Our efforts led to the identification of new and more potent inhibitors. For example, compound **6g** has a K_i value of 180 nM binding to XIAP BIR3, in a competitive binding assay and represents a promising lead compound for further optimization.

Apoptosis, or programmed cell death, is a genetically regulated cell death mechanism.[1] Dysfunction of the apoptosis machinery plays a major role in many human diseases, including cancer. X-Linked inhibitor of apoptosis protein (XIAP) is a potent and effective cellular inhibitor of apoptosis.[2–5] XIAP has been found to be overexpressed in many human cancer cell lines.[6] XIAP is considered as a promising cancer therapeutic target because inhibition of XIAP can promote apoptosis in cancer cells with overexpression of XIAP and sensitize cancer cells to apoptosis induction.[7] One of the major cellular functions of XIAP is the inhibition of the activity of caspase-9 by binding to caspase-9 through its BIR3 domain and trapping caspase-9 in its inactive form.[8] Smac/DIABLO protein (second mitochondria-derived activator of caspase or direct IAP-binding protein with low pI) has been discovered as an endogenous cellular inhibitor of XIAP,[9,10] and promotes apoptosis in cells at least in part by binding to the BIR3 domain of XIAP where caspase-9 binds and relieving the inhibition of XIAP to caspase-9.[11] There is a strong research interest in the design of peptidomimetics and non-peptidic small-molecule inhibitors to target the XIAP BIR3 domain where Smac and caspase-9 bind.[12–20] Such small-molecule inhibitors are predicted to promote apoptosis in cancer cells and may have great therapeutic potential to be developed as an entirely new class of anticancer drugs.

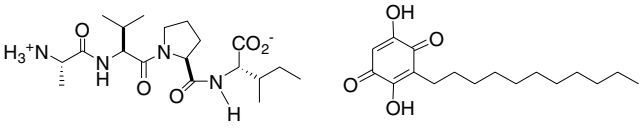

Smac AVPI Peptide — **1** (Embelin)

Through structure-based database searching, we have previously discovered embelin as a fairly potent, non-peptide, small-molecule inhibitor of XIAP.[20] Embelin was determined to bind to the XIAP BIR3 domain with a K_i value of 0.40 μM in our competitive fluorescence-polarization (FP)-based assay (Table 1). To the best of our knowledge, embelin is the only known class of non-peptide inhibitor that binds to the XIAP BIR3 domain, whose chemical structure is not related to the AVPI peptide in Smac. Hence, embelin represents a promising initial lead for optimization toward our ultimate goal of developing a new class of anticancer drugs to target XIAP. In this paper, we wish to report our design, synthesis, and biochemical evaluation of a series of new embelin analogues as inhibitors of XIAP.

Keywords: XIAP; Embelin; Small-molecule inhibitors.
* Corresponding author. Tel.: +1 734 615 0362; fax: +1 734 647 9647; e-mail: shaomeng@umich.edu

0960-894X/$ - see front matter © 2006 Elsevier Ltd. All rights reserved.
doi:10.1016/j.bmcl.2006.08.072

Table 1. Binding affinities to the XIAP BIR3 in an FP-based binding assay for **6a**–**g**

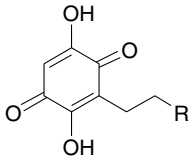

Compound	R	$K_i \pm$ SD (μM) FP-based binding assay
1	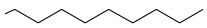	0.40 ± 0.13
6a	H	10.4 ± 1.3
6b	$-CH_2CH_2CH_2CH_2CH_2Me$	1.25 ± 0.9
6c	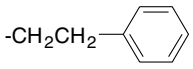	1.3 ± 0.3
6d		0.71 ± 0.17
6e	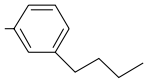	0.48 ± 0.3
6f	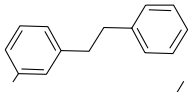	0.38 ± 0.09
6g	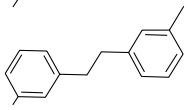	0.18 ± 0.09

Embelin consists of the dihydroxyquinone core and a long hydrophobic tail. Our modeling predicted that the hydrophilic dihydroxyquinone core forms a number of hydrogen bonds with XIAP and the hydrophobic tail interacts with the hydrophobic pocket where the isoleucine residues in the AVPI Smac peptide bind. In the present study, we have kept the dihydroxyquinone core intact and focused our modifications on the hydrophobic tail portion of the molecule.

A series of embelin analogues **6a**–**g** with different hydrophobic tails were designed and synthesized. The synthesis of compounds **6a**–**g** is shown in Scheme 1. Briefly, commercially available or easily prepared corresponding triphenylphosphonium bromide **2a**–**g** were treated with 1:1 equivalent of *n*-butyllithium, followed by reaction with aldehyde **3**, which was prepared according to a published method[21] and hydrogenation afforded the key intermediates **4a**–**g**. Oxidation of **4a**–**g** with ceric ammonium nitrate gave [1,2]benzoquinones **5a**–**g**.[22] The final target compounds **6a**–**g** were obtained by the treatment of **5a**–**g** with 70% perchloric acid and concentrated hydrochloric acid at room temperature for 48 h.[23]

Compounds **6a**–**g** were tested for their binding affinities to recombinant XIAP BIR3 protein using our established quantitative fluorescence-polarization (FP)-based competitive binding assay[24] and compared directly to embelin (**1**) and the AVPI Smac peptide. The results are summarized in Table 1. In our FP-based binding assay, embelin (**1**) and the Smac AVPI peptide were determined to have K_i values of 0.40 and 0.58 μM, respectively.

Compound **6a** was designed to test the importance of the $C_{11}H_{23}$ long hydrophobic tail, in which the $C_{11}H_{23}$ tail was replaced by a much shorter ethyl group. Our FP-based binding assay showed that compound **6a** has a K_i value of 10.4 μM to XIAP BIR3, thus 25 times less potent than embelin. This suggests that the $C_{11}H_{23}$ long hydrophobic tail is critical for the binding of embelin to XIAP BIR3. Based upon this result, we have designed and synthesized compound **6b** with an *n*-octyl side chain. Compound **6b** has a K_i value of 1.25 μM. Hence, although compound **6b** is 3 times less potent than embelin, it is 8 times more potent than compound **6a**, further confirming the importance of the long hydrophobic tail in the binding of embelin to XIAP BIR3.

The crystal and NMR structures of XIAP BIR3 in complex with Smac protein or peptide showed that the binding of Smac to XIAP BIR3 is mediated primarily by the AVPI four amino acid residues in Smac and a well-defined surface binding groove in XIAP BIR3.[25,26] While the alanine residue in the Smac AVPI-binding motif forms an extensive hydrogen bonding network with XIAP BIR3, the proline residue has hydrophobic contacts with Trp323 in XIAP. Our modeling suggested that the hydrophilic dihydroxyquinone core in embelin mimics the alanine residue in the Smac AVPI peptide to form a hydrogen bonding network. We have designed two new analogues, **6c** and **6d**, to explore whether a phenyl ring would be able to mimic the interaction between the proline ring in the Smac AVPI peptide and Trp323 in XIAP. As can be seen, while compound **6c** with a $(CH_2)_4$ linker between the dihydroxyquinone group and the phenyl ring has a K_i value of 1.3 μM, compound **6d** with a $(CH_2)_2$ linker has a K_i value of 0.71 μM. Hence, compound **6d** is 2 and 15 times more potent than **6c** and **6a**, respectively. Thus, we have made further modifications based upon compound **6d**.

The isoleucine residue in the Smac AVPI peptide binds to a hydrophobic pocket in XIAP BIR3 and plays an important role for their binding. Our modeling suggested that the long hydrophobic tail in embelin interacts with this hydrophobic pocket in XIAP. We have thus designed and synthesized a series of new analogues based upon compound **6d** in an attempt to capture the hydrophobic interaction between the isoleucine residue in the Smac AVPI peptide and the hydrophobic pocket in XIAP BIR3.

Compound **6e** with an *n*-butyl group attached to the *meta*-position on the phenyl ring in compound **6d** has a K_i value of 0.48 μM, which is slightly more potent than **6d**. Encouraged by this result, we replaced the *n*-butyl group with a phenylethyl group since it was previously shown that replacement of the isoleucine in the Smac

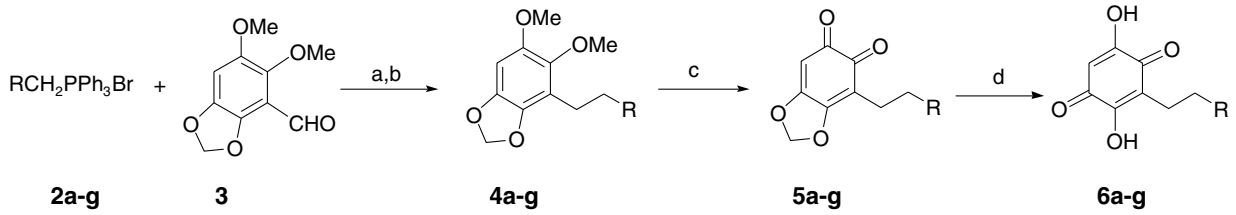

Scheme 1. Synthesis of compounds **6a**–**g**. Reagents and conditions: (a) *n*-BuLi, THF, 0 °C, 10 min; (b) H_2, 10% Pd–C, EtOAc, room temperature; (c) CAN, CH_3CN–H_2O, 0 °C, 1 h; (d) $HClO_4$, HCl, dioxane, room temperature, 48 h.

AVPI peptide by a phenylalanine residue increased the binding affinity of the resulting peptide.[27] This resulted in compound **6f**, which has a K_i value of 0.38 μM binding to XIAP and is as potent as embelin.

Compound **6g** was designed and synthesized to further explore the interaction between the terminal phenyl ring and XIAP by installation of a methyl group on the *meta*-position the binding affinity of the resulting peptide.[28] Compound **6g** has a K_i value of 0.18 μM and is thus 2 times more potent than embelin for binding to XIAP BIR3.

We have evaluated compound **6g** for its activity in inhibition of cell growth in the MDA-MB-231 (2LMP) human breast cancer line and the PC-3 human prostate cancer cell line. Both of these two cancer cell lines have high levels of XIAP (data not shown). The results are shown in Figure 1. As can be seen, compound **6g** is effective in inhibition of cell growth with IC_{50} values of 5.0 and 5.5 μM in the MDA-MB-231 and PC-3 cell lines, respectively.

In summary, embelin represents a novel class of non-peptide small-molecule inhibitor of XIAP. Our present study focused on the modifications of the hydrophobic tail in embelin. Our study yielded new inhibitors with binding affinities better than embelin and provided preliminary structure–activity relationship for this class of inhibitors. The most potent inhibitor **6g** binds to XIAP BIR3 with a K_i value of 180 nM. Importantly, **6g** is effective in inhibition of cell growth in human breast and prostate cancer cell lines with high levels of XIAP. Hence, compound **6g** represents a promising new lead compound for further optimization toward our ultimate goal of developing a new class of anticancer drugs by targeting XIAP and promoting apoptosis in cancer cells.

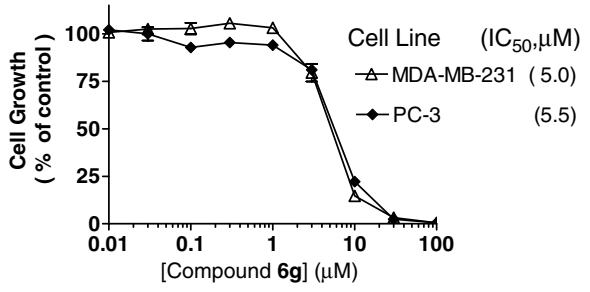

Figure 1. Inhibition of cell growth by compound **6g** in the MDA-MB-231 (2LMP) human breast cancer cell line and the PC-3 human prostate cancer cell line. Cells were treated by compound **6g** for 4 days and cell growth was determined using the WST assay.

Acknowledgments

We are grateful for the financial support from the Department of Defense Prostate Cancer Program (PC030410), the Susan G. Komen Foundation, and the National Cancer Institute, National Institutes of Health (R21CA104802).

References and notes

1. Lowe, S. W.; Lin, A. W. *Carcinogenesis* **2000**, *21*, 485.
2. Deveraux, Q. L.; Reed, J. C. *Genes Dev.* **1999**, *13*, 239.
3. LaCasse, E. C.; Baird, S.; Korneluk, R. G.; MacKenzie, A. E. *Oncogene* **1998**, *17*, 3247.
4. Kasof, G. M.; Gomes, B. C. *J. Biol. Chem.* **2001**, *276*, 3238.
5. Salvesen, G. S.; Duckett, C. S. *Nat. Rev. Mol. Cell Biol.* **2002**, *3*, 401.
6. Tamm, I.; Kornblau, S. M.; Segall, H.; Krajewski, S.; Welsh, K.; Kitada, S.; Scudiero, D. A.; Tudor, G.; Qui, Y. H.; Monks, A.; Andreeff, M.; Reed, J. C. *Clin. Cancer Res.* **2000**, *6*, 1796.
7. Holcik, M.; Gibson, H.; Korneluk, R. G. *Apoptosis* **2001**, *6*, 253.
8. Shiozaki, E. N.; Chai, J.; Rigotti, D. J.; Riedl, S. J.; Li, P.; Srinivasula, S. M.; Alnemri, E. S.; Fairman, R.; Shi, Y. *Mol. Cell* **2003**, *11*, 519.
9. Du, C.; Fang, M.; Li, Y.; Wang, X. *Cell* **2000**, *102*, 33.
10. Verhagen, A. M.; Ekert, P. G.; Pakusch, M.; Silke, J.; Connolly, L. M.; Reid, G. E.; Moritz, R. L.; Simpson, R. J.; Vaux, D. L. *Cell* **2000**, *102*, 43.
11. Shiozaki, E. N.; Shi, Y. *Trends Biochem. Sci.* **2004**, *29*, 486.
12. MacKenzle, A.; LaCasse, E. *Cell Death Differ.* **2000**, *7*, 866.
13. Fulda, S.; Wick, W.; Weller, M.; Debatin, K.-M. *Nat. Med.* **2002**, *8*, 808.
14. Arnt, C. R.; Chiorean, M. V.; Heldebrant, M. P.; Gores, G. J.; Kaufmann, S. H. *J. Biol. Chem.* **2002**, *277*, 44236.
15. Yang, L.; Mashima, T.; Sato, S.; Mochizuki, M.; Sakamoto, H.; Yamori, T.; Oh-Hara, T.; Tsuruo, T. *Cancer Res.* **2003**, *63*, 831.
16. Sun, H.; Nikolovska-Coleska, Z.; Yang, C.-Y.; Xu, L.; Liu, M.; Tomita, Y.; Pan, H.; Yoshioka, Y.; Krajewski, K.; Roller, P. P.; Wang, S. *J. Am. Chem. Soc.* **2004**, *126*, 6686.
17. Sun, H.; Nikolovska-Coleska, Z.; Yang, C.-Y.; Xu, L.; Tomita, Y.; Krajewski, K.; Roller, P. P.; Wang, S. *J. Med. Chem.* **2004**, *47*, 4147.

18. Oost, T. K.; Sun, C.; Armstrong, R. C.; Al-Assaad, A. S.; Betz, S. F.; Deckwerth, T. L.; Ding, H.; Elmore, S. W.; Meadows, R. P.; Olejniczak, E. T.; Oleksijew, A.; Oltersdorf, T.; Rosenberg, S. H.; Shoemaker, A. R.; Tomaselli, K. J.; Zou, H.; Fesik, S. W. *J. Med. Chem.* **2004**, *47*, 4417.
19. Li, L.; Thomas, R. M.; Suzuki, H.; De Brabander, J. K.; Wang, X.; Harran, P. G. *Science* **2004**, *305*, 1471.
20. Nikolovska-Coleska, Z.; Xu, L.; Hu, Z.; Tomita, Y.; Li, P.; Roller, P. P.; Wang, R.; Fang, X.; Guo, R.; Zhang, M.; Lippman, M. E.; Yang, D.; Wang, S. *J. Med. Chem.* **2004**, *47*, 2430.
21. Dallacker, F.; Sanders, G. *Chemiker-Zeitung* **1986**, *110*, 369.
22. Dallacker, F.; Lohnert, G. *Chem. Ber.* **1972**, *105*, 1586.
23. Dallacker, F.; Lohnert, G. *Chem. Ber.* **1972**, *105*, 614.
24. Nikolovska-Coleska, Z.; Wang, R.; Fang, X.; Pan, H.; Tomita, Y.; Li, P.; Roller, P. P.; Krajewski, K.; Saito, N.; Stuckey, J.; Wang, S. *Anal. Biochem.* **2004**, *15*, 261.
25. Wu, G.; Chai, J.; Suber, T. L.; Wu, J. W.; Du, C.; Wang, X.; Shi, Y. *Nature* **2000**, *408*, 1008.
26. Liu, Z.; Sun, C.; Olejniczak, E. T.; Meadows, R.; Betz, S. F.; Oost, T.; Herrmann, J.; Wu, J. C.; Fesik, S. W. *Nature* **2000**, *408*, 1004.
27. Kipp, R. A.; Case, M. A.; Wist, A. D.; Cresson, C. M.; Carrell, M.; Griner, E.; Wiita, A.; Albiniak, P. A.; Chai, J.; Shi, Y.; Semmelhack, M. F.; McLendon, G. L. *Biochemistry* **2002**, *41*, 7344.
28. NMR and elemental analysis data for compound **6g** (2,5-dihydroxy-3-{2-[3-(2-*m*-tolyl-ethyl)-phenyl]-ethyl}-[1,4]benzoquinone). ^{1}H NMR (300 MHz, $CDCl_3$) δ 7.67 (br s, 2H), 7.27–7.14 (m, 2H), 7.12–6.97 (m, 6H), 6.05 (s, 1H), 2.88 (s, 4H), 2.78 (s, 4H), 2.35 (s, 3H); ^{13}C NMR (75 MHz, $CDCl_3$) δ 142.1, 141.8, 141.1, 137.9, 129.2, 128.6, 128.4, 128.2, 126.6, 126.3, 126.0, 125.4, 115.9, 102.3, 38.0, 33.8, 24.6, 21.4; Anal. Calcd for $C_{23}H_{22}O_4$: C, 76.22; H, 6.12. Found: C, 75.88; H, 5.95.

J|A|C|S
Journal of the American Chemical Society

Published by
The American Chemical Society

Alanna Schepartz, *Associate Editor*

Department of Chemistry
Yale University
P.O. Box 208107
New Haven, CT 06520

Office: (203) 432-6052
Fax: (203) 432-7496
Email: JACS@yale.edu
http://pubs.acs.org/jacs

28 August 2007

Manuscript Number: JA074725F
Title: "Design, Synthesis and Characterization of A Potent, Non-Peptide, Cell-Permeable, Bivalent Smac Mimetic that Concurrently Targets both the BIR2 and BIR3 Domains in XIAP"

Dear Dr. Wang:

We are pleased to inform you that your manuscript has been accepted for publication in the *Journal of the American Chemical Society*, and we have forwarded your manuscript to the ACS Publication office.

You will be contacted in the near future by the ACS Journal Publishing Staff regarding the page proofs for your manuscript. Your paper will be published on the web approximately 48 hours after you approve these proofs. In view of this fast publication time, it is important to review your page proofs carefully. Once a manuscript appears on the web, it is published, and any change after that point must be considered as an addition or correction to the final publication.

Once again, congratulations!

Sincerely,

Alanna Schepartz
Associate Editor
Milton Harris '29 Ph. D. Professor of Chemistry
Professor of Molecular, Cellular, and Developmental Biology

Design, Synthesis and Characterization of A Potent, Non-Peptide, Cell-Permeable, Bivalent Smac Mimetic that Concurrently Targets both the BIR2 and BIR3 Domains in XIAP

*Haiying Sun[+], Zaneta Nikolovska-Coleska[+], Jianfeng Lu[+], Jennifer L. Meagher[∃], Chao-Yie Yang[+], Su Qiu[+], York Tomita[¶], Yumi Ueda[¶], Sheng Jiang[#], Krzysztof Krajewski[#], Peter P. Roller[#], Jeanne A. Stuckey[∃†], and Shaomeng Wang[+]**

[+]Departments of Internal Medicine, Pharmacology and Medicinal Chemistry and Comprehensive Cancer Center, [∃]Life Sciences Institute, and [†] Biological Chemistry, Biophysics Research Division, University of Michigan, 1500 E. Medical Center Drive, Ann Arbor, MI 48109, USA; [¶]Lombardi Cancer Center, Georgetown University Medical Center, Washington DC 20007, USA; [#]Laboratory of Medicinal Chemistry, National Cancer Institute-Frederick, NIH, Frederick, Maryland 21702, USA.

RECEIVED DATE (automatically inserted by publisher); shaomeng@med.umich.edu

Running Title: A Novel, Non-peptide, Bivalent Smac Mimetic as a Potent Antagonist of XIAP

CORRESPONDING AUTHOR: Shaomeng Wang, Phone: (734) 615-0362; Fax: (734) 647-9647; Email: shaomeng@umich.edu

ABSTRACT. XIAP is a central apoptosis regulator that inhibits apoptosis by binding to and inhibiting the effectors caspase-3/-7 and an initiator caspase-9 through its BIR2 and BIR3 domains, respectively. Smac protein in its dimeric form effectively antagonizes XIAP by concurrently targeting both its BIR2 and BIR3 domains. We report the design, synthesis and characterization of a non-peptide, cell-permeable, bivalent small-molecule (SM-164) which mimics Smac protein for targeting XIAP. Our study shows that SM-164 binds to XIAP containing both BIR domains with an IC_{50} value of 1.39 nM, being 300 and 7000-times more potent than its monovalent counterparts and the natural Smac AVPI peptide, respectively. SM-164 concurrently interacts with both BIR domains in XIAP and functions as an ultra-potent antagonist of XIAP in both cell-free functional and cell-based assays. SM-164 targets cellular XIAP and effectively induces apoptosis at concentrations as low as 1 nM in leukemia cancer cells, while having a minimal toxicity to normal human primary cells at 10,000 nM. The potency of bivalent SM-164 in binding, functional and cellular assays is 2-3 orders of magnitude higher than its corresponding monovalent Smac mimetics.

TOC Graphics

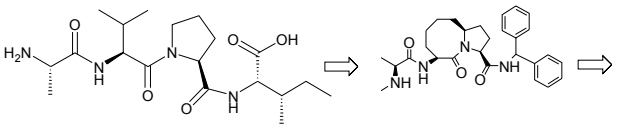

Smac AVPI Peptide (IC_{50} =10,396 nM) **1** (Monovalent Smac Mimetic, IC_{50} = 438 nM)

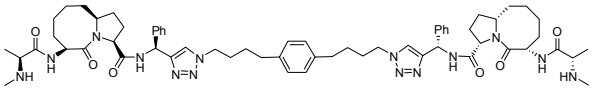

4 (Bivalent Smac Mimetic, IC_{50} = 1.39 nM)

Introduction:

Apoptosis, or programmed cell death, is a critical cell process in normal development and homeostasis of multicellular organisms. Inappropriate regulation of apoptosis has been implicated in many human diseases, including cancer.[1-3] It is now recognized that dysfunction of the apoptosis machinery is a hallmark of cancer.[2] Accordingly, targeting critical apoptosis regulators is an attractive approach for the development of new classes of therapies for the treatment of cancer and other human diseases.[1-3]

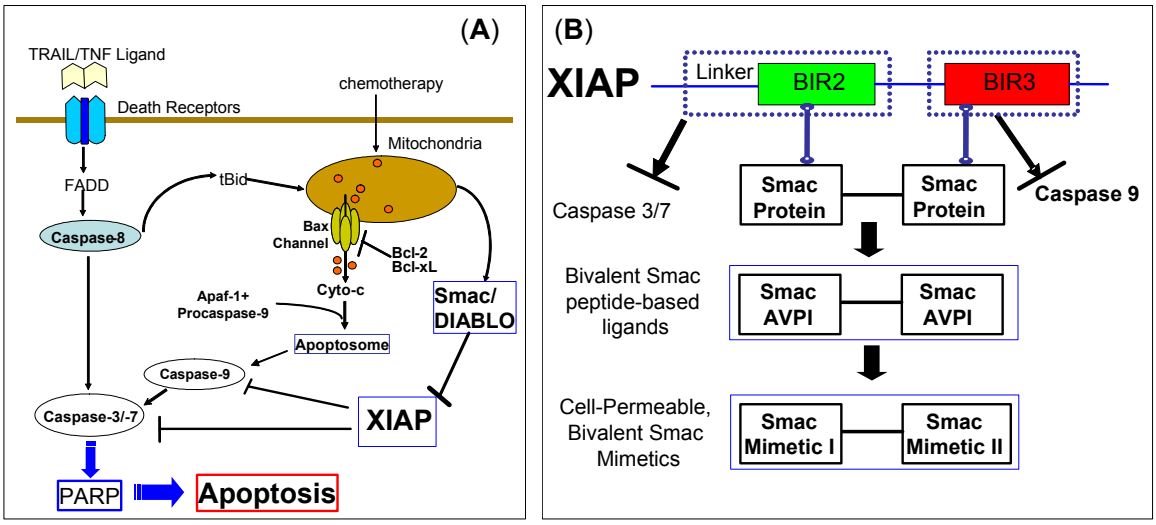

Figure 1. (**A**). A schematic, simplified apoptosis pathway. XIAP inhibits apoptosis by directly binding to and inhibition of caspase-9, caspase-3 and -7. Smac protein binds to XIAP and antagonizes XIAP to promote activation of caspases and apoptosis. (**B**). Design of bivalent Smac mimetics to target both the BIR2 and BIR3 domains of XIAP by mimicking the binding of dimeric Smac protein.

The X-linked inhibitor of apoptosis protein (XIAP) is a member of IAP proteins and a central apoptosis regulator, although its role may not be limited to the regulation of apoptosis.[5,6] XIAP potently inhibits apoptosis by directly binding to and effectively inhibiting three members of caspases, the two effectors, caspase-3 and -7, and an initiator, caspase-9 (**Figure 1A**), whose activity is critical for execution of apoptosis. XIAP contains three baculovirus IAP repeat (BIR) domains. The third BIR domain (BIR3) of XIAP selectively targets caspase-9, whereas the BIR2 domain, together with the linker preceding BIR2, inhibits both caspase-3 and caspase-7 (**Figure 1B**).[5] Consistent with its potent apoptosis-suppressing function, XIAP is found to be highly expressed in many human tumor cell lines

and tumor samples from patients[6] and plays an important role in conferring resistance on cancer cells to a variety of anticancer drugs.[7]

In cells, the anti-apoptotic function of XIAP is antagonized by Smac/DIABLO (second mitochondria-derived activator of caspases or direct IAP binding protein with low pI) (**Figure 1A**).[8,9] Smac/DIABLO has been identified as a protein released from mitochondria into the cytosol in response to apoptotic stimuli.[8,9] It forms an elongated dimer[10] and targets both the BIR2 and BIR3 domains in XIAP (**Figure 1B**).[11] It removes the XIAP inhibition of caspase-9 by binding to the BIR3 domain in XIAP through its AVPI tetrapeptide binding motif and directly competing with a similar ATPF tetrapeptide in the processed caspase-9 (**Figure 1B**).[11-15] Conclusive understanding of the mechanism by which Smac removes the inhibition of XIAP to caspase-3/-7 remains elusive.[11] Crystal structures[16-18] show that the linker preceding BIR2 in XIAP binds to caspase-3/-7 and is the major energetic determinant, while the BIR2 domain itself plays a regulatory role. Modeling suggests that Smac protein also binds to XIAP BIR2 through its AVPI motif and prevents the binding of XIAP to caspase-3/-7.[16-19] In this manner, dimeric Smac protein effectively removes the inhibition of XIAP to caspase-9 and to caspase-3/-7 by concurrently targeting both the BIR2 and BIR3 domains in XIAP (**Figure 1B**).[19]

Because XIAP blocks apoptosis at the down-stream effector phase, a point where multiple signaling pathways converge, it represents a particularly attractive molecular target for the design of new classes of anticancer drugs aimed at overcoming the apoptosis resistance of cancer cells.[7] To date, a number of research laboratories, including ours, have pursued the design of small-molecule antagonists of XIAP.[20-28] One approach focuses on the design of small molecules that target the XIAP BIR3 domain, antagonizing the inhibition of XIAP to caspase-9.[20-25] These efforts have so far yielded small-molecules that bind to the XIAP BIR3 domain with high affinities. A number of these compounds are effective in inhibition of cell growth and induction of apoptosis in cancer cells.[20-25] Another approach is to design small-molecule inhibitors that target the BIR2 domain, blocking the interaction of XIAP with caspase-3/-7.[26,27] For example, polyurea compounds that target the caspase-3/XIAP interaction have

been shown to achieve broad anticancer activity and are synergistic when used in combination with chemotherapeutic agents.[27] Collectively, these studies have provided convincing evidence that targeting XIAP is an effective strategy to overcome the apoptosis resistance of cancer cells.

Since both the BIR2 and BIR3 domains in XIAP effectively suppress apoptosis by targeting caspase-3/-7 and caspase-9 respectively, we reason that bivalent small molecules which concurrently interact with both BIR domains could be particularly efficient and potent XIAP antagonists (**Figure 1B**). Indeed, a small-molecule mimic containing two Smac AVPI binding motifs was shown to antagonize XIAP with a potency exceeding that of Smac protein in a cell-free functional assay and to enhance apoptosis induction of other therapeutic agents in cancer cells.[28] It was proposed[28] that its high potency as an XIAP antagonist is attributable to its bivalency, but its precise mode of action in targeting XIAP remains unclear.

In this study, we present the structure-based design, synthesis and detailed characterization of a novel, non-peptidic, bivalent small-molecule (SM-164) using a series of complementary biochemical, functional and cellular assays. We demonstrate that SM-164 concurrently targets the BIR2 and BIR3 domains in the same XIAP molecule, achieves an extremely high binding affinity to XIAP, and functions as an ultra-potent antagonist of XIAP in cell-free functional and cellular assays. It binds potently to cellular XIAP and effectively induces apoptosis in leukemia cancer cells at concentrations as low as 1 nM. Importantly, SM-164 has minimal toxicity to normal human primary cells at concentrations as high as 10,000 nM. Its potency in binding, functional and cellular assays is 2-3 orders of magnitude higher than its corresponding monovalent Smac mimetics.

Results:

Design of a cell-permeable monovalent Smac mimetic

Smac protein binds to both the BIR2 and BIR3 in XIAP *via* its AVPI binding motif.[11] It was shown[13] that short Smac-based peptides containing the AVPI sequence bind to recombinant XIAP BIR3 and BIR2 proteins with K_d values of 0.4-0.7 μM and 6-9 μM, respectively. The Smac-based AVPI peptide thus provides a suitable template for the design of bivalent small molecules that can concurrently interact with both the BIR2 and BIR3 domains. Unfortunately, Smac-based peptides are not cell-permeable. Thus, for the design of cell-permeable, bivalent Smac mimetics, it was essential to first derive cell-permeable, monovalent Smac mimetics that can bind to both XIAP BIR2 and BIR3 with good affinities.

We have employed a structure-based strategy to design potent, cell-permeable, small molecules (monovalent Smac mimetics) that mimic the Smac AVPI binding motif, although our initial purpose was to target the XIAP BIR3 domain.[21-23] Using this approach, we have designed compound **1** (SM-122) as a conformationally constrained, Smac AVPI mimetic containing a [8,5] bicyclic system (**Figure 2**) and evaluated its binding affinities to XIAP BIR2 and BIR3 proteins. To facilitate the investigation of the molecular mechanism of action for Smac mimetics, we have also designed a biotinylated analogue of SM-122 (**2**, named BL-SM-122, **Figure 2**).

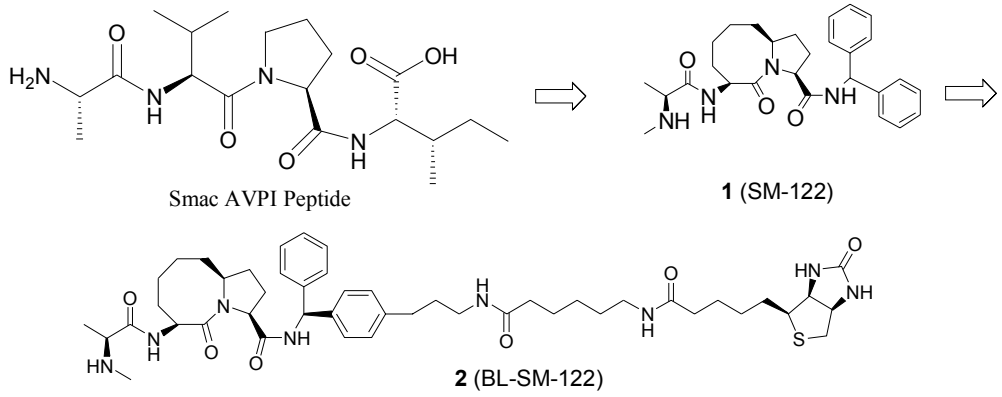

Figure 2. Design of a potent, conformationally constrained, monovalent Smac mimetic SM-122 and its biotinylated analogue.

The binding affinities of compounds **1**, **2** and the Smac AVPI peptide to the XIAP BIR3 domain protein were evaluated using a previously established sensitive fluorescence-polarization (FP) assay (**Figure 3**).[29] Compound **1** binds to XIAP BIR3 protein with an IC_{50} value of 91 nM. Its biotinylated analogue **2** has an IC_{50} value of 112 nM, very close to that of compound **1**, indicating that the biotin label does not have a significant effect on the binding of compound **1** to XIAP BIR3 protein. In comparison, the Smac AVPI peptide has an IC_{50} value of 1,183 nM and its calculated K_i value is 425 nM, similar to the reported K_d value for this peptide.[30] Therefore, compound **1** binds to XIAP BIR3 with an affinity 13-times higher than that of the Smac AVPI peptide.

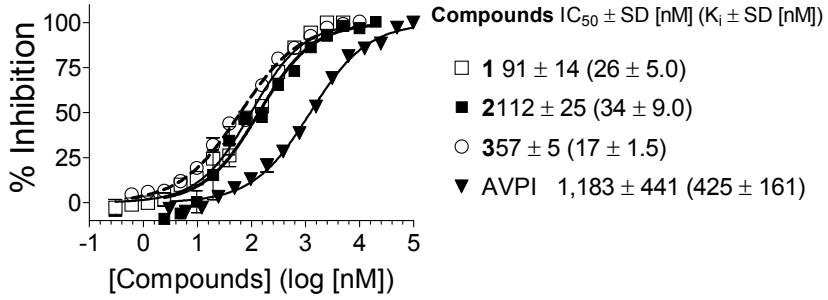

Figure 3. Competitive binding of our designed monovalent Smac mimetics **1**, **2**, **3** and the AVPI peptide to XIAP BIR3 (residues 240-356) as determined using an FP-based assay.

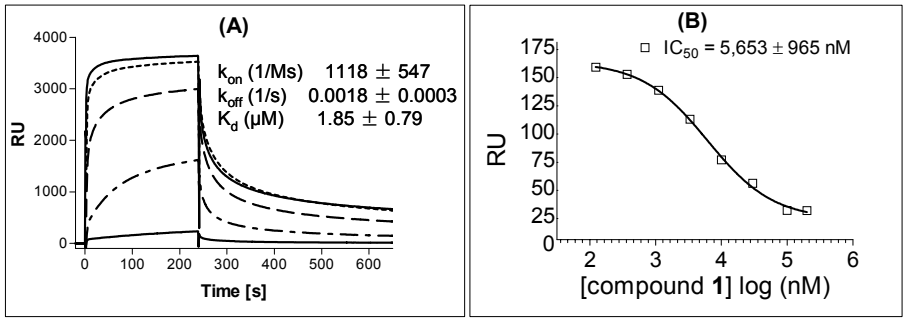

Figure 4. (A). Analysis of the binding of biotin-labeled compound **2** to XIAP L-BIR2 protein (residues 120-240) using the Biacore surface plasmon resonance (SPR) technique with different concentrations of the protein (from the top: 50, 25, 12.5, 6.25 and 3.125 μM). (B) Competitive binding of compound **1** to XIAP L-BIR2 as determined using the Biacore SPR technique. Biotinylated SM-122-BL was immobilized on the streptavidin chip.

We next evaluated the binding affinity of SM-122 (**1**) to XIAP BIR2. For this purpose, we attempted to develop an FP assay for XIAP BIR2, similar to that for XIAP BIR3.[29] Unfortunately, the

fluorescently labeled Smac-based peptide tracer we used previously to establish the competitive binding FP assay for XIAP BIR3 domain[29] has a low binding affinity to XIAP BIR2, and is unsuitable as a tracer for the development of an FP assay for XIAP BIR2. To address this limitation, we employed the Biacore surface plasmon resonance (SPR) technique to directly evaluate the binding affinity of biotinylated compound **2** to XIAP BIR2 protein with compound **2** immobilized on the streptavidin chip. Our analysis showed that compound **2** binds to XIAP BIR2 with a K_d value of 1.85 μM (K_{on} = 1118 1/Ms and K_{off} = 0.0018 1/s) (Figure 4A). We next evaluated compound **1** for its binding to XIAP BIR2 in a competitive SPR assay with biotinylated compound **2** immobilized on the streptavidin chip and XIAP BIR2 protein and compound **1** in the mobile phase. Our results showed that compound **1** blocks the binding of XIAP BIR2 to compound **2** in a dose-dependent manner and has an IC_{50} value of 5.6 μM (Figure 4B). Therefore, our SPR experiments showed that both compounds **1** and **2** bind to XIAP BIR2 with a good affinity.

Our FP and SPR assays showed that compound **1** binds to XIAP BIR2 and BIR3 proteins with good affinities. Importantly, as will be demonstrated later in the paper, compound **1** effectively inhibits cell growth and induces apoptosis in cancer cells, indicative of its excellent cell permeability. Hence, compound **1** represents a promising monovalent Smac mimetic template for the design of bivalent Smac mimetics to target concurrently the BIR2 and BIR3 domains.

Design of bivalent Smac mimetics

We next identified suitable sites in compound **1** for chemically tethering two molecules together for the design of bivalent Smac mimetics. For this purpose, we employed computational modeling to predict the binding of **1** to BIR2 and BIR3 domains of XIAP using high-resolution crystal structures of these individual domains.[12,18] The predicted binding models (Figure 5) showed that one phenyl group of **1** in the pro-(*S*) configuration does not insert into the binding pocket of either BIR2 or BIR3 and consequently is exposed, making this phenyl ring suitable as an anchoring site for tethering two molecules of **1** together to produce bivalent Smac mimetics.

Modeling also suggested that the pro-(*S*) phenyl group in **1** may be replaced by other aromatic rings without compromising the binding. Thus, compound **3** was designed and synthesized to test if the pro-(*S*) phenyl group can be replaced by a [1,2,3]-triazole so that the "click chemistry," a highly efficient coupling method[31], can be readily applied to facilitate the synthesis of bivalent Smac mimetics (Figure 6). Consistent with our modeling prediction, compound **3** was determined to bind to XIAP BIR3 with an IC_{50} value of 57 nM, essentially the same as that of compound **1** (91 nM) (Figure 3). In addition, compound **3** was also shown to bind to XIAP BIR2 with the same affinity as that of compound **1** in our SPR assay (data not shown). Thus, compounds **1** and **3** have similar binding affinities to either BIR2 or BIR3 domain.

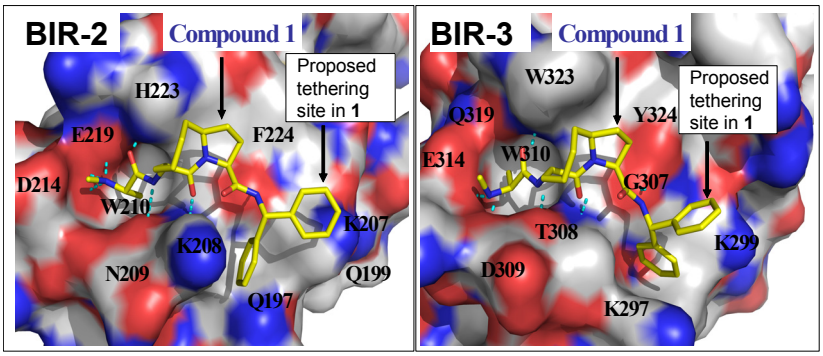

Figure 5. Predicted binding model of Smac mimetic **1** in complex with (**A**) XIAP BIR2 domain and (**B**) BIR3 domain.

The experimentally determined three-dimensional structure of XIAP containing both BIR2 and BIR3 domains has not been reported but our modeling analysis showed that the linker region between BIR2 and BIR3 containing approximately 25 residues is quite flexible. Accordingly, we designed a bivalent Smac mimetic SM-164 (**4**, **Figure 6**), which contains two monovalent Smac mimetics tethered together through a flexible linker which when extended, provides a distance of approximately 15 Å between the two triazole rings. We reasoned that such a linker would provide sufficient length and flexibility for the two monovalent binding units in **3** to bind concurrently to both the BIR2 and BIR3 domains in the same XIAP molecule. Based upon our predicted binding models for compound **1** (Figure 5), the methyl group in **1** inserts into a small hydrophobic cavity in both BIR2 and BIR3 and the *N*-methyl amino group participates in a hydrogen-bonding network with protein residues in both models.

To confirm our predicted binding models and to determine the specificity of bivalent Smac mimetic **4,** compound **5** was designed as an inactive control (Figure 6). In **5**, the methyl group in each monovalent binding unit was replaced by a (1*H*-indolyl)-methyl group, a much larger hydrophobic group, to disrupt the hydrophobic interactions at this site and the methylamino group was replaced by an acetamido group to block the hydrogen bond formation. To test if the stereospecificity is critical for binding, compound **6**, a stereoisomer of **4**, was designed and synthesized.

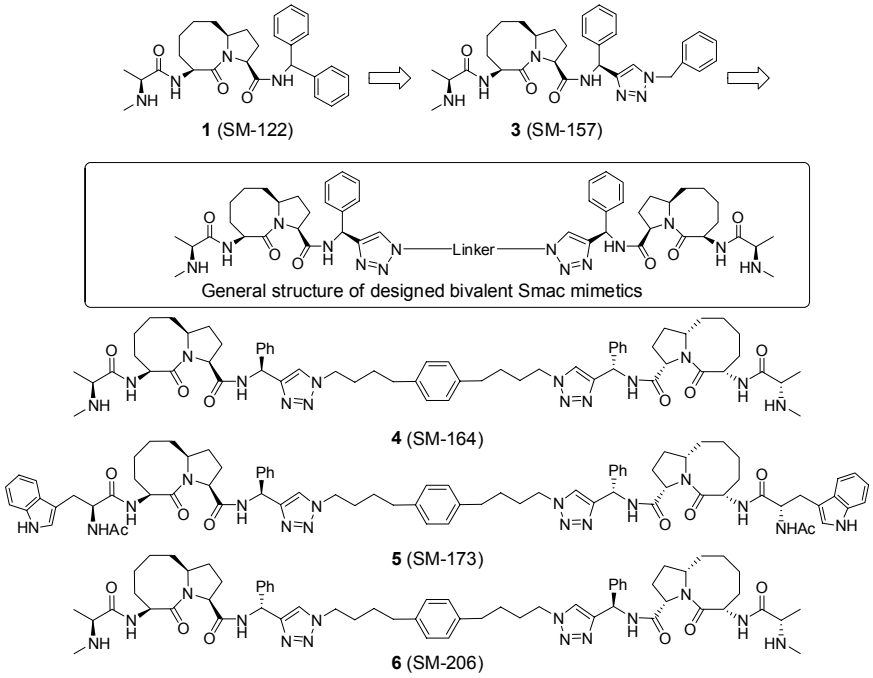

Figure 6. Design of a new class of bivalent Smac mimetics based upon a conformationally constrained monovalent Smac mimetic.

Chemistry

The synthesis of compound **1** is shown in Scheme 1. The key intermediate **8** was synthesized from pyroglutamic acid **7** in eight steps according to a reported method.[32] Hydrogenation of the double bond in **8** catalyzed by 10% Pd-C, followed by hydrolysis of the methyl ester gave the acid **9**. Condensation of **9** with aminodiphenylmethane followed by removal of the Boc protecting group yielded an ammonium salt, condensation of which with Boc-N-methyl-*L*-alanine furnished an amide. Removal of the Boc protecting group from this amide afforded compound **1** (SM-122).

The synthesis of SM-157 (**3**) is shown in Scheme 2. The chiral amine **11** was prepared according

to a reported method from the alcohol **10** in five steps.[33] Condensation of acid **9** with amine **11** gave an amide **12**. After removal of the Boc protecting group, the resulting ammonium salt was condensed with Boc-*N*-methyl-*L*-alanine to afford amide **13**. Cycloaddition of **13** with azidomethylbenzene catalyzed by $CuSO_4$-(+)-sodium-*L*-ascorbate yielded a triazole.[31] Removal of the Boc protecting group from this triazole furnished compound **3** (SM-157).

Scheme 1. Synthesis of compound **1**

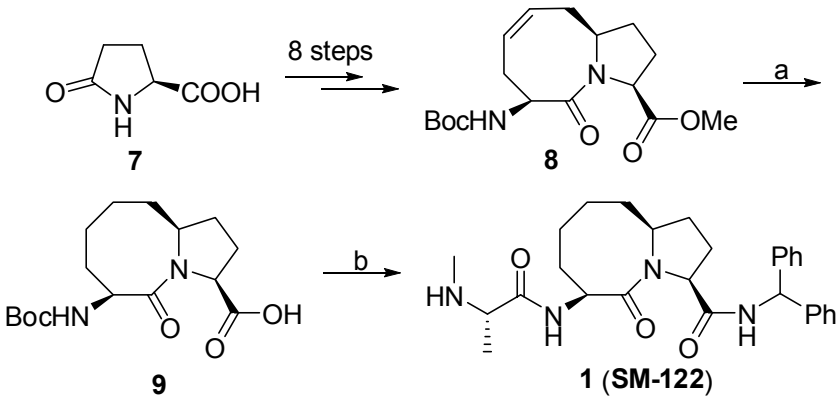

Reagents and Conditions: (a) i. 10% Pd-C, H_2, MeOH; ii. 2N LiOH, 1,4-dioxane, then 1N HCl, 96% over two steps; (b) i. aminodiphenylmethane, EDC, HOBt, N,N-diisopropylethylamine, CH_2Cl_2, overnight; ii. 4N HCl in 1,4-dioxane, MeOH; iii. Boc-N-methyl-L-alanine, EDC, HOBt, N,N-diisopropylethylamine, CH_2Cl_2; iv. 4N HCl in 1,4-dioxane, MeOH, 72% over four steps.

Scheme 2. Synthesis of compound **3**.

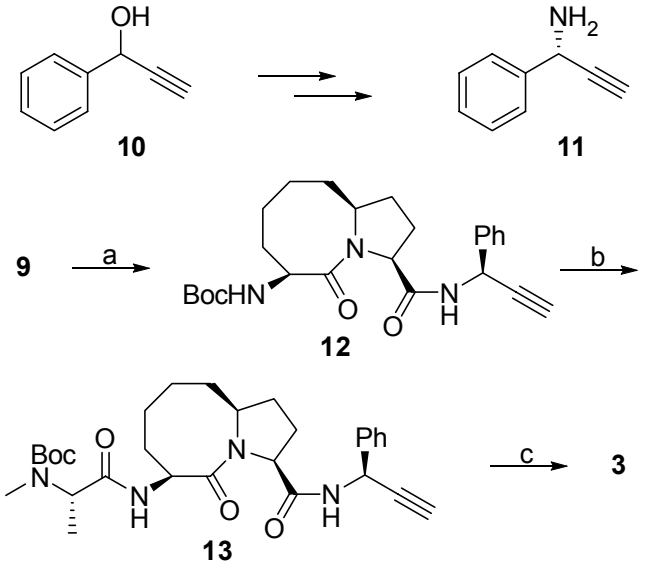

Reagents and conditions: (a) **11**, EDC, HOBt, N,N-diisopropylethylamine, CH_2Cl_2, overnight, 91%; (b) i. 4 N HCl in 1,4-dioxane, MeOH; ii. Boc-N-methyl-L-alanine, EDC, HOBt, N,N-diisopropylethylamine, CH_2Cl_2, 86% over two steps; (c) i. azidomethylbenzene, $CuSO_4$, (+)-sodium -L-ascorbate, *tert*-butanol - H_2O 2:1; ii. 4 N HCl in 1,4-dioxane, MeOH, 74% over two steps.

The synthesis of the bivalent compounds **4** (SM-164), **5** (SM-173) and **6** (SM-206) is shown in Scheme 3. The chiral amine **14** was prepared according to a reported method.[33] Compound **15** was synthesized with the same method as that used for compound **13**. Removal of the Boc protecting group in **12** followed by condensation of the resulting ammonium salt with *L*-Nα-Boc-Trp yielded an amide. Removal of the two Boc protecting group in this amide followed by condensation of the resulting salt with acetic anhydride provided compound **16**. Cycloaddition of 2 eq of compound **13** or **15** with 1 eq of 1,4-bis-(4-azidobutyl)-benzene respectively under the catalysis of $CuSO_4$-(+)-sodium-L-ascorbate gave two bis-triazoles.[31] Removal of the two Boc protecting groups in these bis-triazoles yielded compounds **4** and **6**, respectively. Cycloaddition of 2 eq of compound **16** with 1 eq of 1,4-bis-(4-azido-butyl)-benzene catalyzed by $CuSO_4$-(+)-sodium-*L*-ascorbate gave compound **5**.[31]

Scheme 3. Synthesis of compounds **4**, **5** and **6.**

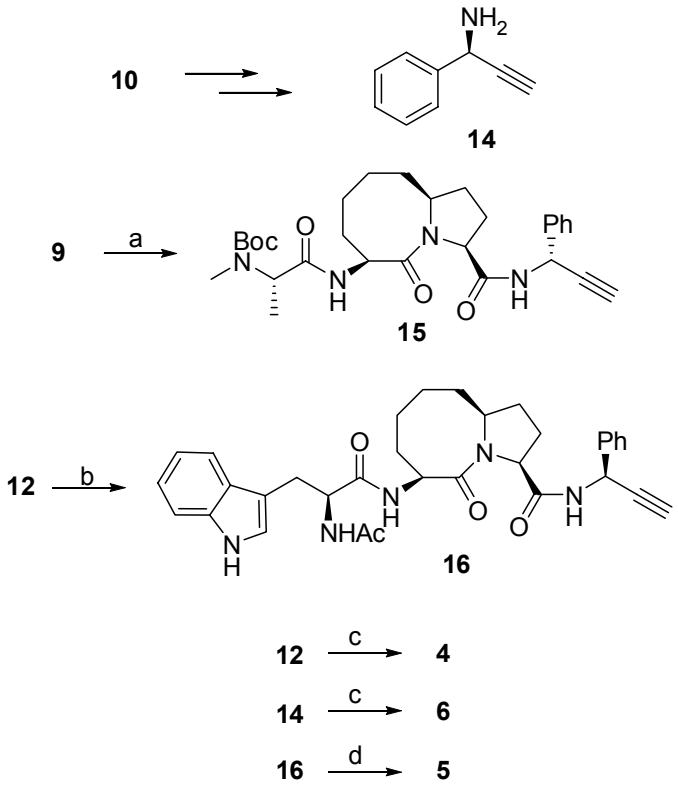

Reagents and conditions: (a) i. **14**, EDC, HOBt, *N,N*-diisopropylethylamine, CH_2Cl_2, overnight; ii. 4 N HCl in 1,4-dioxane, MeOH; iii. Boc-*N*-methyl-L-alanine, EDC, HOBt, *N,N*-diisopropylethylamine, CH_2Cl_2, 73% over three steps; (b) i. 4 N HCl in 1,4-dioxane; ii. N-Boc-L-Trp, EDC, HOBt, *N,N*-diisopropylethylamine, CH_2Cl_2; iii. 4 N HCl in 1,4-dioxane, MeOH, iv. acetic anhydride, N,N-diisopropylethylamine, CH_2Cl_2, 67% over four steps; (c) i. 1,4-bis-(4-azido-butyl)-benzene, $CuSO_4$, (+)-sodium -L-ascorbate, *tert*-butanol - H_2O 2:1; ii. 4 N HCl in 1,4-dioxane, MeOH, 68% for **4** and 66% for **6**; (d) 1,4-bis-(4-azido-butyl)-benzene, $CuSO_4$, (+)-sodium -L-ascorbate, *tert*-butanol - H_2O 2:1, 76%.

The synthesis of biotinylated compound **2** (BL-SM-122) is shown in Scheme 4. The chiral amine **18** was synthesized according to our reported method.[34] Condensation of acid **9** with **18** followed by removal of the Boc protecting group and condensation of the resulting ammonium salt with *L*-*N*-Boc-*N*-methyl-alanine yielded an amide. Cleavage of the Cbz protecting group in this amide by hydrogenation followed by condensation of the resulting amine with Cbz-6-aminohexanoic acid provided amide **19**. Removal of the Cbz protecting group in this amide (**19**) followed by condensation with (+)-biotin *N*-hydroxy-succinimide ester furnished a biotinylated amide. Removal of the Boc protecting group in the amide gave our designed biotinylated compound **2** (BL-SM-122).

Scheme 4. Synthesis of compound **2** (BL-SM-122)

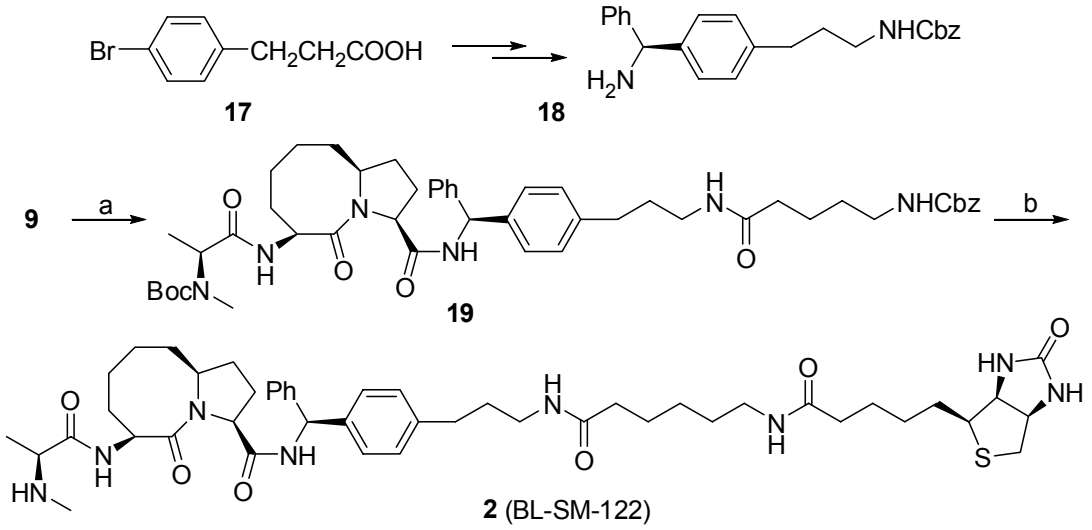

Reagents and conditions: (a) i. **18**, EDC, HOBt, *N,N*-diisopropylethylamine, CH_2Cl_2, overnight; ii. 4 N HCl in 1,4-dioxane, MeOH; iii. Boc-*N*-methyl-L-alanine, EDC, HOBt, *N,N*-diisopropylethylamine, CH_2Cl_2; iv. H_2, 10% Pd-C, MeOH; v. Cbz-6-aminohexanoic acid, EDC, HOBt, *N,N*-diisopropylethylamine, CH_2Cl_2, 42% over five steps; (b). i. H_2, 10% Pd-C, MeOH; ii. (+)-biotin N-hydroxy-succinimide ester, *N,N*-diisopropylethylamine, CH_2Cl_2; iii. 4 N HCl in 1,4-dioxane, MeOH, 74% over three steps.

Design of a fluorescently tagged, bivalent Smac peptide and development of a competitive binding assay to XIAP containing BIR2 and BIR3 domains

To evaluate accurately the binding affinities of our designed bivalent Smac mimetics, it was critical to develop a sensitive and reliable binding assay for XIAP containing both BIR2 and BIR3 domains. For this purpose, we designed and synthesized a fluorescently tagged Smac-based peptide,

Smac-1F (**Figure 7**), which contains two basic binding units (AKPF) chemically tethered through two lysines by a flexible linker. This design was based upon a biochemical study,[30] which showed that the second residue (valine) in the Smac AVPI peptide can be replaced by a lysine and the fourth residue by a phenylalanine to yield new peptides with a better binding affinity than the original Smac AVPI peptide to XIAP BIR3. Saturation experiments determined that Smac-1F binds to L-BIR2-BIR3 (residues 120-356) with a K_d value of 2.3 nM (**Figure 7**). We further determined that the linker preceding BIR2 does not contribute to the binding to Smac-1F.[35] Our extensive investigations conclusively showed that Smac-1F indeed interacts with both BIR2 and BIR3 domains simutaneously in XIAP.[35] Using Smac-1F and XIAP L-BIR2-BIR3 protein, we have established a competitive fluorescence-polarization (FP) assay to determine quantitatively the binding affinities of our designed Smac mimetics to XIAP containing both BIR2 and BIR3 domains.

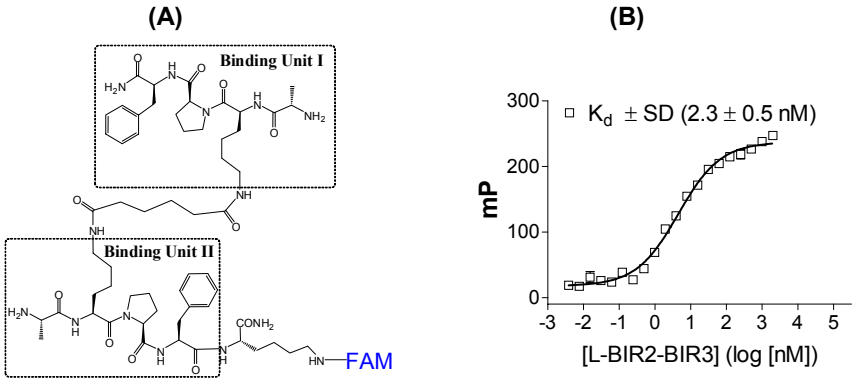

Figure 7. (A). Chemical structure of Smac-1F, a bivalent Smac-based peptide labeled with a fluorescence probe. (B). Saturation curve of XIAP (residues 120-356) containing both BIR2 and BIR3 domains to Smac-1F.

Quantitative determination of the binding affinities of designed Smac mimetics to XIAP protein

The binding affinities of compounds **1**, **3**, **4**, **5**, **6** and the Smac AVPI peptide to XIAP L-BIR2-BIR3 protein were determined in a competitive FP assay using Smac-1F as the tracer (**Figure 8**). Compounds **1**, **3**, **4**, **6** and the Smac AVPI peptide bind to XIAP with IC_{50} values of 438, 376, 1.39, 71.5 and 10,396 nM, respectively, whereas the designed inactive control **5** shows no appreciable binding at

100 μM. Hence, the bivalent Smac mimetic **4** is 271-351 times more potent than the monovalent compounds **1** and **3** and >7,000 times more potent than the Smac AVPI peptide, respectively. The stereoisomer **6** is 51-times less potent than compound **4**, confirming the importance of the stereospecificity. There was no significant difference with binding affinities for each of these Smac mimetics when either XIAP L-BIR2-BIR3 or BIR2-BIR3 protein (residues 156-356) was used in the binding assays (data not shown), indicating that the linker preceding BIR2 domain does not interact with these Smac mimetics. Our binding data demonstrate that the designed bivalent Smac mimetic **4** achieves an extremely high binding affinity to XIAP proteins containing both BIR2 and BIR3 domains and is much more potent than monovalent Smac mimetics **1** and **2** and the natural Smac AVPI peptide.

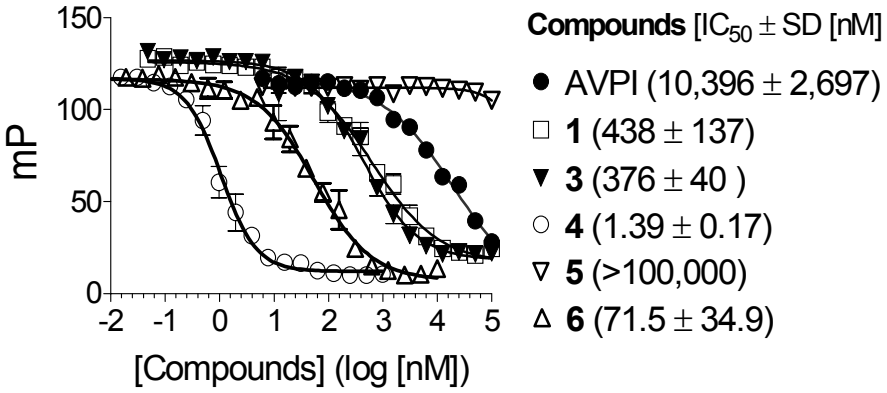

Figure 8. Competitive binding of Smac mimetics to XIAP protein (residues 120-356) containing BIR2 and BIR3 domains determined in a competitive FP-based assay.

Probing the binding modes of Smac mimetics to XIAP proteins by analytical gel filtration

Although compound **4** was designed to target both the BIR2 and BIR3 domains in XIAP simultaneously, it was unclear if this is indeed happening. To probe the binding mode of **1**, **3** and **4** to XIAP, we performed analytical gel filtration experiments using recombinant XIAP BIR3 (residues 241-356) and BIR2-BIR3 (residues 156-356) proteins (**Figure 9**). The BIR2-BIR3 protein without the linker preceding the BIR2 domain was used because this protein has a better solubility than the L-BIR2-BIR3

protein and compound **4** binds to these two proteins with the same affinities in our FP binding assay.

When the recombinant XIAP protein containing only the BIR3 domain was used in the gel filtration experiment, compound **4** induced dimerization of the protein (**Figure 9A**), indicating that each of the two monovalent binding units in **4** binds to one XIAP BIR3-only protein and forms a 1:2 complex between **4** and the XIAP BIR3-only protein. In sharp contrast, when the recombinant XIAP protein containing both BIR2 and BIR3 domains was used in the gel filtration experiment, compound **4** did not induce dimerization of the protein (**Figure 9B**). Instead, compound **4** appeared to make the protein become more compact, judging by the apparent molecular weight derived from the gel filtration data. Furthermore, monovalent compounds **1** and **3** failed to cause dimerization of either BIR3 or BIR2-BIR3 protein. These data suggest that when **4** interacts with the BIR3-only protein, one molecule of compound **4** binds to two molecules of XIAP BIR3 protein and induces dimerization of the protein. But when presented with XIAP containing both BIR2 and BIR3 domains, it binds simultaneously to both the BIR2 and BIR3 domains in the same XIAP molecule.

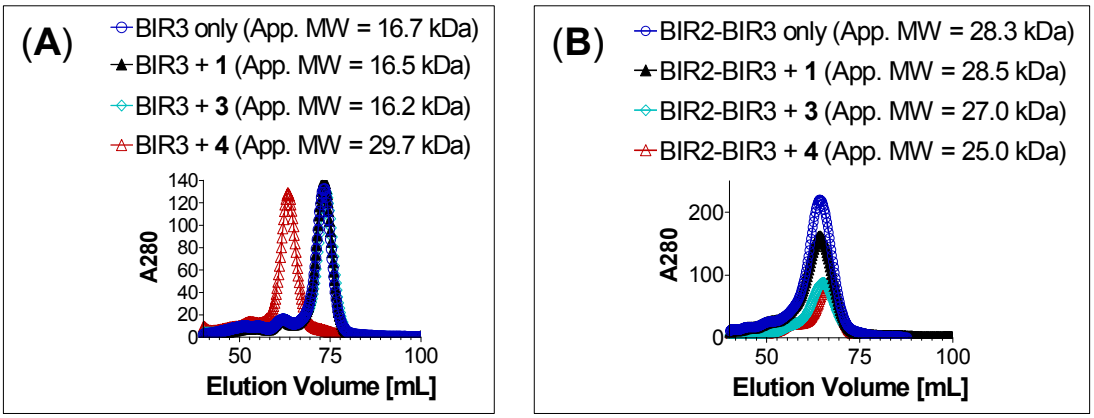

Figure 9. Analytical gel filtration of (**A**) XIAP BIR3-only protein or (**B**) XIAP BIR2-BIR3 protein alone or in the presence of monovalent Smac mimetics **1** and **3** and bivalent Smac mimetic **4.** The apparent molecular weights are shown in parentheses. The calculated molecular weight (MW) for BIR3 and BIR2-BIR3 proteins in monomeric form are 15.7 and 28.0 kDalton, respectively.

Although our binding data and gel filtration experiments using wild-type XIAP proteins strongly suggested that bivalent Smac mimetic **4** interacts simultaneously with both the BIR2 and BIR3 domains in the same XIAP molecule, these data alone do not conclusively show that either BIR2 or BIR3 is

directly involved in the binding. To confirm that both BIR2 and BIR3 domains are directly involved in the binding of XIAP BIR2-BIR3 protein to the bivalent Smac mimetic **4**, we generated mutations in each of the BIR domains. Based upon our modeling, E219 in the BIR2 domain is involved in a charge-charge interaction with compound **1** (Figure 5A), suggesting an important role of E219 in the interaction between **1** and the BIR2 domain. Our modeled structure also showed that the E314 residue in the BIR3 domain has a strong charge-charge interaction with **1** and W323 has hydrophobic contacts with the 8-membered ring in **1**, suggesting that these two residues may play a key role in the binding of **1** to XIAP BIR3. Accordingly, we have prepared two mutated proteins, BIR2(E219R)-BIR3 and BIR2-BIR3(E314S,W323E), and used them to probe the involvement of these two individual domains in the binding of compound **4** to wild-type XIAP BIR2-BIR3. The gel filtration experiments using wild-type and mutated XIAP proteins containing both BIR2 and BIR3 domains showed that in the absence of **4**, all these proteins behave as a monomer (**Figure 10A**). In the presence of compound **4**, complete

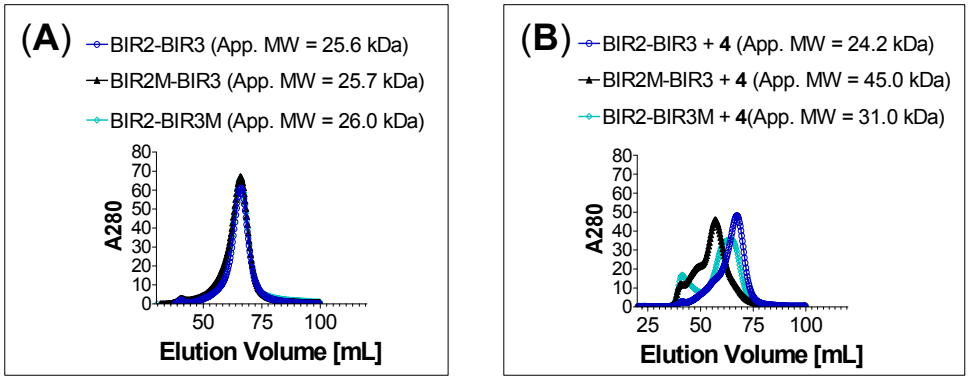

Figure 10. Analytical gel filtration of (**A**) wild-type XIAP BIR2-BIR3, BIR2(E219R)BIR3 (BIR2M-BIR3), BIR2-BIR3(E314S,W323E) (BIR2-BIR3M) proteins alone (**B**) or in the presence of bivalent Smac mimetic **4.** The apparent molecular weights (App. MW) are shown in parentheses.

dimerization of the XIAP BIR2(E219R)-BIR3 mutated protein is observed, which is in sharp contrast to the absence of dimerization when the wild-type XIAP BIR2-BIR3 protein was used (**Figure 10B**). These data clearly showed that BIR2 is directly involved in the interaction of XIAP BIR2-BIR3 with compound **4**. The gel filtration experiments further showed that compound **4** induces partial dimerization of the XIAP BIR2-BIR3(E314S,W323E) mutated protein, presumably *via* binding to two

native BIR2 domains (**Figure 10B**). The incomplete dimerization of the XIAP BIR2-BIR3(E314S,W323E) protein may be due to the relatively weak binding of its monovalent binding unit in **4** to the BIR2 domain but nevertheless clearly demonstrates that BIR3 is also directly involved in the binding of XIAP BIR2-BIR3 with compound **4**. These gel filtration experiments using both native and mutated proteins, together with the binding data, provide clear and convincing evidence that the bivalent Smac mimetic **4** interacts simultaneously with both the BIR2 and BIR3 domains in XIAP, achieving an extremely tight binding to the protein.

Analysis of the binding of Smac mimetics to XIAP BIR2-BIR3 protein by HSQC NMR spectroscopy

Heteronuclear single quantum correlation (HSQC) NMR spectroscopy was employed to further investigate if a single molecule of bivalent compound **4** concurrently interacts with the BIR2 and BIR3 domains in XIAP and if monovalent compound **1** and bivalent compound **4** have different binding modes to XIAP containing both BIR domains. The BIR2-BIR3 protein (residues 156-356) was also used in our NMR experiments for its better solubility than the L-BIR2-BIR3 protein.

It was found that most of the resonances within the BIR3 domain in XIAP BIR2-BIR3 protein appear at identical positions as those from the BIR3-only protein (residues 241-356), indicating that the BIR3 domain structure is well preserved in XIAP BIR2-BIR3 protein (data not shown). By comparing the spectra of BIR2-only, BIR3-only and BIR2-BIR3 proteins, we were able to assign most of the peaks for the BIR3 domain and to identify peaks associated with the BIR2 domain in the XIAP BIR2-BIR3 protein.

When compound **4** was added to uniformly ^{15}N labeled BIR2-BIR3 protein, ^{15}N HSQC spectra showed that many residues in the protein are affected by the compound (Supporting Information). Line width analysis of the residues within the core structural domains indicated that XIAP BIR2-BIR3 protein, with or without compound **4**, has approximately the same molecular size, confirming that compound **4** does not cause dimerization of the protein, consistent with our gel filtration results.

There are striking differences between the ^{15}N HSQC spectra of XIAP BIR2-BIR3 protein with

compounds **1** and **4** (Supporting Information). Overall, more of the protein residues are affected by compound **4** than by compound **1**, and the changes are apparent at the lowest concentration (10 μM) of compound **4** tested, which is at 1:10 ratio of the protein concentration used in the NMR experiments. In comparison, higher concentrations of compound **1** are required for similar changes in chemical shifts, indicating that compound **1** has a lower binding affinity to XIAP than compound **4**, consistent with FP binding data.

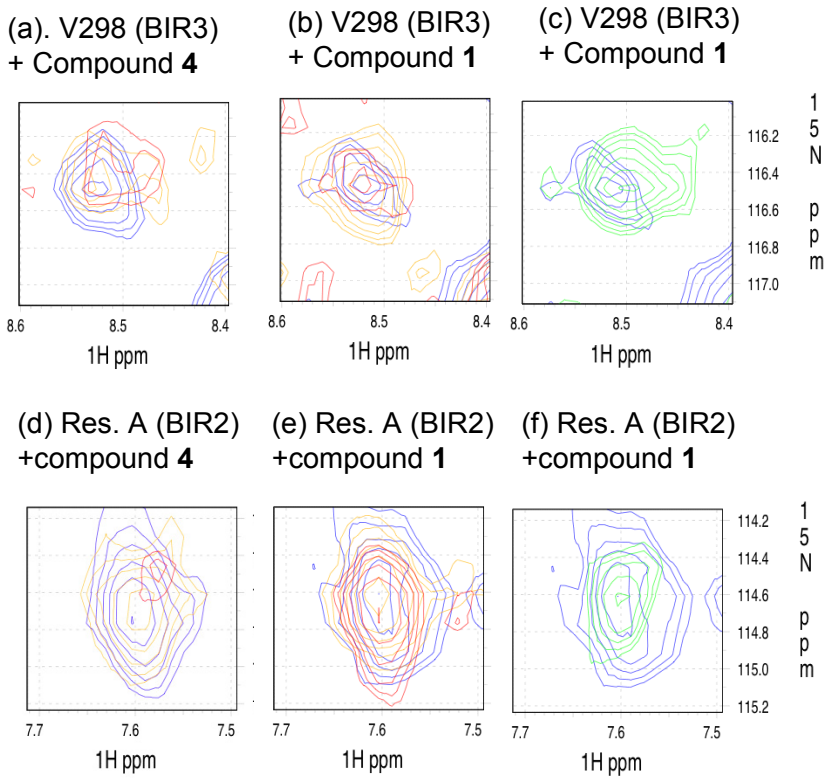

Figure 11. Small regions of overplayed ^{15}N HSQC NMR spectra of ^{15}N labeled XIAP BIR2-BIR3 with various concentrations of compounds **1** and **4** (blue: 0 μM, orange: 10 μM, red: 30 μM, and green: 150 μM (for panels e and f only). (a)-(c) Residue valine 298 (V298) in BIR3 domain of BIR2-BIR3 protein with different concentrations of compounds **4** and **1**, respectively; (d)-(f) a residue in BIR2 domain of BIR2-BIR3 proteins with different concentrations of compounds **4** and **1**, respectively.

Analysis of the residues in BIR3 domain of BIR2-BIR3 protein showed that compounds **1** and **4** affected the same BIR3 residues (Supporting Information), indicating that they bind to the same site in the BIR3 domain. However, compound **4** at the same concentrations has a greater effect on these BIR3 residues than compound **1**. For example, both compounds **4** and **1** induce significant chemical shifts on valine 298 (V298) (Figure 11(a)-(c)) and a number of other residues (Supporting Information) located in

the BIR3 domain at the lowest concentration tested, but compound **4** at the same concentrations has a greater effect than compound **1**. These data showed that although both compounds bind to BIR3 strongly, compound **4** binds to BIR3 with an even higher affinity than compound **1**. Of note, V298 directly contacts with compound **1** in our predicted binding model (Figure 5) and with the isoleucine residue in the Smac AVPI peptide in both crystal and NMR solution structures.[12,13]

The BIR2 residues affected with different concentrations of compound **4** follow the same trends as seen with the BIR3 residues and there are also significant changes in chemical shifts for BIR2 residues when compound **4** was tested at 1:10 ratio of the protein concentration. In sharp contrast, even at the highest concentration (150 μM) of compound **1** tested, which is 50% in excess of the protein concentration, BIR2 residues are affected much more weekly than the BIR3 residues (**Figure 11** and Supporting Information). These data showed that compound **1** binds to BIR2 with a much weaker affinity than to BIR3 but compound **4** binds to both BIR domains with high affinities.

Taken together, our NMR data provide additional and strong evidence that bivalent compound **4** interacts concurrently with both BIR2 and BIR3 domains in the same XIAP molecule and monovalent compound **1** binds to the BIR3 domain with a higher affinity than to the BIR2 domain. Furthermore, compound **4** binds to XIAP with a higher affinity than compound **1**. These NMR data are entirely consistent with binding data and the results from gel filtration experiments using native and mutated XIAP proteins.

Antagonism by Smac mimetics of XIAP activation of caspase-9 and –3/-7 in cell free functional assays

Since XIAP functions as a potent inhibitor of caspase-9, -3 and -7, we evaluated **1**, **4**, **5** and the AVPI peptide for their ability to antagonize XIAP in cell-free caspase functional assays (**Figure 12**). In these assays, XIAP L-BIR2-BIR3 (residues 120-356) was found to dose-dependently inhibit the activity of caspase-9 and caspase-3/-7 and achieve complete inhibition at 50 nM (**Figure 12**). Both compounds **1** and **4** antagonize XIAP in a dose-dependent manner and are capable of restoring the activity of

caspase-9, as well as that of caspase-3/-7. Consistent with their binding affinities to XIAP, compound **4** is 100 times more potent than **1**, and significantly, at an equal molar concentration of XIAP, it completely overcomes the inhibition of XIAP and fully restores the activity of caspase-9 and -3/-7, indicating its extremely high potency to antagonize XIAP. In comparison, 100 μM of the Smac AVPI peptide, (2,000 times of the concentration of XIAP protein) is needed to completely restore the activity of caspase-9 and caspase-3/-7 and the inactive control **5** has a minimal effect at 100 μM. These functional data show that bivalent Smac mimetic **4** functions as an ultrapotent antagonist of XIAP and is 100- and 2000-times more potent than the corresponding monovalent Smac mimetic **1** and the Smac AVPI peptide, respectively, entirely consistent with their binding affinities to XIAP.

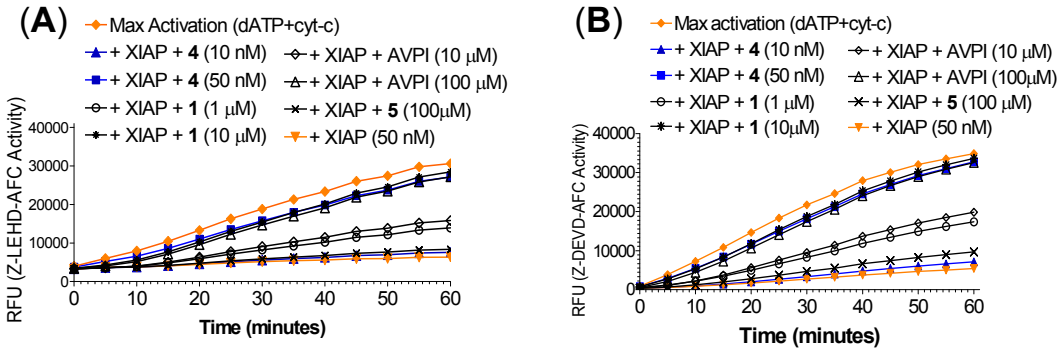

Figure 12. Functional antagonism of Smac mimetics to XIAP protein (residues 120-356) in cell-free (**A**) caspase-9 and (**B**) caspase-3/-7 activity assays.

Cellular antagonism to XIAP in isogenic cell lines transfected with XIAP or vector control

Our cell-free functional assays demonstrate that our designed bivalent Smac mimetic **4** functions as an ultrapotent antagonist of XIAP and is much more potent than its monovalent counterpart **1**. We next determined if compounds **1** and **4** are capable of antagonizing XIAP in cells and if **4** is also much more potent than **1**. For this purpose, we employed a pair of isogenic Jurkat cell lines transfected with either XIAP (XIAP-JK) or vector control (Vec-JK).[36] Western blot analysis showed that XIAP-JK cells have much higher levels of XIAP than Vec-JK cells and transfection of XIAP did not alter the levels of other IAP proteins, including cIAP-1 and cIAP-2 (**Figure 13A**). XIAP-JK cells become highly resistant to TRAIL (tumor necrosis factor-related apoptosis-inducing ligand) as compared to Vec-JK cells

(**Figure 13B**). Both **1** and **4** can antagonize XIAP to cell death induction by TRAIL, but **4** is 100-times more potent than **1** in overcoming the resistance of XIAP to cell death induction by TRAIL. Of note, both **1** and **4** have no significant effect on their own in these two Jurkat cell lines. These data clearly showed that **4** is a highly effective, cell-permeable antagonist of XIAP and is 100-times more potent than its monovalent counterpart **1**.

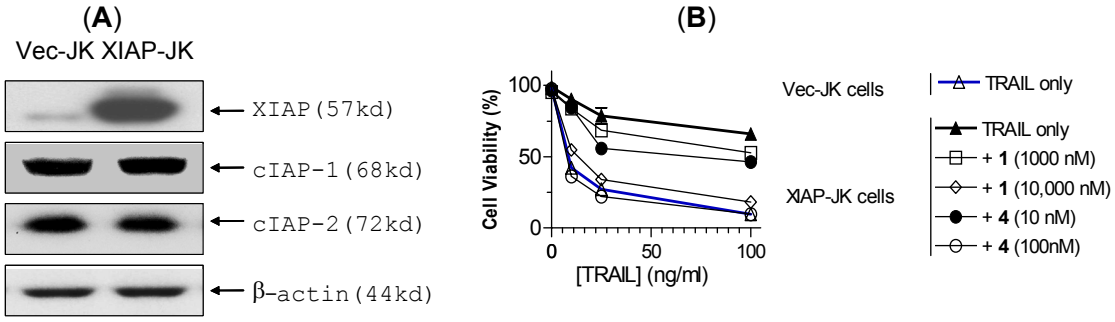

Figure 13. (**A**). Western blot analysis of expression levels of IAP proteins in Jurkat cells transfected with vector control (Vec-JK), or full length of XIAP (XIAP-JK). (**B**). Induction of cell death by TRAIL alone or in combination with compounds **1** and 4. Cells were treated with TRAIL alone or in combination for 24 hours and cell viability was assessed by trypan blue exclusion assay.

Inhibition by Smac mimetics of cell growth and induction of apoptosis in leukemia cells

Consistent with its role as a potent inhibitor of apoptosis, XIAP is highly expressed in many cancer cell lines and tumor samples from patients.[6] We hypothesize that in some, but not all, cancer cell lines, XIAP may function as the final defensive mechanism to protect cancer cells from apoptosis induction and a potent Smac mimetic may be capable of inducing apoptosis and inhibiting cell growth as a single agent without using another apoptotic stimulus by efficiently antagonizing the XIAP mediated protection.

Indeed, we found that compounds **1**, **3**, **4** and **6** effectively inhibit cell growth in the HL-60 human leukemia cell line (**Figure 14A**) and a number of other cancer cell lines with diverse tumor types. Compound **4** achieves an IC_{50} value of 1 nM in inhibition of cell growth in the HL-60 cell line. In comparison, monovalent compounds **1** and **3** have IC_{50} values of 1400 and 2000 nM, respectively, the stereoisomer **6** has an IC_{50} value of 90 nM and the inactive control **5** has an IC_{50} value >3000 nM. Therefore, the bivalent Smac mimetic **4** is 1000-times more potent than the monovalent compounds **1**

and **3** in inhibition of cell growth and their cell growth activities correlate well with their binding affinities to XIAP.

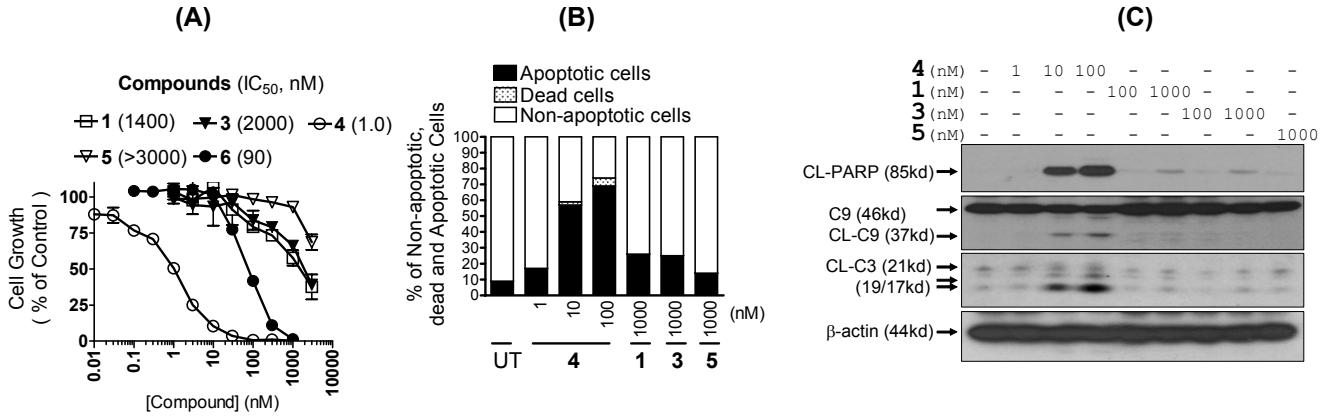

Figure 14. (A). Inhibition of cell growth by Smac mimetics in the HL-60 leukemia cancer cell line. HL-60 cells were treated with these Smac mimetics for 4 days and cell growth was analyzed by the WST-8 assay. **(B).** Induction of apoptosis by Smac mimetics **1**, **3**, **4** and **5** in the HL-60 leukemia cell line. HL-60 cells were treated with compounds **1**, **3**, **4** and **5** for 24 hours. Cells were harvested, stained with annexin-V-FITC and Propidium Iodide (PI) double staining and analyzed by flow cytometer. (C). Western blot analysis of cleavage of PARP (CL-PARP), caspase-3 (CL-C3) and -9 (CL-C9) in the HL-60 cell line induced by compounds **1**, **3**, **4** and **5**. HL-60 cells were treated with Smac mimetics for 24 hours. Whole cell lysates were analyzed with Western blotting using specific antibodies. β-actin was used as the loading control.

Because cell growth inhibition is a combination of cell growth arrest and cell death induction, we examined if compounds **1**, **3**, **4** and **5** can induce apoptosis in the HL-60 cell line by flow cytometry (**Figure 14B**). Our data showed that compound **4** potently and effectively induces apoptosis in the HL-60 cell line in a dose-dependent manner (**Figure 14B**). Compound **4** at 10 and 100 nM for 24-hours induces 57% and 69% of HL-60 cells to undergo apoptosis, respectively. In fact, compound **1** at concentrations as low as 1 nM for 24-hours induces 17% of HL-60 cells to undergo apoptosis, higher than the untreated control (9%). Monovalent Smac mimetics **1** and **3** at 1000 nM induce 25% of HL-60 cells to undergo apoptosis but are at least 100-times less effective than compound **4**. Importantly, the inactive control compound **5** at 1000 nM has no significant effect, indicating the specific effect by compound **4**.

Since compound **4** effectively antagonizes XIAP and promotes activation of caspase-9 and -3 in cell-free systems, we evaluated if **4** also activates caspase-9 and -3 in the HL-60 leukemia cells. In addition, we investigated the ability of compound **4** to induce cleavage of PARP (poly(ADP-ribose)-

polymerase), a substrate of caspase-3 and a biochemical marker of apoptosis. The results are shown in **Figure 14C**. As shown, within 24 hours compound **4,** at concentrations as low as 10 nM, induces robust activation of caspase-9 and -3 and cleavage of PARP and is 100-times more effective than the monovalent Smac mimetics **1** and **3**. The inactive control compound **5** has no effect on caspase activation and PARP cleavage at 1000 nM.

Taken together, our data showed that these Smac mimetics can effectively inhibit cell growth and induce apoptosis as single agents and the bivalent Smac mimetic **4** is 100-1000 times more potent than the corresponding monovalent Smac mimetics **1** and **3**. Compound **4** achieves an IC_{50} value of 1 nM in the HL-60 leukemia cell line in the cell growth assay and induces significant apoptosis at concentrations as low as 1 nM in a 24-hour treatment. The activity for compound **4** is highly specific since the inactive control compound **5** has no or minimal effect in all these assays at concentrations as high as 1000 nM.

Intracellular targets of designed Smac mimetics; co-immunoprecipitation assay

Our data show that compound **4** potently induces apoptosis in the HL-60 leukemia cell line at low nanomolar concentrations. To provide direct evidence that Smac mimetics **1**, **3** and **4** target XIAP in cells, we have performed co-immunoprecipitation assays using biotinylated BL-SM-122 in the HL-60 cell lysates (**Figure 15**).

These studies showed that BL-SM-122 pulls down XIAP protein in a dose-dependent manner in the HL-60 cell lysates. Compound **4** effectively competes off the binding of BL-SM-122 to XIAP dose-dependently. Compound **4** at 10 nM competes off more than 50% of XIAP bound to BL-SM-122 at 10 μM, and at 100 nM completely blocks the binding of XIAP to BL-SM-122. Monovalent Smac mimetics **1** and **3** at 1 μM reduce the amount of XIAP protein bound to BL-SM-122 only slightly, whereas the inactive control compound **5** has no effect at 1 or 3 μM. These data clearly indicate that bivalent Smac mimetic **4** binds to cellular XIAP with a much higher binding affinity than BL-SM-122 and the

unlabeled monovalent Smac mimetics **1** and **3**.

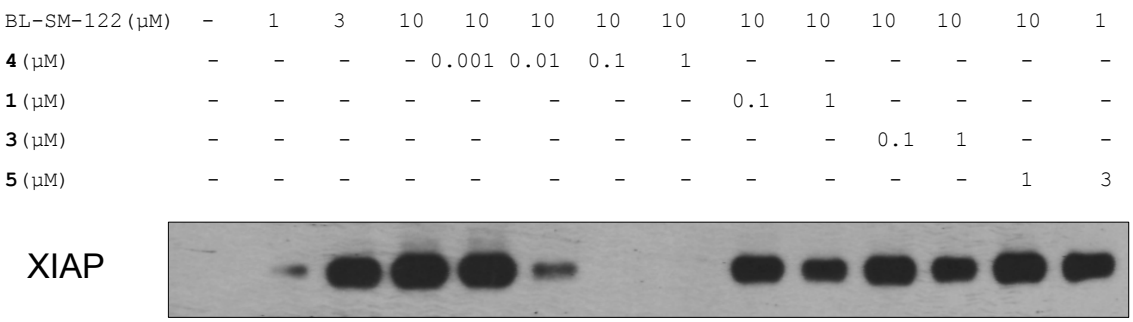

Figure 15. Probing the interaction of Smac mimetics to cellular XIAP in the HL-60 leukemia cell line by a competitive, co-immunoprecipitation pull-down assay using biotinylated SM-122 (BL-SM-122). HL-60 whole cell lysates were incubated with BL-SM-122 alone, or pre-incubated with compounds **1**, **3**, **4** and **5**, followed by co-incubation with BL-SM-122. Complexes formed between BL-SM-122 and its targeted proteins were recovered by incubation with Streptavidin-argarose beads. XIAP protein associated with beads was eluted by heating and detected by western blotting using a monoclonal XIAP antibody.

Summary

We have designed compound **4** (SM-164) as a cell-permeable, bivalent Smac mimetic to mimic the mode of binding of Smac protein to XIAP. Our study showed that SM-164 binds to XIAP protein containing both the BIR2 and BIR3 domains with an IC_{50} value of 1.39 nM and functions as an extremely potent antagonist of XIAP in our cell-free functional assays and in cells. Our gel filtration experiments using wild-type and mutated XIAP proteins, together with our NMR experiments, established that SM-164 achieves an extremely high affinity to XIAP by concurrently interacting with both the BIR2 and BIR3 domains. It potently binds to cellular XIAP protein, promotes activation of caspases and effectively induces apoptosis in leukemia cancer cells at concentrations as low as 1 nM. Significantly, SM-164 has a minimal toxicity to normal human primary cells at concentrations as high as 10,000 nM, displaying an outstanding selectivity. Our study provides convincing evidence that concurrent targeting of the BIR2 and BIR3 domains in XIAP using a non-peptide, bivalent small-molecule is a highly effective strategy to antagonize XIAP, promoting apoptosis in cancer cells. SM-164 is a powerful tool for further elucidation of the cellular functions of XIAP and a very promising lead compound in the development of a new class of anticancer therapy aimed at overcoming apoptosis resistance of cancer cells.

Experimental Section.

I. Chemistry

General Methods: ^{1}H NMR spectra were acquired at 300 MHz and ^{13}C spectra at 75 MHz. ^{1}H chemical shifts are reported with $CDCl_3$ (7.27 ppm) or HDO (4.70 ppm) as internal standards. ^{13}C chemical shifts are reported relative to $CDCl_3$ (77.00 ppm) or 1,4-dioxane (67.16 ppm) as internal standards. The final products were purified by C18 reverse phase semi-preparative HPLC column with solvent A (0.1% of TFA in H_2O) and solvent B (0.1% of TFA in CH_3CN) as eluents.

(3S,6S,10aS)-6-(tert-Butoxycarbonylamino)-5-oxodecahydropyrrolo[1,2-a]azocine-3-carboxylic acid (9). To a solution of compound **8** (1.35 g, 4 mmol) in MeOH (20 mL) was added 10% Pd-C (0.2 g). The mixture was stirred under H_2 for 8 h then filtered through celite and the filtrate was evaporated to give an ester. To a solution of this ester in 1,4-dioxane (5 mL) was added 2N LiOH (6 mL). The mixture was stirred at room temperature for 2 h and then neutralized with 1N HCl until the pH was 4. After extraction of the mixture with ethyl acetate (3x30 mL), the combined organic layers were dried over Na_2SO_4 and removal of the solvent gave the acid **9** (1.25 g. 96% over two steps). This acid can be used in the following steps without purification or can be purified by recrystallization from ethyl acetate/hexane (1:1). ^{1}H NMR ($CDCl_3$) δ 5.62 (brs, 1H), 4.63 (m, 1H), 4.50 (m, 1H), 4.25 (m, 1H), 2.41-2.09 (m, 3H), 2.07-1.50 (m, 9H), 1.45 (brs, 9H); ^{13}C NMR (75 MHz, $CDCl_3$) δ 174.77, 172.50, 155.24, 79.72, 59.96, 59.59, 50.97, 36.39, 32.21, 28.36, 26.56, 25.24, 22.65; ESI MS: *m/z* 349.2 $(M+Na)^+$; HR ESI MS for $C_{16}H_{26}N_2O_5Na$ required: 349.1739, found: 349.1727.

(3S,6S,10aS)-N-benzhydryl-6-((S)-2-(methylamino)propanamido)-5-oxodecahydropyrrolo[1,2-a]azocine-3-carboxamide (1). To a solution of the acid **9** (160 mg, 0.5 mmol) in CH_2Cl_2 (10 mL) was added aminodiphenylmethane (140 mg, 0.77 mmol), EDC (150 mg, 0.77 mmol), HOBt (105 mg, 0.78 mmol) and *N,N*-diisopropylethyl amine (0.5 mL) at $0^{o}C$ with stirring. The mixture was stirred at room temperature for eight hours and then condensed. The residue was purified by chromatography to give an amide. To a solution of this amide in MeOH (5 mL) was added HCl (4N in 1,4-dioxane, 3 mL). The

solution was stirred at room temperature overnight and then evaporated to give an ammonium salt. To a mixture of this salt in CH_2Cl_2 (10 mL) was added Boc-*N*-methyl-L-alanine (150 mg, 0.74 mmol), EDC (154 mg, 0.8 mmol), HOBt (103 mg, 0.76 mmol) and *N,N*-diisopropylethyl amine (0.7 mL) at 0^{o}C with stirring. The mixture was stirred at room temperature overnight and then condensed. The residue was purified by chromatography to give an amide. To a solution of this amide in MeOH (5 mL) was added HCl solution (4N in 1,4-dioxane, 3 mL). The solution was stirred at room temperature overnight and then condensed to give crude compound **1** as a salt with HCl (184 mg, 72% over four steps). The crude product was purified by C18 reversed-phase semi-preparative HPLC with a gradient from 70% of solvent A and 30% of solvent B to 50% of solvent A and 50% of solvent B in 40 min. ^{1}H NMR (300 M Hz, D_2O) δ 7.30-7.18 (m, 10H), 5.95 (s, 1H), 4.74 (m, 1H), 4.34 (m, 1H), 4.24 (m, 1H), 3.83 (m, 1H), 2.57 (s, 3H), 2.21-1.50 (m, 11H), 1.40 (d, J = 7.0 Hz, 3H), 1.38 (m, 1H); ^{13}C NMR (D_2O) δ 173.77, 172.62, 169.95, 141.56, 141.28, 129.54, 129.44, 128.40, 128.35, 128.01, 127.82, 62.50, 61.40, 58.19, 57.49, 51.42, 36.16, 33.30, 32.64, 31.61, 28.07, 25.36, 22.14, 15.95; ESI MS: *m/z* 477.3 $(M+H)^+$; HR ESI MS for $C_{28}H_{37}N_4O_3$ required: 477.2866, found: 477.2849.

tert-Butyl-(3S,6S,10aS)-5-oxo-3-((R)-1-phenylprop-2-ynylcarbamoyl)decahydropyrrolo[1,2-a]azo-cin-6-ylcarbamate (**12**). To a solution of acid **9** (650 mg, 2 mmol) in CH_2Cl_2 (20 mL) was added the chiral amine **11** (380 mg, 2.9 mmol), EDC (580 mg, 3 mmol), HOBt (405 mg, 3 mmol) and *N,N*-diisopropylethyl amine (1.5 mL) at 0 ^{o}C with stirring. The mixture was stirred at room temperature for a further eight hours and then condensed. The residue was purified by chromatography to give amide **12** (798 mg, 91%). ^{1}H NMR ($CDCl_3$): δ 7.80 (brd, J = 8.6 Hz, 1H), 7.50-7.40 (m, 2H), 7.33-7.20 (m, 3H), 5.91 (dd, J = 8.6, 2.4 Hz, 1H), 5.45 (brd, J = 7.9 Hz, 1H), 4.64 (dd, J = 8.3, 6.3 Hz, 1H), 4.52 (m, 1H), 4.10 (m, 1H), 2.60 (m, 1H), 2.45 (d, J = 2.4 Hz, 1H), 2.20-1.60 (m, 5H), 1.40-1.22 (m, 14H), 1.05 (m, 1H); ^{13}C NMR ($CDCl_3$): δ 172.25, 169.30, 154.95, 138.50, 128.55, 128.04, 127.04, 81.71, 79.53, 72.75, 59.50, 59.09, 50.95, 44.70, 36.48, 36.28, 31.92, 28.29, 24.89, 23.87, 22.94; ESI MS: *m/z* 439.3

$(M+Na)^+$; HR ESI MS for $C_{25}H_{33}N_3O_4Na$ required: 462.2369, found: 462.2354.

tert-Butylmethyl((S)-1-oxo-1-((3S,6S,10aS)-5-oxo-3-((R)-1-phenylprop-2-ynylcarbamoyl)deca-hydropyrrolo[1,2-a]azocin-6-ylamino)propan-2-yl)carbamate (**13**). To a solution of compound **12** (440 mg, 1 mmol) in MeOH (5 mL) was added HCl solution (4N in 1,4-dioxane, 5 mL). The solution was stirred at room temperature overnight and then condensed to give an ammonium salt. To a mixture of this salt and CH_2Cl_2 (10 mL) was added Boc-N-methyl-L-alanine (303 mg, 1.5 mmol), EDC (287 mg, 1.5 mmol), HOBt (204 mg, 1.5 mmol) and N,N-diisopropylethyl amine (1.2 mL) at 0^oC with stirring. The mixture was stirred at room temperature overnight then condensed. The residue was purified by chromatography to give amide **13** (450 mg, 86% over two steps). ^1H NMR ($CDCl_3$): δ 7.75 (brd, J = 8.5 Hz, 1H), 7.50-7.40 (m, 2H), 7.33-7.20 (m, 3H), 5.91 (dd, J = 8.5, 2.3 Hz, 1H), 6.88 (brs, 1H), 4.80 (m, 1H), 4.60 (dd, J = 8.4, 6.3 Hz, 1H), 4.58 (brm, 1H), 4.10 (m, 1H), 2.80 (s, 3H), 2.60 (m, 1H), 2.49 (d, J = 2.3 Hz, 1H), 2.20-1.60 (m, 5H), 1.50-1.05 (m, 18H); ^{13}C NMR ($CDCl_3$): δ 171.55, 170.51, 169.29, 154.95, 138.52, 128.59, 128.11, 127.09, 81.69, 80.57, 72.81, 59.59, 59.03, 49.88, 44.77, 36.50, 35.86, 31.92, 30.04, 28.36, 24.85, 23.98, 23.01, 13.72; ESI MS: *m/z* 547.3 $(M+Na)^+$; HR ESI MS for $C_{29}H_{40}N_4O_5Na$ required: 547.2896, found: 547.2897.

(3S,6S,10aS)-N-((S)-(1-Benzyl-1H-1,2,3-triazol-4-yl)(phenyl)methyl)-6-((S)-2-(methylamino)-propanamido)-5-oxodecahydropyrrolo[1,2-a]azocine-3-carboxamide (3). To a solution of compound **13** (105 mg, 0.2 mmol) and azidomethylbenzene (201 mg, 1.5 mmol) in *tert*-butanol (10 mL) was added a mixture of $CuSO_4$ (20 mg, 0.13 mmol) and (+)-sodium-L-ascorbate (60 mg) in H_2O (5 mL). The mixture was stirred at room temperature overnight and then extracted with CH_2Cl_2 (3x15 mL). The combined organic layer was washed with brine, dried over Na_2SO_4 and condensed. The residue was purified by chromatography to give a triazole. To a solution of this triazole in MeOH (5 mL) was added HCl solution (4N in 1,4-dioxane, 2 mL). The solution was stirred at room temperature overnight and

then condensed to give crude compound **3** as a salt with HCl (88 mg, 74% over two steps). This crude product was purified by C18 reversed phase semi-preparative HPLC and the purity was determined by analytical HPLC to be over 98%. The gradient ran from 70% of solvent A and 30% of solvent B to 50% of solvent A and 50% of solvent B in 40 min. ^{1}H NMR (D_2O) δ 7.66 (s, 1H), 7.35-7.10 (m, 10H), 6.04 (m, 1H), 5.36 (s, 2H), 4.70 (m, 1H), 4.28 (m, 1H), 4.19 (m, 1H), 3.80 (m, 1H), 2.56 (s, 3H), 2.20-1.50 (m, 11H), 1.40 (d, J = 7.1 Hz, 3H), 1.38 (m, 1H); ^{13}C NMR (D_2O) δ 173.14, 172.21, 169.50, 148.55, 139.09, 134.99, 129.40, 129.27, 129.04, 128.50, 128.31, 127.38, 124.02, 61.97, 60.97, 57.20, 54.22, 51.08, 50.36, 35.91, 33.05, 32.28, 31.32, 27.65, 25.06, 21.92, 15.63; ESI MS: *m/z* 580.3 $(M+Na)^+$; HR ESI MS for $C_{31}H_{39}N_7O_3Na$ required: 580.3012, found: 580.3017.

(S,3S,3'S,6S,6'S,10aS,10a'S)-N,N'-((1S,1'S)-(1,1'-(4,4'-(1,4-Phenylene)bis(butane-4,1-diyl))bis(1H-1,2,3-triazole-4,1-diyl))bis(phenylmethylene))bis(6-((S)-2-(methylamino)propanamido)-5-oxodecahydropyrrolo[1,2-a]azocine-3-carboxamide) (**4**). To a solution of compound **13** (280 mg, 0.53 mmol) and 1,4-bis-(4-azidobutyl)-benzene (71 mg, 0.26 mmol) in *tert*-butanol (10 mL) was added a mixture of $CuSO_4$ (20 mg, 0.13 mmol) and (+)-sodium-L-ascorbate (60 mg) in H_2O (5 mL). The mixture was stirred at room temperature overnight and then extracted with CH_2Cl_2 (3x30 mL). The combined organic layer was washed with brine, dried over Na_2SO_4 and evaporated to give a residue which was purified by chromatography to give a bis-triazole. To a solution of this bis-triazole in MeOH (5 mL) was added HCl solution (4N in 1,4-dioxane, 5 mL). The solution was stirred at room temperature overnight and then condensed to give crude compound **4** as a salt with HCl (215 mg, 68% over two steps). This crude product was purified by C18 reversed phase semi-preparative HPLC and the purity checked by analytical HPLC to be over 98%. ^{1}H NMR (D_2O): δ 7.40 (s, 2H), 7.20-7.05 (m, 10H), 6.60 (s, 4H), 6.05 (s, 2H), 4.70 (m, 2H), 4.28 (m, 2H), 4.15 (m, 2H), 4.06 (m, 4H), 3.80 (m, 2H), 2.55 (s, 6H), 2.28-1.04 (m, 38H); ^{13}C NMR (D_2O): δ 172.75, 172.09, 169.49, 148.33, 139.53, 129.24, 128.54, 127.41, 123.44, 61.89, 60.89, 57.18, 51.02, 50.30, 35.95, 34.28, 33.09, 32.35, 31.34, 29.22, 27.86,

25.11, 21.92, 15.69; ESI MS: *m/z* 1121.6 $(M+H)^+$; HR ESI MS for $C_{62}H_{85}N_{14}O_6$ required: 1121.6777, found: 1121.6777.

(3S,6S,10aS)-6-((S)-2-Acetamido-3-(1H-indol-3-yl)propanamido)-5-oxo-N-((R)-1-phenylprop-2-ynyl)decahydropyrrolo[1,2-a]azocine-3-carboxamide (16). To a solution of compound **12** (434 mg, 1 mmol) in MeOH (5 mL) was added HCl solution (4N in 1,4-dioxane, 5 mL). The solution was stirred at room temperature overnight and then condensed to give an ammonium salt. To a mixture of this salt in CH_2Cl_2 (10 mL) was added Nα-Boc-L-Trp (360 mg, 1.2 mmol), EDC (290 mg, 1.5 mmol), HOBt (202 mg, 1.5 mmol) and N,N-diisopropylethyl amine (1.2 mL) at 0^oC with stirring. The mixture was stirred at room temperature overnight and then condensed. The residue was purified by chromatography to give an amide. To a solution of this amide in MeOH (5 mL) was added HCl solution (4N in 1,4-dioxane, 5 mL). The solution was stirred at room temperature overnight and then evaporated to give an ammonium salt. To a mixture of this salt was added acetic anhydride (0.3 mL) and N,N-diisopropylethyl amine (0.8 mL) at 0^oC with stirring. The mixture was stirred at room temperature overnight then condensed and the residue was purified by chromatography to give the amide **16** (379 mg, 67% over four steps). ^1H NMR ($CDCl_3$): δ 8.71 (brs, 1H), 8.13 (d, J = 1.6 Hz, 1H), 8.01 (d, J = 8.5 Hz, 1H), 7.45-7.15 (m, 7H), 7.10-6.92 (m, 2H), 6.77 (d, J = 1.6 Hz, 1H), 6.39 (d, J = 8.5 Hz, 1H), 5.91 (dd, J = 8.5, 2.4 Hz, 1H), 5.20 (m, 1H), 5.05 (m, 1H), 4.34 (t, J = 8.2 Hz, 1H), 4.12 (m, 1H), 3.20 (m, 1H), 2.90 (m, 1H), 2.45 (d, J = 2.4 Hz, 1H), 2.20-1.45 (m, 15H); ^{13}C NMR ($CDCl_3$): δ 170.79, 170.72, 170.66, 170.11, 137.60, 135.81, 128.61, 127.83, 127.59, 127.06, 122.57, 121.69, 118.94, 118.30, 111.13, 110.55, 81.66, 72.60, 60.45, 60.18, 53.37, 49.38, 44.47, 36.59, 35.96, 31.99, 30.05, 26.44, 25.56, 22.98, 22.34, 20.63; ESI MS: *m/z* 590.3 $(M+Na)^+$; HR ESI MS for $C_{33}H_{37}N_5O_4Na$ required: 590.2743, found: 590.2748.

(S,3S,3'S,6S,6'S,10aS,10a'S)-N,N'-((1S,1'S)-(1,1'-(4,4'-(1,4-Phenylene)bis(butane-4,1-diyl))bis(1H-1,2,3-triazole-4,1-diyl))bis(phenylmethylene))bis(6-((S)-2-acetamido-3-(1H-indol-3-yl)propan-

amido)-5-oxodecahydropyrrolo[1,2-a]azocine-3-carboxamide) (5). To a solution of compound **16** (190 mg, 0.34 mmol) and 1,4-bis-(4-azidobutyl)-benzene (45 mg, 0.17 mmol) in *tert*-butanol (10 mL) was added a mixture of $CuSO_4$ (20 mg, 0.13 mmol) and (+)-sodium-L-ascorbate (60 mg) in H_2O (5 mL). The mixture was stirred at room temperature overnight then extracted with CH_2Cl_2 (3x30 mL). The combined organic layer was washed with brine, dried over Na_2SO_4 and evaporated to give a residue which was purified by chromatography to give compound **5** (282 mg, 76%). ^{1}H NMR ($CDCl_3$): δ 8.70 (s, 2H), 8.32 (d, J = 8.0 Hz, 2H), 7.60 (d, J = 7.4 Hz, 2H), 7.40-6.80 (m, 26 H), 6.47 (d, J = 7.9 Hz, 2H), 6.25 (d, J = 8.0 Hz, 2H), 4.81 (m, 2H), 4.70 (m, 2H), 4.50 (m, 2H), 4.27 (t, J = 7.1 Hz, 4H), 3.95 (m, 2H), 3.30-3.08 (m, 4H), 2.60 (t, J = 2.61 Hz, 4H), 2.45-2.25 (m, 2H), 2.12-1.20 (m, 36H); ^{13}C NMR ($CDCl_3$): δ 170.78, 170.41, 170.14, 169.88, 148.00, 140.45, 138.98, 136.19, 128.53, 128.44, 127.68, 127.56, 127.28, 123.70, 121.67, 121.55, 119.13, 118.57, 111.29, 110.25, 59.98, 59.06, 54.01, 50.40, 50.20, 50.01, 47.76, 35.93, 34.61, 31.74, 29.53, 29.09, 28.08, 24.83, 23.30, 22.95, 20.82; ESI MS: *m/z* 1429.7 $(M+Na)^+$; HR ESI MS for $C_{80}H_{94}N_{16}O_8Na$ required: 1429.7338, found: 1429.7341.

tert-Butylmethyl((S)-1-oxo-1-((3S,6S,10aS)-5-oxo-3-((S)-1-phenylprop-2-ynylcarbamoyl)deca-hydropyrrolo[1,2-a]azocin-6-ylamino)propan-2-yl)carbamate (15). To a solution of the acid **9** (480 mg, 1.47 mmol) in CH_2Cl_2 (15 mL) was added chiral amine **14** (290 mg, 2.21 mmol), EDC (430 mg, 2.25 mmol), HOBt (297 mg, 2.2 mmol) and *N,N*-diisoopropylethyl amine (1.5 mL) at 0 ^oC with stirring. The mixture was stirred at room temperature for eight hours and then condensed. The residue was purified by chromatography to give an amide. To a solution of this amide in MeOH (5 mL) was added HCl solution (4N in 1,4-dioxane, 5 mL). The solution was stirred at room temperature overnight and then condensed to give an ammonium salt. To a mixture of this salt in CH_2Cl_2 (10 mL) was added Boc-N-methyl-L-alanine (404 mg, 2.0 mmol), EDC (390 mg, 2.0 mmol), HOBt (272 mg, 2.0 mmol) and N,N-diisopropylethyl amine (2.0 mL) at 0^oC with stirring. The mixture was stirred at room temperature overnight and then concentrated. The residue was purified by chromatography to give the amide **15** (563 mg, 73% over three steps). ^{1}H NMR ($CDCl_3$): δ 7.85 (brd, J = 8.5 Hz, 1H), 7.50-7.42 (m, 2H), 7.35-7.20

(m, 3H), 6.98 (brd, 1H), 4.86 (m, 1H), 5.90 (dd, J = 8.5, 2.4 Hz, 1H), 4.73 (brm, 1H), 4.62 (m, 1H), 4.21 (m, 1H), 2.81 (s, 3H), 2.55 (m, 1H), 2.42 (d, J = 2.4 Hz, 1H), 2.13 (m, 1H), 2.08-1.55 (m, 10H), 1.38 (brs, 9H), 1.32 (d, J = 7.1 Hz, 3H); ^{13}C NMR ($CDCl_3$): δ 172.23, 171.10, 170.27, 138.61, 129.13, 128.55, 127.35, 82.06, 73.18, 59.89, 59.54, 50.37, 44.93, 37.22, 36.60, 32.29, 30.53, 28.78, 25.66, 24.38, 23.92, 14.29; ESI MS: *m/z* 547.3 $(M+Na)^+$; HR ESI MS for $C_{29}H_{40}N_4O_5Na$ required: 547.2896, found: 547.2906.

(S,3S,3'S,6S,6'S,10aS,10a'S)-N,N'-((1R,1'R)-(1,1'-(4,4'-(1,4-Phenylene)bis(butane-4,1-diyl))bis(1H-1,2,3-triazole-4,1-diyl))bis(phenylmethylene))bis(6-((S)-2-(methylamino)propanamido)-5-oxodeca-hydropyrrolo[1,2-a]azocine-3-carboxamide) (**6**). To a solution of compound **14** (240 mg, 0.46 mmol) and 1,4-bis-(4-azidobutyl)-benzene (60 mg, 0.22 mmol) in *tert*-butanol (10 mL) was added a mixture of $CuSO_4$ (20 mg, 0.13 mmol) and (+)-sodium-L-ascorbate (60 mg) in H_2O (5 mL). The mixture was stirred at room temperature overnight and then extracted with CH_2Cl_2 (3x30 mL). The combined organic layer was washed with brine, dried over Na_2SO_4 and condensed. The residue was purified by chromatography to give a bis-triazole. To a solution of this bis-triazole in MeOH (5 mL) was added HCl solution (4N in 1,4-dioxane, 5 mL). The solution was stirred at room temperature overnight and then condensed to give compound **6** as a salt with HCl (180 mg, 66% over two steps). The product was purified by C18 reversed phase semi-preparative HPLC and the purity determined by analytical HPLC to be over 98%. ^1H NMR (D_2O): δ 7.44 (s, 2H), 7.30-6.80 (m, 10H), 6.49 (s, 4H), 5.99 (s, 2H), 4.63 (m, 2H), 4.28 (m, 2H), 4.06 (m, 2H), 3.92 (m, 2H), 3.80 (m, 4H), 2.55 (s, 6H), 2.28-0.95 (m, 42H); ^{13}C NMR (D_2O): δ 175.04, 174.33, 171.97, 150.65, 143.08, 141.97, 131.63, 131.00, 130.59, 129.60, 126.25, 64.31, 63.33, 59.74, 53.47, 52.92, 38.47, 36.87, 35.85, 34.86, 33.87, 31.85, 30.42, 27.65, 24.52, 18.26. ESI MS: *m/z* 1143.7 $(M+Na)^+$; HR ESI MS for $C_{62}H_{85}N_{14}O_6Na$ required: 1143.6596, found: 1143.6616.

(3S,6S,10aS)-6-[2-(tert-Butoxycarbonyl-methyl-amino)-propionylamino]-5-oxo-decahydro-

pyrrolo[1,2-a]azocine-3-carbonic acid (S)-1-(4-(3-(4-benzoxycarbonylamino-butyrylamino)-propyl)-phenyl)-1'-phenyl amide (18). To a solution of acid **9** (220 mg, 0.67 mmol) in CH_2Cl_2 (10 mL) was added amine **17** (250 mg, 0.67 mmol), EDC (190 mg, 1.0 mmol), HOBt (135 mg, 1.1 mmol) and *N,N*-diisopropylethyl amine (1 mL) at 0°C with stirring. The mixture was stirred at room temperature for eight hours and then evaporated. The residue was purified by chromatography to give an amide. To a solution of this amide in MeOH (5 mL) was added HCl (4N in 1,4-dioxane, 3 mL). The solution was stirred at room temperature overnight and then condensed to give an ammonium salt. To a mixture of this salt in CH_2Cl_2 (10 mL) was added Boc-*N*-methyl-*L*-alanine (160 mg, 0.79 mmol), EDC (191 mg, 1.0 mmol), HOBt (140 mg, 1.04 mmol) and N,N-diisopropylethyl amine (1 mL) at 0°C with stirring. The mixture was stirred at room temperature overnight and then condensed. The residue was purified by chromatography to give an amide. To a solution of this amide in MeOH (10 mL) was added 10% Pd-C (100 mg). The solution was stirred under 1 atm of H_2 at room temperature overnight before being filtered through celite and condensed. The residue was dissolved in CH_2Cl_2 (10 mL) and Cbz-6-amino-hexanoic acid (212 mg, 0.8 mmol), EDC (193 mg, 1 mmol), HOBt (134 mg, 1 mmol) and *N,N*-diisopropylethyl amine (1 mL) were added at 0°C with stirring . The mixture was stirred at room temperature overnight and then concentrated to give a residue which was purified by chromatography to give compound **19** (245 mg, 42% over five steps). ^{1}H NMR ($CDCl_3$) δ 7.95 (brd, J = 8.5 Hz, 1H), 7.40-7.05 (m, 14H), 6.95 (brm, 1H), 6.19 (brd, J = 8.6 Hz, 1H), 5.49 (m, 1H), 5.10 (brs, 2H), 4.95-4.76 (m, 2H), 4.70 (m, 1H), 4.60 (brm, 1H), 4.14 (m, 1H), 3.33-3.12 (m, 4H), 2.86 (s, 3H), 2.68-2.49 (m, 3H), 2.20-1.15 (m, 33H); ^{13}C NMR ($CDCl_3$) δ172.71, 171.65, 170.58, 169.54, 156.41, 141.80, 140.50, 139.28, 136.59, 128.57, 128.47, 128.05, 127.45, 127.26, 127.14, 80.61, 66.54, 59.90, 59.16, 56.88, 50.00, 40.74, 39.11, 36.47, 35.91, 32.88, 31.94, 31.12, 30.04, 29.61, 28.37, 26.20, 25.14, 24.89, 24.12, 23.17, 13.77; ESI MS: *m/z* 903.5 $(M+Na)^+$; HR ESI MS for $C_{50}H_{68}N_6O_8$ required: 903.4996, found: 903.5009.

(3S,6S,10aS)-6-((S)-2-(Methylamino)propanamido)-5-oxo-N-((S)-(4-(3-(6-(5-((3aS,4S,6aR)-2-oxohexahydro-1H-thieno[3,4-d]imidazol-4-yl)pentanamido)hexanamido)propyl)phenyl)(phenyl)-methyl)decahydropyrrolo[1,2-a]azocine-3-carboxamide (2, BL-SH-122). To a solution of compound **19** (110 mg, 0.13 mmol) in MeOH (10 mL) was added 10% Pd-C (50 mg). The solution was stirred under 1 atm of H_2 at room temperature overnight before filtering through celite and concentration. The residue was dissolved in CH_2Cl_2 (10 mL) and (+)-biotin N-hydroxy-succinimide ester (48 mg, 0.15 mmol) and N,N-diisoopropylethylamine (0.5 mL) were added to the solution. The mixture was stirred overnight and then condensed. The residue was purified by chromatography to yield a biotinylated amide. To a solution of the amide in MeOH was added a solution of HCl in 1,4-dioxane. The solution was stirred at room temperature overnight and then the solvent was evaporated to give a crude product which was purified by C18 reversed phase semi-preparative HPLC to give compound **19** (84 mg, 74% over three steps). The purity was checked by analytical HPLC to be over 98%. The gradient ran from 70% of solvent A and 30% of solvent B to 50% of solvent A and 50% of solvent B in 40 min. ^{1}H NMR (D_2O): δ 7.22-7.04 (m, 5H), 7.02-6.90 (m, 4H), 5.87 (s, 1H), 4.65 (m, 1H), 4.32 (m, 1H), 4.22 (m, 1H), 4.12 (m, 1H), 4.01 (m, 1H), 3.80 (m, 1H), 3.05-2.82 (m, 5H), 2.62 (m, 1H), 2.52 (s, 3H), 2.46 (m, 1H), 2.45-2.30 (m, 2H), 2.18-1.05 (m, 33H); ^{13}C NMR (D_2O): δ 176.33, 176.30, 172.70, 172.07, 169.46, 165.37, 141.42, 139.27, 129.10, 127.94, 127.63, 62.31, 62.03, 60.99, 60.46, 57.43, 57.19, 55.76, 51.00, 40.08, 39.40, 39.24, 35.98, 35.83, 32.59, 31.31, 30.56, 28.49, 28.37, 28.08, 25.99, 25.66, 25.47, 15.66; ESI MS: *m/z* 895.5 $(M+Na)^+$; HR ESI MS for $C_{47}H_{68}N_8O_6S$ required: 895.4880, found: 895.4878.

II. Molecular modeling

The crystal structure of XIAP BIR3 in a complex with the Smac protein[12] (PDB code:1G73) was used to predict the binding models of XIAP BIR3 bound to designed compounds. The XIAP BIR2 structure from the X-ray structure[18] of the complex of XIAP BIR2 and caspase-3 (PDB code: 1I3O) was used to predict the binding models of designed compounds to XIAP BIR2.

A previous study[37] has demonstrated that the N-terminus of the small subunit of caspase 3 (sequence: SGVDD) interacts with XIAP BIR2 in the same binding groove as is involved in the XIAP BIR2-Smac peptide interaction. This groove can be seen clearly in the asymmetric crystallographic unit between XIAP BIR2 and caspase 3. The Swiss PDB viewer program was used to generate the asymmetric crystallographic unit in 1I3O while retaining the structure of XIAP BIR2 and the SGVDDDM peptide from caspase 3 for further molecular dynamics simulations. Our initial experiments docking compound **1** with XIAP BIR2 using the X-ray structure of XIAP BIR2 from 1I3O failed to yield satisfactory results. Examination of the crystal structure of XIAP BIR2 and comparison with that of XIAP BIR3 showed that the first aspartic acid residue, D in the SGVDDDM peptide interacts with the side chain of Q197 of XIAP BIR2. Thus, the binding pocket in the crystal structure of XIAP BIR2, which interacts with this aspartate residue, may be forced to adopt a conformation that is incompatible with its interaction with a hydrophobic residue in the fourth position of the Smac AVPI peptide. To resolve this problem, we performed an extensive molecular dynamics simulation of the XIAP BIR2 structure. In order to investigate if a hydrophobic residue in the fourth position can induce a conformational change of the XIAP BIR2 and achieve favorable interactions, we used Sybyl[38] to mutate this residue, converting SGVDDDM to SGVFDDM and added an N-methyl group to the C-terminus of the peptide. A molecular dynamics simulation of XIAP BIR2 in a complex with this mutated peptide was then performed to refine the structure.

Prior to the MD simulation, counter ions were added to neutralize the peptide-protein complex

before solvating the system with a 10Å cube of explicit waters. The four residues bonded with the Zn^{2+} ion were constrained by moderate harmonic forces to prevent unfolding of the protein. The protocol for the MD simulation was as follows: A 1000-step minimization of the solvated system was performed and followed by 6 ps of MD simulation to gradually heat the system from 0K to 298K. The system was then equilibrated and refined by a further 94 ps simulation at 298 K. During the simulation, the four residues covalently bonded with the zinc ion and the backbone atoms of the remaining residues in XIAP BIR2 are constrained by harmonic forces with force constants equal to 15 kcal/mol. Based on this protocol, only the side chain atoms of XIAP BIR2 are refined and adapted to the mutated peptide (SGVFDDM) as compared to the SGVDDM determined in the crystal structure. This refined structure of XIAP BIR2 was then used to predict the models of our designed compounds binding to XIAP BIR2.

We used the Amber program suite[39] (version 7) to perform all molecular dynamics (MD) simulations. A recent version of the Amber force field (ff96)[40] was used for the natural amino acids in the complex and the TIP3P model[41] was used for water molecules. There is one Zn^{2+} ion covalently bound to C200, C203, H220, and C227 in the XIAP BIR2 domain and to C300, C303, H320, and C327 in the XIAP BIR3 domain. This Zn^{2+} ion, while important for structural integrity, has no direct interaction with the ligands. We used parameters developed by Ryde[42] for the Zn^{2+} ion and its coordination with the neighboring four residues to model this chelating structure in our simulation. All the MD simulations were carried out at NTP. The SHAKE algorithm[43] was used to fix the bonds involving hydrogen. The PME method[44] was used to account for long range electrostatic interactions and the non-bonded cutoff distance was set at 10Å. The time step was 2 fs, and the neighboring pairs list was updated after every 20 steps. For the refinement of the structure between SM-122 and XIAP BIR2 and BIR3, the protocol is as follows: A 500-step minimization of the solvated system was performed followed by 6 ps of MD simulation to gradually heat the system from 0K to 298K. The system was then equilibrated by another 34 ps simulation at 298K. Finally, the 1 ns production simulation was run and the snapshots of conformations (typically 2000), evenly spaced in time, were collected for structural

analysis.

All the binding poses of designed ligands with XIAP BIR2 and BIR3 were developed with the GOLD program [45] (version 2.2). The centers of the binding sites for XIAP BIR2 and BIR3 were set at T208 and T308 respectively and the radius of the binding site was defined as 13 Å, large enough to cover the binding pockets. For each genetic algorithm (GA) run, a maximum number of 200,000 operations were performed on a population of 5 islands of 100 individuals. Operator weights for crossover, mutation and migration were set to 95, 95 and 10 respectively. The docking simulations were terminated after 20 runs for each ligand. GoldScore implemented in Gold 2.2 was used as the fitness function to evaluate the docked conformations. The 20 conformations ranked highest by each fitness function were saved for analysis of the predicted docking modes. For the docking poses reported, these were the highest ranked conformations from the docking simulations.

III. Protein expression and purification, binding assays to different constructs of XIAP, cell-free functional assays for the activity of caspase-9 and caspase-3/-7, and analytical gel filtration assays

Protein expression and purification

Different constructs of human XIAP proteins, including linker-BIR2-BIR3 (residues 120-356), BIR3 (residues 241-356) and linker-BIR2 (residues 120-240) were cloned into a pET28 vector (Novagen) containing an N-terminal 6xHis tag. BIR2-BIR3 (residues 156-356), without the linker preceding BIR2, was cloned into a modified HIS-TEV vector with an N-terminal 8xHis tag. The mutated proteins, BIR2(E219R)-BIR3 and BIR2-BIR3(E314S,W323E) were created using QuikChange mutagensis (Stratagene) on a BIR2-BIR3 (residues 156-356) template. Proteins were produced in *E. coli* BL21(DE3) cells grown at 37°C in 2xYT containing kanamycin to an OD_{600} of 0.6. Protein expression was induced by 0.4 mM IPTG at 20°C for 20 hours (linker-BIR2-BIR3), 20°C for 4 hours (BIR2-BIR3), 37°C for 3 hours (linker-BIR2), or 27°C for 4 hours (BIR3). Cells were lysed by sonication in buffer containing Tris pH 7.5 (50 mM), NaCl (200 mM), ZnAc (50 μM), 0.1% βME and Leupectin/Aprotin protease inhibitors. Proteins were purified from the soluble fraction using Ni-NTA resin (QIAGEN) followed by gel filtration on a Superdex 75 column in Tris pH 7.5 (20 mM), NaCl (200 mM), ZnAc (50 μM), and dithiothretal (DTT, 1 mM). After purification, DTT was added to a final concentration of 10 mM.

Fluorescence-polarization-based binding for XIAP BIR3 protein

A sensitive *in vitro* binding assay using the fluorescence polarization (FP)-based method[29] was used to determine the binding affinity of Smac mimetics to XIAP BIR3 protein. In this assay, 5-carboxyfluorescein was coupled to the lysine side chain of a mutated Smac peptide with the sequence (AbuRPFK-Fam). This fluorescently tagged peptide, named SM5F, was used as the fluorescent tracer in the FP-based binding assay of different compounds to the XIAP BIR3 protein. The recombinant XIAP

BIR3 protein of human XIAP (residues 241-356) fused to His-tag was stable and soluble, and was used for the FP-based binding assay. The K_d value of SM5F peptide to XIAP BIR3 protein was determined to be 17.9 nM.[29]

Dose-dependent binding experiments were carried out with serial dilutions of the tested compounds. An aliquot of the samples and preincubated XIAP BIR3 protein (0.030 μM) and SM5F peptide (5 nM) in the assay buffer (100 mM potassium phosphate, pH 7.5; 100 μg/ml bovine gamma globulin; 0.02% sodium azide, purchased from Invitrogen Life Technology), were added to Dynex 96-well, black, round-bottom plates (Fisher Scientific). For each assay, the controls included XIAP BIR3 protein and SM5F (equivalent to 0% inhibition), and SM5F only (equivalent to 100% inhibition). The polarization values were measured after 3 hours of incubation using an ULTRA READER (Tecan U.S. Inc., Research Triangle Park, NC). IC_{50} values, the inhibitor concentration at which 50% of the bound tracer is displaced, were determined from a plot using nonlinear least-squares analysis. Curve fitting was performed using GRAPHPAD PRISM software (GraphPad Software, Inc., San Diego, CA).

Surface Plasmon Resonance (SPR) affinity measurements and SPR competitive binding assays to XIAP BIR2 and BIR3 domains

SPR experiments were performed at room temperature on a Biacore 3000 biosensor with HBS-P [HEPES, (pH 7.4, 10 mM), NaCl (150 mM), and 0.005% Tween 20] as the running buffer. Biotin labeled Smac mimetic, BL-SM-122, was immobilized onto streptavidin (SA) sensorchips by using streptavidin-biotin coupling chemistry. BL-SM-122 was immobilized on two chips with different densities, 272 and 105 response units on the sensor chip surface.

To collect kinetic binding data of BIR2 XIAP protein for BL-SM-122 directly, the BIR2 protein solution with different concentrations in running buffer was injected over the ligand and reference flow cells at a constant flow rate of 20 μl/min. During each injection, the ligand/protein complex was allowed to associate/dissociate for 240 and 300 seconds, respectively. Residual bound protein was desorbed with

NaOH (50 mM), followed by two washes with the running buffer. Binding kinetics were derived from sensorgrams after subtraction of baseline responses and the data were fit globally to a 1:1 interaction model (A + B = AB) by using the BIA evaluation software.

For competitive binding assay, a fixed concentration of XIAP BIR2-only protein (1 μM) was incubated with different concentrations of the tested compound in HBS-P buffer for ~2 hr at room temperature. The mixtures were then injected over a sensorchip containing a channel with BL-SM-122 immobilized on the chip and a control without BL-SM-122. The baseline response (control) was subtracted to obtain the specific binding response. Taking the response for the protein alone as the maximal response (100%), the relative residual binding (%) in the presence of different concentrations of the tested compound at a given injection time point (225 s) was then calculated. The relative residual responses were plotted against initial concentrations of the tested compound and fitted using a nonlinear least-squares equation using GRAPHPAD PRISM software (GraphPad Software, Inc., San Diego, CA).

Fluorescence-polarization-based binding for XIAP L-BIR2-BIR3 protein

A FP-based competitive binding assay was established for quantitative determination of the binding affinities of our designed Smac mimetics to XIAP containing both BIR2 and BIR3 domains. In the competitive binding experiments, the tested compound was incubated with XIAP protein (residues 120-356, 3 nM) and **Smac-1F** (0.5 nM) in the assay buffer [potassium phosphate, pH 7.5 (100 mM); bovine gamma globulin (100 μg/ml); 0.02% sodium azide] in Dynex 96-well, black, round-bottom plates (Fisher Scientific). In each experiment, the controls included XIAP and **Smac-1F** peptide (equivalent to 0% inhibition), and **Smac-1F** only (100% of inhibition). Polarization values were measured after 2 hours incubation, using the Ultra plate reader. The IC_{50} value, the inhibitor concentration at which 50% of bound tracer was displaced, was determined from the plot using nonlinear least-squares analysis For each assay, Smac AVPI peptide was used as the control. Curve fitting was performed using GRAPHPAD PRISM software (GraphPad Software, Inc., San Diego, CA).

Cell-free caspase functional assays

MDA-MB-231 cell lysates were prepared by solubilizing cells in ice cold buffer containing KCl (50 mM), EGTA (5 mM), $MgCl_2$ (2 mM) DTT (1 mM), 0.2% CHAPS and HEPES, (pH 7.5 50 mM), containing cocktail protease inhibitors, incubating on ice for 10 minutes, then freezing in liquid nitrogen. Cytochrome c and dATP were added to the cell lysates, which were then incubated at 30^{o}C in a water bath for 60 minutes to activate caspase-9 and -3/-7. Addition of recombinant XIAP L-BIR2-BIR3 protein (50 nM) in the cell lysates completely suppressed the activity of caspase-9, and caspase-3/-7. Different concentrations of a tested Smac mimetic (1 nM - 100 μM) were added to determine the restoration of the activity of these caspases.

For determination of caspase activity, 25 μM of either caspase-9 substrate (Z-LEHD-AFC), or caspase-3/-7 substrate (Z-DEVD-AFC) (BioVision Inc.) was added. Fluorescence detection of substrate cleavage by caspase-9 or -3/-7 for their specific substrate was carried out on an ULTRA READER using an excitation wavelength of 400 nm and an emission wavelength of 505 nm. The reaction was monitored for 1-2 hours.

Analytical gel filtration experiments

To probe the binding mode of the designed Smac mimetics to XIAP proteins, we performed analytical gel filtration experiments with BIR3 (residues 241-356) protein, BIR2-BIR3 (residues 156-356) protein, BIR2(E219R)-BIR3 (residues 156-356) protein, and BIR2-BIR3(E314S,W323E) protein. Analytical gel filtration experiments were performed on a Superdex 75 column (GE Healthcare) attached to an AKTA Purifier-10 system in Tris-HCl, (pH 7.5, 20 mM), NaCl (200 mM), zinc acetate (50 μM), and DTT (1 mM). Recombinant protein was run on the column at a concentration of 1 mg/ml alone or after incubation with a 1:1 molar ratio of Smac mimetic. Molecular weight standards from Amersham-Pharmacia were used to calibrate the column.

IV. NMR HSQC Experiments

Expression and purification of ^{15}N labeled proteins

The BIR3 domain (residues 241-356) of human XIAP fused to His-tag (pET28b, Novagen), the BIR2 domain (residues 156-260) and the BIR2-BIR3 protein (residues 156-356) of human XIAP in pHis-TEV vector were used to express respective proteins from BL21(DE3) cells (Nogaven) in M9 medium containing $^{15}NH_4Cl$ to label the protein uniformly with ^{15}N. Most of the proteins were found in the soluble fraction and they were purified using TALON (Clontech) affinity chromatography, followed by Q-XL ion exchange and G75 size-exclusion chromatography (GE Healthcare) with AKTA purifier (GE Healthcare).

NMR HSQC experiments

^{15}N HSQC NMR spectra were recorded on a Bruker AVANCE 500MHz NMR spectrometer with samples containing 100 μM of the ^{15}N labeled proteins in 50 mM Tris (pH 7.2), 50 μM $ZnCl_2$, 1 mM DTT at 25°C with or without test compound at a final concentration between 10-150 μM. The spectra were then compared in order to identify residues affected by the interaction with the test compound. Within the BIR3 domain, the known chemical shift assignments of the backbone atoms,[13,46] were used to identify the residues corresponding to the affected peaks. The backbone atom resonance assignments of the BIR3 domain were also confirmed by 3D NMR triple resonance experiments (HNCA, HNCACB, HN(CO)CBCA, HNCO, TOCSY-HSQC, C(CO)NH). All NMR data were processed and analyzed using the nmrPipe/nmrDraw package (Dr. Frank Delaglio, NIDDK, NIH).[47]

V. Assays for cell growth, cell viability, apoptosis, Western blotting and biotin-streptavidin pull-down

Cell lines

Human HL-60 leukemia cell line was purchased from the American Type Culture Collection

(Manassas, Virginia, USA), maintained in RPMI 1640 (Invitrogen), supplemented with 10% fetal bovine serum (Invitrogen) and 1% penicillin-streptomycin, at 37°C in 5% CO_2. Human Jurkat T leukemic cell lines stably transfected with the pEBB-HA (VEC-JK), pEBB-HA-XIAP (XIAP-JK) were a kind gift of Dr. Colin Duckett (Departments of Pathology and Internal Medicine, University of Michigan). Jurkat cell lines were cultured in RPMI 1640 supplemented with 10% fetal bovine serum (Invitrogen) and 1% penicillin-streptomycin in the presence of puromycin from EMD Biosciences (2 μg/ml).

Cell growth assay

The effect of Smac mimetics on HL-60 cell growth was evaluated by a WST-8 [2-(2-methoxy-4-nitrophenyl)-3-(4-nitrophenyl)-5-(2,4-disulfophenyl)-2*H*-tetrazolium, monosodium salt assay (Dojindo Molecular Technologies, Inc). Cells (3000-4000 cells in each well) were cultured in 96-well tissue culture plates in medium (200 μl) containing various concentrations of Smac mimetics for indicated time. At the end of incubation, WST-8 dye (20 μl) was added to each well and incubated for an additional 1-3 h, then the absorbance was measured in a microplate reader (Molecular Devices) at 450 nm. Cell growth inhibition was evaluated as the ratio of the absorbance of the sample to that of the control.

Cell viability assay

Cell viability was quantitated by microscopic examination in a trypan blue exclusion assay. Cells were treated in triplicate for 24 hours, harvested and stained with an equal volume of 0.04% trypan blue. Both blue cells and morphologically shrunk cells were scored as non-viable cells. At least 100 cells from each treatment, performed in triplicate, were counted.

Apoptosis assay

Apoptosis assays were performed with an annexin-V/propidium iodide (PI) apoptosis detection kit

(Roche) according to manufacturer's instructions. Briefly, cells were harvested, washed with ice-cold PBS and then stained with annexin-V-FITC and PI for 15 minutes at room temperature in the dark. Stained cells were analyzed in a FACS calibur flow cytometer. Annexin-V (+) cells were measured as apoptotic cells, annexin V (-) and PI (+) cells were measured as death cells.

Western blotting

Cells were harvested and washed with cold PBS. Cell pellets were lysed in double lysis buffer (DLB; 50 mmol/L Tris, 150 mmol/L sodium chloride, (1 mmol)/L EDTA, 0.1% SDS and 1% NP-40) in the presence of L PMSF (1 mmol) and protease inhibitor cocktail (Roche) for 10 min on ice, then centrifuged at 13,000 rpm at 4°C for 10 min. Protein concentrations were determined using a Bio-Rad protein assay kit (Bio-Rad Laboratories).

Proteins were electrophoresed onto either 4% or 20% gradient SDS-PAGE (Invitrogen) then transferred to PVDF membranes. Following blocking in 5% milk, membranes were incubated with a specific primary antibody, washed, and incubated with horseradish peroxidase–linked secondary antibody (Amersham). The signals were visualized with the Chemiluminescent HRP antibody detection reagent (Denville Scientific). When indicated, the blots were stripped and reprobed with a different antibody. Primary antibodies against caspase-9, cleaved caspase 3 and β-actin were purchased from Cell Signaling Technology; primary antibody against cleaved PARP was purchased from Epitomics.

Biotin-avidin pull-down assay

The interaction between compounds **1**, **2**, **3** and **4** and cellular XIAP was investigated using a biotin-streptavidin pull-down assay. Cells were lysed in lysis buffer [20 mmol/L Tris, NaCl (150 mM/L) and 1% NP40] for 20 min. Cell lysates were precleared with streptavidin-agarose beads, incubated with biotinylated SM-122, named BL-SM-122, alone for pull-down assay, or pre-incubated with compound **1**, **2**, **3** and **4** for 5 min followed by co-incubation with BL-SM-122 for competitive experiments.

Complexes formed between the Smac mimetics and the associated proteins were recovered by incubation with streptavidin-agarose beads (100 μl) on a shaker for 2 h at 4°C then centrifuged at 1000 × g for 1 min. The complexes were then washed 3 times with lysis buffer at 4°C and eluted from the beads by boiling in SDS loading buffer (100 μl). The eluted proteins were detected by Western blotting.

Acknowledgment: We are grateful for the financial support from the Breast Cancer Research Foundation, the Prostate Cancer Foundation, the Department of Defense Prostate Cancer Program (W81XWH-04-1-0213), Ascenta Therapeutics, and the National Cancer Institute, NIH (R01CA109025). Jurkat cells were kind gifts of Dr. Colin Duckett from the University of Michigan. The authors thank Dr. Dennis Torchia at the National Institute of Diabetes and Digestive and Kidney Diseases, National Institutes of Health for helpful discussions of the NMR experiments, Dr. Jason Gestwicki at the Life Sciences Institute and Department of Pathology at the University of Michigan for assistance and discussions of the SPR experiments, and Dr. G.W.A. Milne for critical reading of the manuscript.

Supporting Information Available: Complete references of 24, 27 and 39, NMR HSQC spectra of XIAP BIR2-BIR3 protein with different concentrations of compounds **1** and **4** and enlarged view for several BIR3 residues available. This material is available free of charge via the Internet at http://pubs.acs.org.

References:

1. Ponder, B. A. *Nature* **2001**, *411*, 336-341.
2. Lowe, S. W. & Lin, A.W. *Carcinogenesis* **2000**, *21*, 485-495.
3. Nicholson, D.W. *Nature* **2000**, *407*, 810-816.
4. Deveraux Q. L. Reed JC. *Genes Dev.* **13**, 239-252.
5. Salvesen G. S.; Duckett, C. S. *Nat Rev Mol Cell Biol* **2002**, *3*, 401-410.
6. Tamm I.; Kornblau S. M.; Segall, H.; Krajewski, S.; Welsh, K.; Kitada, S.; Scudiero, D. A.; Tudor, G.; Qui, Y. H.; Monks, A.; Andreeff, M.; Reed, J. C. *Clin. Cancer Res.* **2000**, *6*, 1796-1803.
7. Holcik, M.; Gibson, H.; Korneluk, R. G. *Apoptosis*, **2001**, *6*, 253-261.
8. Du, C.; Fang, M.; Li, Y.; Wang, X. *Cell*, **2000**, *102*, 33-42.
9. Verhagen, A. M.; Ekert, P. G.; Pakusch, M. ; Silke, J. ; Connolly, L. M. ; Reid, G. E. ; Moritz, R. L. ; Simpson, R. J. ; Vaux, D. L. *Cell*, **2000**, *102*, 43-53.

10. Chai J. ; Du, C. ; Wu, J. W. ; Kyin, S. ; Wang, X. ; Shi, Y. *Nature,* **2000**, *406*, 855-62.

11. Shiozaki, E. N. ; Shi, Y. *Trends Biochem Sci.* **2004**, *29*, 486-494.

12. Wu, G.; Chai, J.; Suber, T. L.; Wu, J.W.; Du, C.; Wang, X.; Shi, Y. *Nature,* **2000**, *408*, 1008-1012.

13. Liu, Z. ; Sun, C. ; Olejniczak, E. T. ; Meadows, R. P. ; Betz, S. F. ; Oost, T. ; Herrmann, J. ; Wu, J. C. ; Fesik, S. W. *Nature*, **2000**, *408*, 1004-1008.

14. Srinivasula, S.; Hegde, R.; Saleh, A.; Datta, P.; Shiozaki, E.; Chai, J.; Lee, R.-A.; Robbins, P. D.; Fernandes-Alnemri, T.; Shi, Y.; and Alnemri, E. S. *Nature,* **2001**, *410*, 112-116.

15. Shiozaki, E. N.; Chai, J.; Rigotti, D. J.; Riedl, S. J..; Li, P.; Srinivasula, S. M.; Alnemri, E. S.; Fairman, R.; Shi, Y. *Mol Cell*, **2003**, *11*, 519-527.

16. Chai, J.; Shiozaki, E.; Srinivasula, S. M.; Wu, Q.; Dataa, P.; Alnemri, E. S.; and Shi, Y. *Cell*, **2001**, 104, 769-780.

17. Huang, Y.; Park, Y. C.; Rich, R. L.; Segal, D.; Myszka, D. G.; Wu, H. *Cell,* **2001**, 104, 781-790.

18. Riedl, S. J.; Renatus, M.; Schwarzenbacher, R.; Zhou, Q.; Sun, C.; Fesik, S. W.; Liddington, R. C.; Salvesen, G. S. *Cell*, **2001**, *104*, 791-800.

19. Huang, Y. Rich, R. L. Myszka, D. G. and Wu, H. *J. Biol. Chem*. **2003**, 278, 49517-49522.

20. Fulda, S.; Wick, W.; Weller, M.; Debatin, K. M. *Nature Med.,* **2002***, 8*, 808- 815.

21. Sun, H.; Nikolovska-Coleska, Z.; Yang, C.-Y.; Xu, L.; Liu, M.; Tomita, Y.; Pan, H.; Yoshioka, Y.; Krajewski, K.; Roller, P. P.; Wang, S. *J. Am. Chem. Soc*. **2004**, *126*, 16686- 16687.

22. Sun, H.; Nikolovska-Coleska, Z.; Yang, C.-Y.; Xu, L.; Tomita, Y.; Krajewski, K.; Roller, P. P.; Wang, S. *J. Med. Chem.* **2004**, *47*, 4147-4150.

23. Sun, H.; Nikolovska-Coleska, Z.; Lu, J.; Qiu, S.; Yang, C.-Y.; Gao, W.; Meagher, J.; Stuckey, J.; Wang, S. *J. Med. Chem.* **2006**, *49*, 7916-7920.

24. Oost, T. K.; et al. *J. Med. Chem.* **2004**; *47,* 4417- 4426.

25. Zobel, K. ; Wang, L. ; Varfolomeev, E. ; Franklin, M. C.; Elliott, L. O.; Wallweber, H. J.; Okawa, D. C.; Flygare, J. A.; Vucic, D. ; Fairbrother, W. J.; Deshayes, K. *ACS Chem. Biol*. **2006**; *1*, 525-

533.

26. Wu, T. Y.; Wagner, K. W.; Bursulaya, B.; Schultz, P. G.; Deveraux, Q. L. *Chem Biol.* 2003, **10,** 759-67.

27. Schimmer, A. D.; *et al. Cancer Cell,* **2004***,* **5**, 25-35.

28. Li, L.; Thomas, R. M.; Suzuki, H.; De Brabander, J. K.; Wang, X, Harran, P. G. *Science*, **2004**, *305*, 1471-4.

29. Nikolovska-Coleska, Z., Wang R., Fang, X., Pan, H., Tomita, Y., Li, P., Roller, P. P., Krajewski, K., Saito, N. G., Stuckeys J. A., Wang, S. *Anal Biochem.* **2004**, *332*, 261-73.

30. Kipp, R. A., Case, M. A., Wist, A. D., Cresson, C. M., Carrell, M., Griner, E., Wiita, A., Albiniak, P. A., Chai, J., Shi, Y., Semmelhack, M. F., McLendon, G. L. *Biochemistry*, **2002**, *41*, 7344-7349.

31. Rostovtsev, V. V.; Green, L. G.; Fokin, V. V. and Sharpless, K. B. *Angew. Chem. Int. Ed.* **2002***, 41*, 2596-2599.

32. Duggan, H. M. E.; Hitchcock, P. B. and Young, D. W.; *Org. Biomol. Chem*., **2005**, *3*, 2287-2295.

33. Messina, F.; Botta, M.; Corelli, F.; Schneider, M. P. and Fazio, F.; *J. Org. Chem.* **1999**, *64*, 3767-3769.

34. Sun, H., Nikolovska, C. Z., Yang, C. Y. and Wang, S., *Tetrahedron Letters*, **2005**, *46*, 7015-7018.

35. Nikolovska-Coleska, Z., Meagher, J. L., Jiang, S., Kawamoto, S. A., Gao, W., Yi, H., Qin, D., Roller, P. R., Stuckey, J. A. Wang, S. *Analytical Biochemistry* (submitted).

36. Wilkinson, J.C.; Cepero, E.; Boise, L.H.; and Duckett, C.S. *Mol Cell Biol*, **2004**, *24***,** 7003-7014.

37. Scott, F. L.; Denault, J.-B.; Riedl, S. J.; Shin, H.; Renatus, M.; Salvesen, G. S. *EMBO J.* **2005**, *24*, 645-655.

38. Sybyl, a molecular modeling system, is supplied by Tripos, Inc., St. Louis, MO 63144.

39. Case, D. A.; *et al. AMBER7*, University of California, San Francisco, **2002**.

40. Kollman, P. A.; Dixon, R.; Cornell, W.; Fox, T.; Chipot, C.; Pohorille, A. In Computer Simulation of Biomolecular Systems, Vol. 3, Wilkinson, A.; Weiner, P. and van Gunsteren, W. F., Ed.,

Elsevier, **1997**, p. 83.

41. Jorgensen, W. L.; Chandrasekhar, J.; Madura, J. D.; Impey, R. W.; Klein, M. L. *J. Chem. Phys.* **1983**, *79*, 926-935.

42. Ryde, U. *Proteins: Struct. Funct. Genet.* **1995**, *21*, 41-56.

43. Rychaert, J. P.; Ciccotti, G.; Berendsen, H. J. C. *J. Comput. Phys*. **1977**, *23*, 327-341.

44. Darden, T. A.; York, D. M.; Pedersen, L. *J. Chem. Phys*. **1993**, *98*, 10089-10092.

45. Jones, G.; Willett, P.; Glen, R. C.; Leach, A. R.; Taylor, R. *J. Mol. Biol.* **1997**, *267*, 727-748.

46. Sun, C.; Cai, M.; Meadows, R.P.; Xu, N.; Gunasekera, A.H.; Herrmann, J.; Wu, J.C.; and Fesik, S.W. *J. Biol. Chem.* **2000**, 275, 33777-33781.

47. Delaglio, F., Grzesiek, S., Vuister, G.W., Zhu, G., Pfeifer, J., and Bax, A. *J. Biomol. NMR*, **1995**, 6, 277-293.

JA074725F

Supporting Information

Design, Synthesis and Characterization of A Potent, Non-Peptide, Cell-Permeable, Bivalent Smac Mimetic that Concurrently Targets both the BIR2 and BIR3 Domains in XIAP

*Haiying Sun[+], Zaneta Nikolovska-Coleska[+], Jianfeng Lu[+], Jennifer L. Meagher[∃], Chao-Yie Yang[+], Su Qiu[+], York Tomita[¶], Yumi Ueda[¶], Sheng Jiang[#], Krzysztof Krajewski[#], Peter P. Roller[#], Jeanne A. Stuckey[∃†], and Shaomeng Wang[+]***

[+]Departments of Internal Medicine, Pharmacology and Medicinal Chemistry and Comprehensive Cancer Center, [∃]Life Sciences Institute, and [†] Biological Chemistry, Biophysics Research Division, University of Michigan, 1500 E. Medical Center Drive, Ann Arbor, MI 48109, USA; [¶]Lombardi Cancer Center, Georgetown University Medical Center, Washington DC 20007, USA; [#]Laboratory of Medicinal Chemistry, National Cancer Institute-Frederick, NIH, Frederick, Maryland 21702, USA.

CORRESPONDING AUTHOR:

Shaomeng Wang, Phone: (734) 615-0362; Fax: (734) 647-9647; Email: shaomeng@umich.edu

Complete References:

24. Oost, T. K.; Sun, C.; Armstrong, R. C.; Al-Assaad, A.-S.; Betz, S. F.; Deckwerth, T. L.; Ding, H.; Elmore, S. W.; Meadows, R. P.; Olejniczak, E. T.; Oleksijew, A.; Oltersdorf, T.; Rosenberg, S. H.; Shoemaker, A. R.; Tomaselli, K. J.; Zou, H.; Fesik, S. W. *J. Med. Chem.* **2004**, 47, 4417-4426.

27. Schimmer, A. D.; Welsh, K.; Pinilla, C.; Wang, Z.; Krajewska, M.; Bonneau, M. J.; Pedersen, I. M.; Kitada, S.; Scott, F. L.; Bailly-Maitre, B.; Glinsky, G.; Scudiero, D.; Sausville, E.; Salvesen, G.; Nefzi, A.; Ostresh, J. M.; Houghten, R. A.; Reed, J. C. *Cancer Cell,* **2004**, **5**, 25-35.

39. Case, D. A.; Pearlman, D. A.; Caldwell, J. W.; Cheatham III, T. E.; Wang, J.; Ross, W. S.; Simmerling, C. L.; Darden, T. A.; Merz, K. M.; Stanton, R. V.; Cheng, A. L.; Vincent, J. J.; Crowley, M.; Tsui, V.; Gohlke, H.; Radmer, R. J.; Y. Duan; Pitera, J.; Massova, I.; Seibel, G. L.; Singh, U. C.; Weiner, P. K.; Kollman, P. A. *AMBER7*, University of California, San Francisco, **2002**.

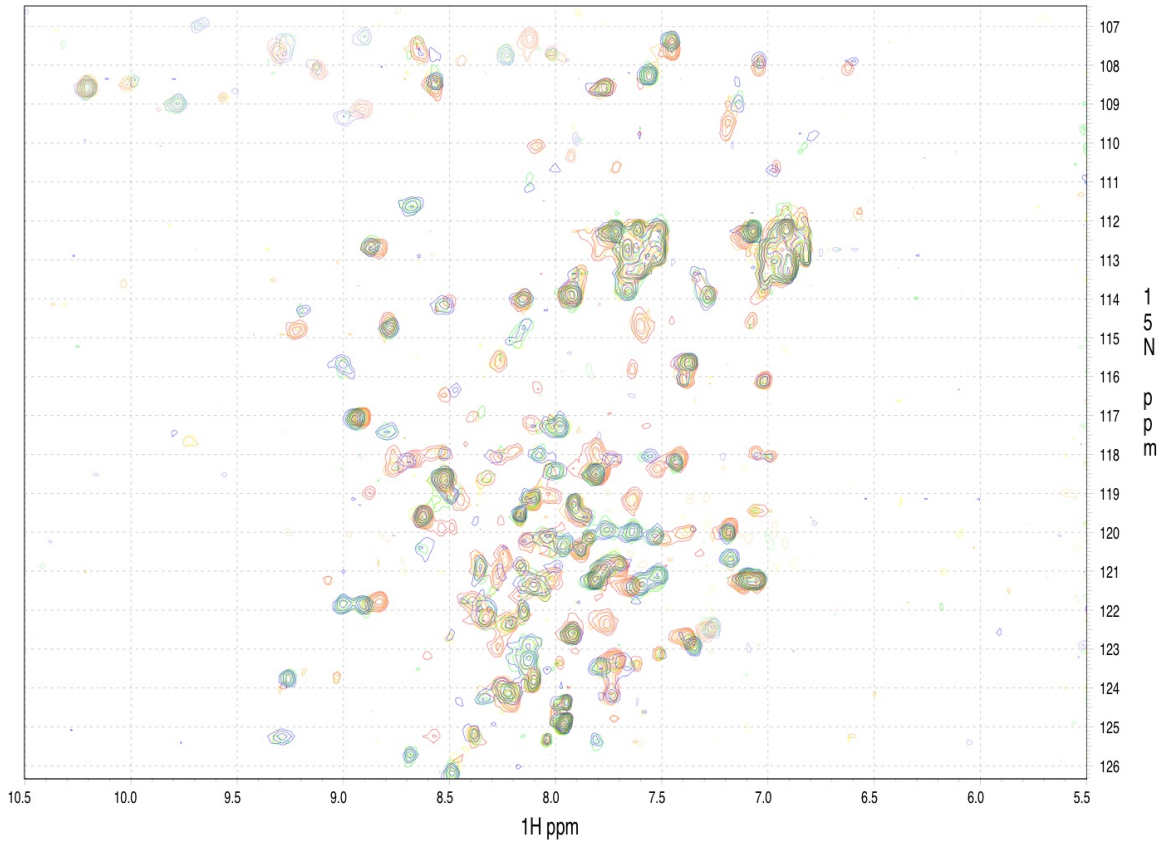

Figure S1.[15]N-HSQC NMR spectra of XIAP BIR2-BIR3 protein at 100 μM with different concentrations of SM-164 (compound **4**) (red: 0; orange: 10; yellow: 30; green: 60; blue 150 μM).

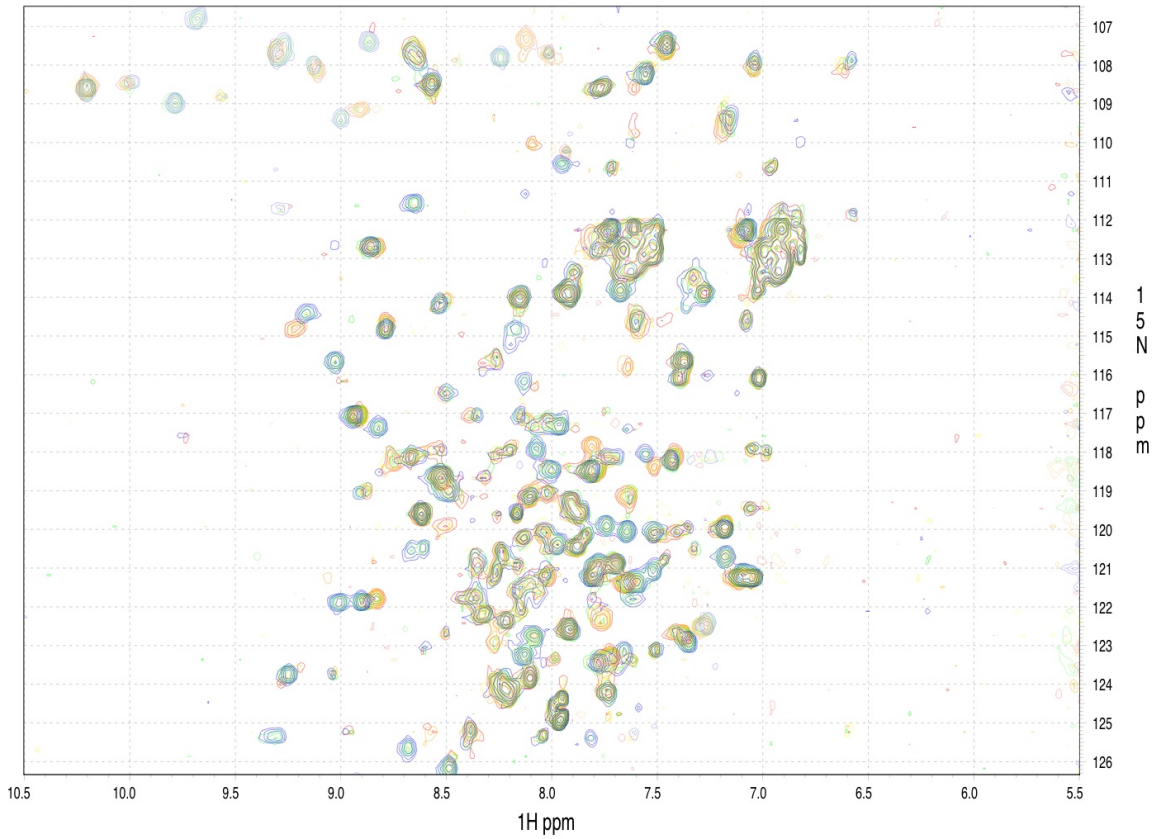

Figure S2. ^{15}N-HSQC NMR spectra of XIAP BIR2-BIR3 protein at 100 μM with different concentrations of SM-122 (compound **1**) (red: 0; orange: 10; yellow: 30; green: 60; blue 150 μM).

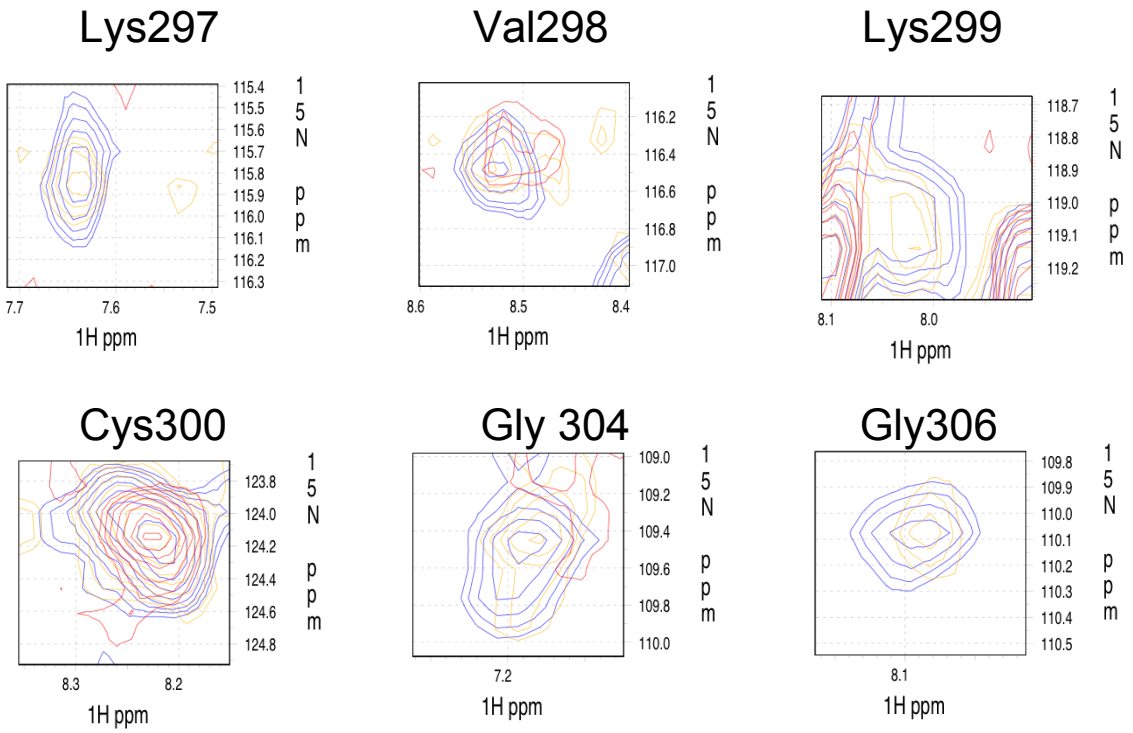

Figure S3.[15]N-HSQC NMR spectra of several BIR3 residues in XIAP BIR2-BIR3 protein (100 μM) with different concentrations of SM-164 (red: 0; orange: 10; yellow: 30; green: 60; blue 150 μM).

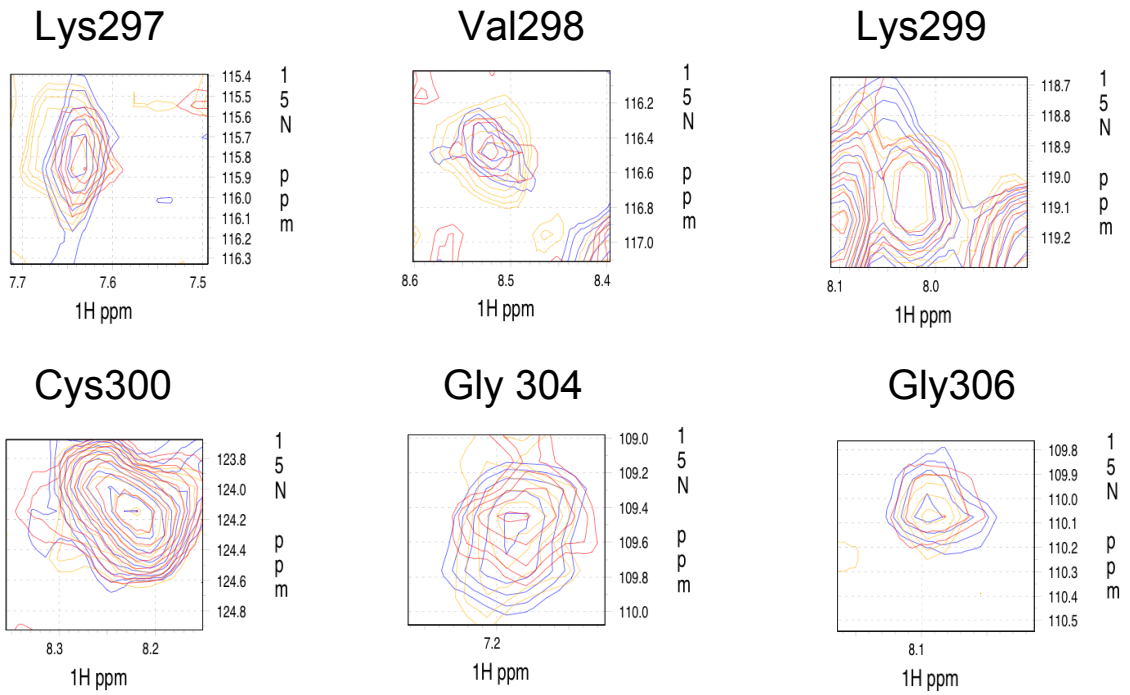

Figure S4.[15]N-HSQC NMR spectra of several BIR3 residues in XIAP BIR2-BIR3 protein (100 μM) with different concentrations of SM-122 (red: 0; orange: 10; yellow: 30; green: 60; blue 150 μM).